FINITE ELEMENT STUDY OF

OIL TANK FOUNDATION SYSTEM

BUI THI YEN

NATIONAL UNIVERSITY OF SINGAPORE

2005

FINITE ELEMENT STUDY ON

OIL TANK FOUNDATION SYSTEM

BUI THI YEN

(M.Eng)

A THESIS SUBMITTED

FOR THE DEGREE OF MASTER OF ENGINEERING

DEPARTMENT OF CIVIL ENGINEERING

NATIONAL UNIVERSITY OF SINGAPORE

2005

Dedicated to my family and friends

ACKNOWLEDGEMENTS

The author would like to express her sincere gratitude and appreciation to her supervisor, Associate Professor Tan Siew Ann, for his continual encouragement and bountiful support that have made her graduate study an educational and fruitful experience.

In addition, the author would also like to thank Associate Professor Leung Chun Fai who gave her the suggestion for this research and supported her all the time here.

Finally, the author is grateful to all her friends and colleagues for their sincere helps and friendships.

TABLE OF CONTENTS

SUMMARY

The thesis focuses on Oil tank foundation system. The finite element code PLAXIS and PLAXIS 3D Foundation were used for the numerical simulation. The research work is aimed at pursuing the objectives: (1) Numerical analysis for single pile, pile raft analysis and compare to some other established methods to validate the FEM program (2) Back analysis of the centrifuge data of 37 end-bearing pile group underneath the sand pad supporting a model oil tank.

The research work done can be summarized as: (1) Single pile was modeled in both 2D Axisymmetry using Plaxis v8 and 3D using Plaxis 3D Foundation. The results from both analyses are compared in order to check the accuracy of Plaxis 3D Foundation program. Plaxis 3D Foundation also is validated in prediction behavior of a piled raft with 6 other established methods (2) Numerical analyses to study the effect of pile cap area, thickness of overlying granular material, number of piles, and stiffness of bed layer of a pile foundation system supporting an oil tank over soft clay. The load distribution among piles, the load transfer characteristics, the maximum settlement, the differential settlement, the shape of settlement and the arching in soil are investigated in each case study. The results are compared to centrifuge data.

Keywords: FEM, PLAXIS, Pile group, Pile raft, settlement profile.

LIST OF TABLES

LIST OF FIGURES

CHAPTER 4: 3D FEM ANALYSIS OF PILE GROUP FOR OIL TANK FOUNDATION ON SOFT GROUND

LIST OF SYMBOLS

Symbol	Units	Meaning
a		Pile cap ratio
A	m^2	Tributary area of one cap
c	kN/m^2	Cohesion
c_i	kN/m^2	Cohesion of interface element
$c_{increment}$	kN/m^2	The increase of cohesion per unit depth
c_{soil}	kN/m^2	Cohesion of soil
c_u	kN/m^2	Undrained shear strength
D	m	Diameter of tank
d_c	m	Shortening of vertical height of conduit
E	MN/m^2	Young's modulus
E_{50}	MN/m^2	Confining stress-dependent stiffness modulus for primary loading
E_{50}^{ref}	MN/m^2	Reference stiff modulus corresponding to the reference confining pressure
EA	kN/m	Elastic axial stiffness
EI	$kN.m^2/m$	Bending stiffness
E_{actual}	MN/m^2	Actual Young's modulus
E_i	MN/m^2	Young's modulus of interface element
$E_{increment}$	MN/m^2	The increase of the Young's modulus per unit of depth
E_{ref}	MN/m^2	Reference Young's modulus
E_s/E_{soil}	MN/m^2	Young's modulus of soil
E_p	MN/m^2	Young's modulus of pile
E_{oed}	MN/m^2	Constrained or oedometric soil modulus
E_{oed}^{ref}	MN/m^2	Tangent stiffness for primary oedometer loading
E_{ur}^{ref}	MN/m^2	Reference Young's modulus for unloading/reloading
F_c		Correction factors of pile settlement
FEM		Finite element method
G	MN/m^2	Shear modulus
H	m	Thickness of the sand above the cap
K		Bulk modulus

K'	MN/m^2	Effective bulk modulus
K_w	MN/m^2	Bulk modulus of water
K_o		Coefficient of lateral stress in in-situ condition
K_o^{NC}		Coefficient of lateral stress in normal consolidation
L	m	Length of Pile
l_e	m	Average element size
m		Power in stress-dependent stiffness relation
n		Porosity
OCR		Over consolidation ratio
p^{ref}	kN/m^2	Reference confining pressure
P_L	kN	Load on piles
P_T	kN	Total load at pile cap level
q_a	kN/m^2	Asymptotic value of the shear strength
q_c	kN/m^2	Average cone resistance
q_f	kN/m^2	Ultimate deviatoric stress
q_s	kN/m^2	Ultimate shaft resistance
R_{inter}		Interface strength reduction factor
r	m	Distance from the center of footing
s	m	Spacing between center of test piles
x_{max}	m	Outer geometry dimension
x_{min}	m	Outer geometry dimension
y_{max}	m	Outer geometry dimension
y_{min}	m	Outer geometry dimension
y_{ref}	m	Reference depth
γ_{unsat}	kN/m^3	Unsaturated unit weight of soil
γ_{sat}	kN/m^3	Saturated unit weight of soil
γ_w	kN/m^3	Unit weight of water
$\underline{\sigma}'$	kN/m^2	Vector notation of effective normal stress
σ_3	kN/m^2	Confining pressure in a triaxial test
σ_h	kN/m^2	Horizontal stress
σ_n	kN/m^2	Normal stress of soil
σ_w	kN/m^2	Pore pressure
τ	kN/m^2	Shear strength of soil
ν		Poisson's ratio

ν_u		Poisson's ratio for undrained
ν_{ur}		Poisson's ratio for unloading and reloading
φ	^{o}	Internal friction angle
ψ	^{o}	Dilatancy angle
Δc_u	kN/m^2	The increase of undrained shear strength per unit depth
ΔE	MN/m^2	The increase of Young's modulus per unit depth

CHAPTER 1

INTRODUCTION

1.1 Oil tank foundation system

It is well known from many studies on oil storage tank foundation systems that stability and settlement are two main factors which may lead to the rupture or even the complete failure of oil tanks (Bell and Iwakiri, 1980; Green and Height, 1975; Marr *et al.,* 1982; D'Orazio and Duncan, 1983 and 1987).

The two modes of foundation stability that have been observed in practice are the edge shear and the base shear. Base shear involves the failure of the entire tank acting as a unit whereas edge shear is referred to local shear failure of a part of the tank perimeter and the nearby portion of the base. In comparison with the absolute magnitude of maximum settlement, differential settlement, the shape of the settlement dish are of more importance in engineering. To avoid problems caused by differential settlement of the tank bottoms, three checks are required: (1) procedure for estimating the magnitude of settlement; (2) procedure for estimating the likely shape of the tank bottom upon settlement; and (3) a criterion for judging the acceptability of the magnitude of differential settlement (D'Orazio and Duncan, 1987).

1.2 Background of project

A thin granular pad can be used to improve the edge shear stability while the use of the pile system would enhance the base shear stability and reduce the settlement as well as the differential settlement. However, the thickness of the granular pad, the

number and configuration of piles, the load distribution among piles in the system to achieve the most effective foundation system are still being studied. One method to enhance the oil tank foundation system and minimize the differential settlement is the use of pile raft foundation. For the case where shallow raft foundation can provide enough bearing capacity but the average settlement and differential settlement is excessive, piles are introduced in order to limit settlements (Randolph, 1994). In this case, the raft and the pile work together such that the raft will take part of the applied load and the piles bear the remaining load in such a way to induce uniform settlement. Available theories can be used to evaluate two failure mechanisms of edge and base shear, and to estimate the settlement in the simple case of a uniform soil layer. However, the real conditions can be much more complicated. Behavior of the foundation system with granular pads and piles in various soil profiles is not easy to idealize.

A field study of Molasses tank in Menstrie, Scotland was carried out by Thornburn et al. (1984). The foundation system consisted of a pile group with individual pile caps taken to more competent soil strata below. A layer of dense compacted granular material was placed over the soft soil with a R.C. membrane laid over the pile caps and the soft ground as shown in Figure 1.1. Since the tanks were able to accommodate reasonably large settlements, the primary purpose of the piles was to provide sufficient bearing capacity in the short term. The results indicate that the selected foundation design appears to provide a suitable foundation for the tank farm. However, relatively few field studies have been reported apart from that by Thornburn.

A numerical study was performed at the National University of Singapore by Khoo (2001) adopting the unit cell concept as a simplification of the pile group

problem. Results were obtained from parametric studies by modeling the soil using both linear elastic and Mohr-Coulomb models. This numerical study is rather simplistic using axisymmetry of single pile which cannot represent correctly all the piles in the group.

A centrifuge model on a foundation system consisting of dense sand pad of 37 end bearing piles on soft soil was reported by Lee (2004). This study investigated the effects of the pile cap size and the thickness of dense granular material to the proportion of applied loads between the piles and the soil, and the distribution of loads among the piles. Some advantages of the centrifuge model are:

- Centrifuge model can model consolidation of soil much faster.
- The failure mechanism in the centrifuge model is similar to real soil as the stresses can be correctly simulated.

However some disadvantages of this model can be listed as:

- Pile installation at 1g and overall model experiment at high g, may affect the result significantly.
- A small bedding error in the centrifuge model is amplified in prototype scale.
- To avoid the base boundary effect especially for friction piles, the model may be too large to operate in the centrifuge test model.
- This model could not be used for a complex soil profile.

With the rapid development of computer technology and finite element technique, some powerful finite element (FEM) programs such as CRISP and PLAXIS are now widely used. These programs were developed with reasonably good soil model to simulate the nonlinear soil behavior. The 3D analysis could address the difficulty of non-uniform soil profile, pile soil interaction etc. As a result, more complex situations can be studied.

1.3 Objective and Scope of Project

This project focuses on oil tank foundation system. The finite element code PLAXIS version 8 and PLAXIS 3D Foundation are used for the numerical simulation. The scopes of this project are:

(1) Validate Plaxis 3D Foundation program in modelling the piles and pile raft.

Firstly, 2D Axisymetry analysis is well known as reliable tool to predict the single pile behavior. In this first part of this research, single pile was modeled in both 2D Axisymetry using Plaxis v8 and 3D using Plaxis 3D Foundation. The results from both analyses are compared in order to check the accuracy of Plaxis 3D Foundation program. Secondly, The Plaxis 3D Foundation will be validated for prediction of pile raft behavior compared to the result from a number of other establish methods. The hypothetical example of 15 piles and 9 piles with raft was modeled in Plaxis 3D to compare the predicted settlements, differential settlements, maximum bending moments in raft and proportion of load carried by piles with that of 6 other established methods.

(2) Numerical analysis to study the effect of pile cap area, thickness of overlying granular material, number of piles, stiffness of founding soil layer of a pile foundation system supporting an oil tank over soft clay. The 3D finite element model was based on the centrifuge model conducted by Lee (2004) as shown in Figure 1.2.

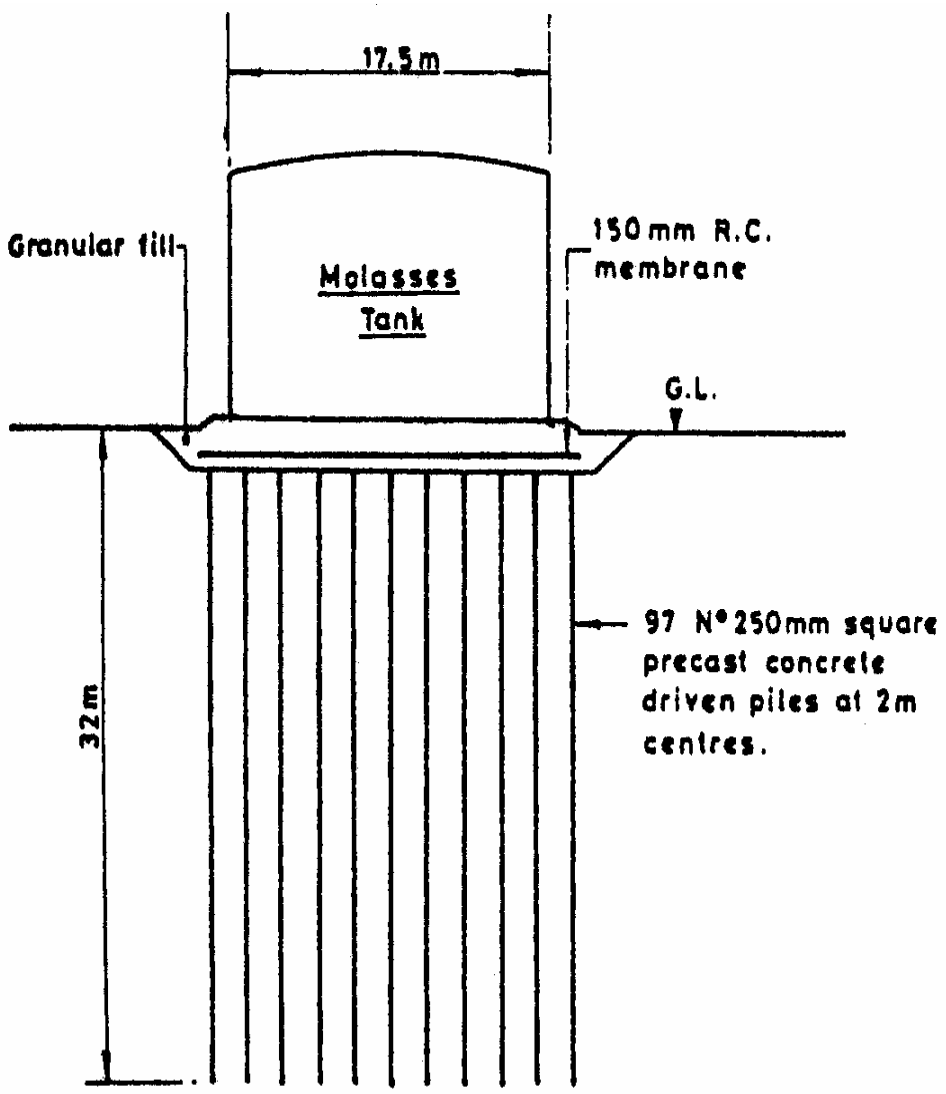

Figure 1.1: Cross section of tank at Menstrie Tank Farm (after Thornburn et al., 1984)

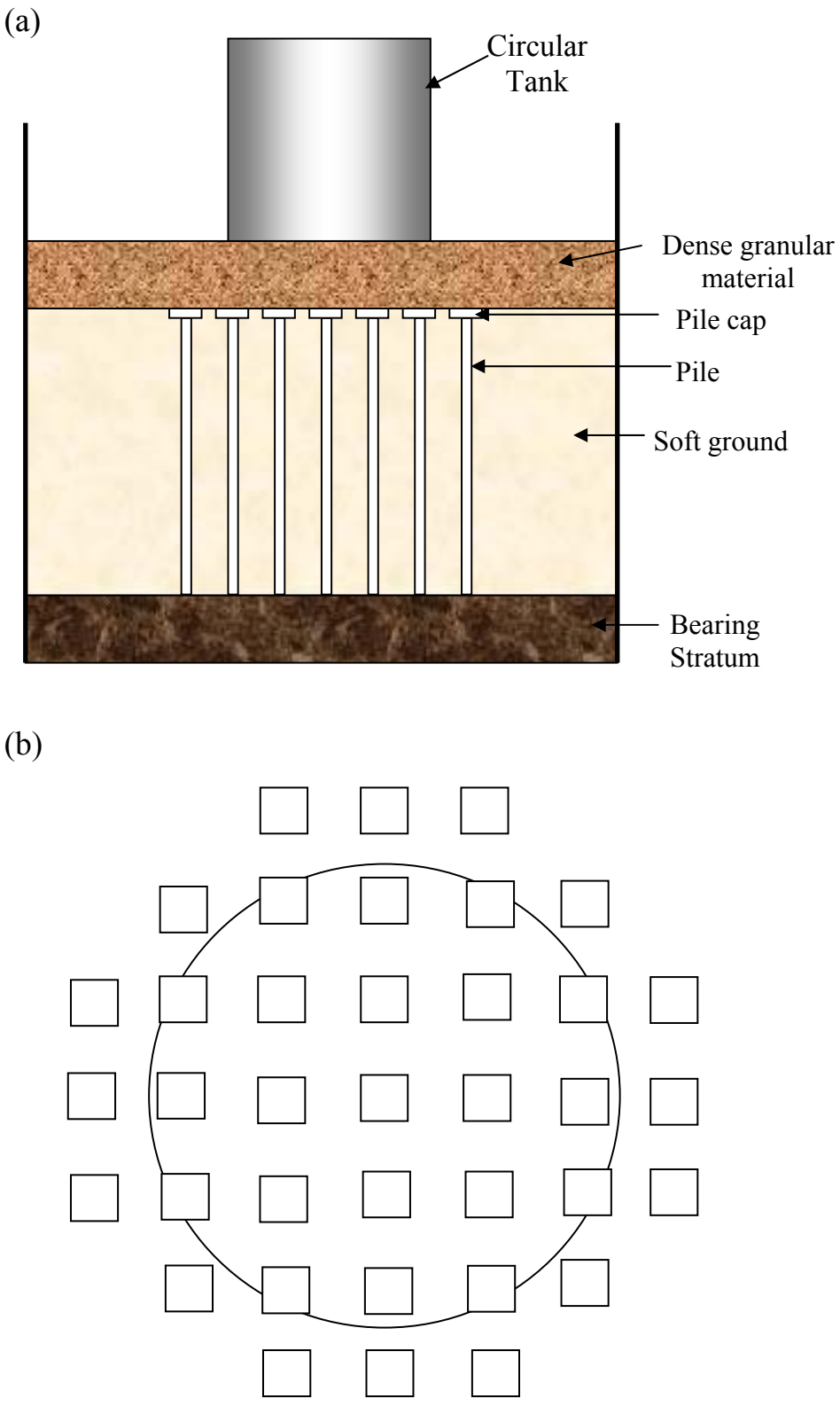

Figure 1.2: Tank supported by a pile group with individual caps: (a) Cross section view, (b) Plan view. (after Lee, 2004)

CHAPTER 2

LITERATURE REVIEW

2.1 Introduction

Several aspects related to oil tanks foundation system will be covered in this literature review. Firstly, the review will focus on previous studies on oil tank foundation. Secondly, since the pile behaviour in oil tank foundation is similar to embankment piles to some extent, the review will also cover embankment piles. Thirdly, arching, the most common phenomenon in embankment piles, will be discussed. Finally, the pile raft foundation will be included in the review because it is believed that a system of pile group underneath sand pad behaves similar to pile raft to some extent and pile raft is also a possible type of oil tank foundation system.

2.2 Tank foundation review

2.2.1 Stability

A tank stability study of 40 tanks, which included 6 foundation shear failures and 2 ruptures, was carried out by Duncan *et al.* (1984). Significant findings of these case histories include:

- Larger non-uniform settlement and tilting of the tank can lead to complete rupture of the tank.

- Either base shear or edge shear can be the critical failure mechanism, thus both should be evaluated.
- Thin weak layers near the surface have greater effects on the edge shear stability, whereas deep and thick weak layers have great effects on base shear stability.
- Either accelerating drainage or slow loading can be used to improve the strength of tank foundation on cohesive soils.
- A thin granular pad can improve edge stability but do not improve base stability.
- Tanks have been successfully stabilitized after failure by: (1) reconstruction on pile foundations or repairing with very slow filling; (2) lifting the tank up, replacing soft foundation soils and constructing stability berms.

All the case studies of this paper were with shallow foundations; theoretical method use to analyze the stability and estimate the settlement could not take in to account the influence of non-uniform soil layer.

2.2.2 Criteria for settlement of tanks

Marr *et al.* (1982) stated that differential settlement is an important factor of tank rupture. Differential settlement is defined as the difference in vertical settlement between two points at the foundation-structure interface. Reasons leading to differential settlement could be non-homogeneous geometry or compressibility of the soil deposit, non-uniform distribution of the load applied to the foundation, and uniform stress acting over a limited area of the soil stratum. These causes exist with varying degrees of importance for a tank foundation.

The settlement pattern shown in Figure 2.1 may influence differently the tank structural elements, which include the shell, bottom plate, connection of shell to bottom plate and roof. Firstly, uniform settlement is not a big concern in practice. Secondly, planar tilt causes additional stress in the shell but apparently not large enough to cause overstressing. Finally, non-planar settlement is most destructive to the tank. Non-planar settlement may radically distort the shell or overstress the shell and it also causes dish-shaped settlement and localized depressions to bottom plate as shown in Figure 2.2. Radial distortion of the shell may lead to malfunction of a floating roof. In addition, overstress may cause rupture and spillage of contents inside the tank.

The paper reported on the control of differential settlement to prevent the damage of each kind of tank structure component. Uniform settlement seems not dangerous but care should be taken in case of non planar settlement.

2.2.3 Differential settlements in steel tanks

Duncan and D'Orazio (1987) studied 31 case histories of tank settlement and damage to investigate which factors controlled the differential settlements of tank and the magnitudes of the differential settlement tolerance. They stated that the shape of the settlement dish, as well as the magnitude of differential settlements is important factors for the tank rupture caused by settlement. They classified the shape of settlement into 3 profiles (Figure 2.3):

Profile A: The maximum settlement is located at the center of the tank. This settlement profile could be seen from the case of flexible raft seated on deep soft soil. The depth of soft soil to produce this settlement profile depends on the factor of safety.

Profile B: Settlement is relatively flat at interior and decreases rapidly toward the tank edge. This settlement profile could be seen from the case of flexible raft

seated on shallower depths of soft soil. It also depends on the factor of safety

Profile C: Maximum settlement is located about two third of the radius from the center of the tank. This settlement profile could be seen from the case of flexible raft seated on a thin layer of soft soil.

Different settlement profiles produce different amounts of distortion for the same magnitude of center settlement. The settlement profile A is the least severe with respect to distortion and profile C is the most severe.

2.2.4 Field study

A case study of storage tanks founded on soft soils reinforced with driven piles in Mentrie, Scotland was presented by Thornburn et al. (1984). The ground condition consists of soft alluvium deposited up to approximately 100 m thick. The foundation system consists of a 2 m thick dense granular material over the 97 piles incorporated with 150 mm thick reinforced concrete membrane as shown in Figure 1.1. The piles were installed in a triangular configuration with 2m center to center spacing, and the piles cap size was 1m square. The piles penetrated to 32m depth below the ground surface. The resistance of the piles comprised both shaft friction and base resistance.

Settlement measurements were taken around each tank periphery and also beneath each tank center. Each tank was subjected to a water test with a full load maintained for 4 hours. The results indicated that generally 75% of the recorded settlements occurred within the first 9 months of the operation and that the settlements appeared to have stabilised after 24 months. The differential settlement between the centre and periphery of the tanks is not significant. The result showed that over 90% of tank loads had been transferred to the piles. This case essentially is a pile foundation with some consolidation effects. The piles are predominantly end-bearing.

2.2.5 Numerical study

A soil-pile composite system was analysed by Khoo (2001) at the National University of Singapore. It consists of a granular fill sitting immediately below the tank and the piles underneath the granular fill to transfer the load to more competent residual soil as shown in Figure 2.4. The granular fill is assumed to behave like a "stiff cushion" to spread the tank load to a wider area below the tank.

All piles in the group are assumed to behave in the same manner. Deformation and stress states are assumed to be identical in any radial direction due to symmetry. The single pile in an axisymmetric model was analysed to represent all the piles in the group as shown in Figure 2.5. Two soil models, linear elastic model and Mohr-coulomb model, were used both in drained and undrained analysis. The analysis aimed to investigate the effect of the pile cap size, the thickness and the stiffness of the granular fill on the percentage of the load carried by the piles.

The results showed that when the thickness of the granular fill is in excess of a minimum required, it seemed to have no effect on the percentage of load taken by the piles. The increase in stiffness of the granular fill improved the load tranfer to the piles. For stiff soil bed, the foundation behaves almost like a raft foundation. Similarly, the larger the pile cap size, the higher the percentage of the load is taken by the piles. Figure 2.6 shows the various percentages of the load taken by the piles with variation of granular fill thickness, granular fill stiffness and the pile cap size for both Mohr-Coulomb and linear elastic model under both drained and undrained conditions.

In reality, the performances of the piles in pile group are not the same, edge pile and centre pile will perform quite differently. The assumption of axisymmetry can not apply to the edge piles. In this study, the single pile used to represent all the piles

in group. The interaction of the piles among pile group was not taken in to account so that the trends of the changes are questionable.

2.2.6 Centrifuge model

A study of 37 piles with individual pile caps by centrifuge models was conducted by Lee (2004) to investigate the effects of pile cap size and thickness of sand pad on the proportion of applied loads between the piles and the soil and distribution of loads among the piles. The centrifuge test model shown in Figure 1.2 was set up with a soil profile consisting of a thin dense sand pad sitting immediately below the tank and then a thick soft soil layer below. The bottom layer was very stiff dense sand. The piles are in a rectangular grid of 2 m center-to-center spacing underneath the sand pad, and the pile toes are set in the very stiff sand layer. The sand pad is assumed to spread the load from the tank to the pile cap and the piles are supposed to transfer the load to the layer of very stiff dense sand below the soft clay. The centrifuge test procedure basically consists of 4 stages: (a) soil pre-consolidation under self-weight, (b) pile installation and sand preparation at 1g, (c) soil re-consolidation under self-weight and (d) application of tank loading.

Lee (2004) found that generally the axial forces carried by center piles are much higher compared to corner piles and piles outside the tank. The settlement was quite uniform and about 60% of ultimate tank settlement had taken place during the loading stage. It continued to increase gradually and practically ceased to increase about 1 year after loading.

Result from series of model tests with pile cap area ratio (defined as the ratio of one pile cap area to the tributary area of the pile, see Figure 4.3) varying from 6% to 30% showed that:

- The proportion of tank loads carried by the pile increases with pile cap area ratio. However, the rate of increase decreases when the pile cap area ratio increases.
- The settlement of tank decreases with increasing pile cap area ratio. The gradient of the load-settlement response of the tank decreases with increasing pile cap area ratios.

Result from series of model test with sand pad thickness varying from 1m to 3m showed that:

- When the thickness of sand pad increases, the proportion of the tank load carried by the pile increases. However, the rate of increase decreases when the thickness of sand pad increases.
- The tank settlement decreases with increasing thickness of sand pad. However, the gradient of the load-settlement response of the tank decreases with increasing sand pad thickness.

Result from series of model tests with a reduced number of piles showed that there was not much difference in the foundation system behavior when the outside piles were removed whereas the increased settlement and effect on the magnitude of load taken by some piles are significant when some corner piles were removed.

2.3 Embankment Piles

Embankment piles are used to carry the load from a fill or a structure into ground. It could be either end bearing piles when the applied load is mainly transferred to the piles tip or floating piles when the applied load is mainly transferred by skin friction. Precast concrete and steel piles are normally used as end bearing piles whereas it is often economical to use small diameter timber piles as floating piles.

2.3.1 Embankment piles by Wong

Wong (1985) suggested that the pile cap on embankment piles should be designed in such a way that the behavior of the piles will be ductile. For the case when one or several of the piles are overloaded, the redistribution of the load among the piles can take place. The pile cap size and the pile spacing also have to be chosen such that the fill does not penetrate between the caps due to soil arching. The allowable load on embankment pile is normally higher than a structure pile because of this redistribution. He reported that it is economical to use the piles with as high an end bearing as possible as in case of high fill or large load. The foundation system with end bearing piles can take more load and give less settlement than the floating piles but it is also less ductile. He also stated that the load sharing of piles cap and the soil between the pile caps depends on the strength and deformation properties of the underlying soil. If the underlying soil is stiff soil, a large part of load will be taken by the soil between pile caps whereas less load will be taken by soil between pile caps in the case of a soft underlying soil.

2.3.2 Load transfer in embankment piles by Tung

Tung (1994) investigated the effect of density of sand fill, height of sand fill, and rigidity of the base board to the load sharing between the piles and the subsoil using a laboratory model. The model consists of 16 piles with individual pile caps (Figure 2.7).

The results showed that:

- Foundation efficacy, defined as the proportion of load taken by piles over the total load, increases with the sand fill height

- The higher the baseboard stiffness, the more is the load tranferred to the piles

2.3.3 Design Guidelines in BS 8006

BS8006 (1995) Code of practice for strengthened/reinforced soils and other fill, provides guidelines for, "Reinforcement used as a component to control embankment stability and settlement". Clause 8.8.8 stated that "the technique of piling enables embankments to be constructed to unrestricted heights at any construction rate with subsequent controlled post-construction settlement". The two most relevant sub-clause discussing the design of embankment piles are **Clause 8.3.3.3 Limit states and Clause 8.3.3.6 Vertical load shedding.**

Clause 8.3.3.3 Limit states

The piles have to be designed based on both ultimate limit state and serviceability limit state as shown in Figures 2.8 and 2.9.

Clause 8.3.3.6 Vertical load shedding

In order to avoid the localization of differential deformations at the surface of embankment, the recommended embankment height, H is

$$H \geq 0.7\ (s-a) \qquad (2.1)$$

where s is the spacing between adjacent piles, and a is the size of the pile caps.

Greater vertical stress on the pile caps than the surrounding ground due to soil arching can be estimated by applying the Marston's formula (1982) for positive projecting subsurface. The ratio of vertical stress on the pile caps, P'_c to the average of vertical stress at the base of embankment, σ', can be expressed as

$$\frac{P_c'}{\sigma'} = \left[\frac{C_c a}{H}\right]^2 \qquad (2.2)$$

where, C_c is arching coefficient

= 1.95H/a – 0.18 for end-bearing piles (unyielding), or

= 1.5H/a – 0.07 for friction and other piles.

2.4 Arching in soil

Arching action is known as "one of the most universal phenomena encountered in the soils both in the field and in the laboratory" (Terzaghi, 1943). Arching effect plays a significant role for load transfer in soil. Many researchers had investigated this effect previously and many assumptions about arch form, stress state, yielding surface etc were made. Some of them will be reviewed in this section.

2.4.1 Terzaghi's Theory

Terzaghi (1943) defined arching effect as "the transfer of pressure from a yielding mass of soil to adjoining stationary parts". He stated that arching happened either when one part of the soil body yielded while the rest remained stationary or one part of yielding support moved out more than the adjoining parts. The shearing resistance opposed this relative movement and maintained the arching.

The state of stress in the arching zone in horizontal support of a bed of sand is shown in Figures 2.10 (a) and (b). The lowering of the trap-door section ab can produce the local yield. The sand located above the trap-door also moved accordingly. The frictional resistance along the boundaries between the moving and stationary mass of sand will oppose this movement so the total pressure on the yielded zone trip decreases while it increases in the adjoining stationary part. The arching is also described when the lateral support of excavation tilts as shown in Figure 2.10(c). The

shortening in a vertical direction of the sliding wedge caused by the frictional resistance along sliding surface tends to oppose the sliding by reducing the stress on the wedge and increasing the stress of adjoining stationary soil.

2.4.2 Hewlett and Randolph

Hewlett and Randolph (1988) developed the arching effect in granular free draining soil by considering the limiting equilibrium of stresses in a curved region of sand which appears between adjacent pile caps, as shown in Figures 2.11 to 2.13. They stated that these "arches of sand" spread the uniform load from the embankment to the pile caps. Arching above a grid of piles is most relevant to embankment piling. He suggested the form of "sand vault" as a series of domes, where the crown of each dome approximate to a hemisphere with radius equal to half of diagonal spacing of the pile grid. They also noted that the arches would fail either at the crown or at the pile cap first, so the estimation of efficacy of two of those regions will be taken separately and the lower value should be used in design. Result from this theory shows that since the pile cap area ratio is about 10% of the ground surface, the efficacy of pile increase with increasing height of embankment.

2.4.3 Marston's formula for load on subsurface conduits

A positive projecting conduit is a conduit which is installed in the shallow bedding with its top projecting some distance above the natural ground surface and then covered by an embankment. The basic concept of Marston's (1982) theory is that the arch action will modify the load due to the weight of the soil column above a conduit and part of this column weight will transfer to the adjacent side prisms at the

plane of relative movement and the load on pipe conduit will not equal to the column weight. He also stated that the load transfer direction due to arching is the same as the relative movement direction as shown in Figures 2.14 and 2.15. The magnitudes and the direction of the relative movements between the interior prism and the adjacent prisms are influenced by the settlement of certain elements of the conduit and the adjacent soil. The settlement ratio is defined as:

$$r_{sd} = \frac{(s_m + s_g) - (s_f + d_c)}{s_m}$$

where r_{sd} = settlement ratio,

s_m = compression strain of side columns of soil of height pB_c

s_g = settlement of natural ground surface adjacent to the conduit

s_f = settlement of conduit into its foundation

d_c = shortening of vertical height of conduit.

If the settlement ratio is positive, the shear forces' direction on the interior prism is downward and resultant load on the structure is greater than the weight of the prism of soil directly above it. It means that some part of vertical pressure in the exterior prisms is transferred to the interior prism by shear force. On the contrary, if the settlement ratio is negative, the shear forces' direction on the interior prism are upward and resultant load on the structure is smaller than the weight of the prism of soil directly above it, it means that part of vertical pressure in the interior prisms is transferred to the exterior prism by shear forces.

He also defined the horizontal plane through the top of conduit as the critical plane as the plane of no relative movement between the exterior and interior prisms that is the plane of equal settlement. When the embankment is sufficiently high, the shear force transfer because of the relative movement will stop at some plane below the top of the embankment.

2.4.4 Arching in pile embankment

Arching effects on load transfer in the embankment fill on soft ground supported by pile with cap beam and geotextile has been investigated by Low et al (1991) using both model tests and theoretical formulations. In their model tests, the cap beam was replaced by sand on soft ground as shown in Figure 2.16. The load on both cap beam and soft ground were recorded and compared with theoretical analysis based on equilibrium of semi-cylindrical sand arches. The arch is considered to occur everywhere if the vertical stress of the soft ground is less than γ (unit weight) times H (thickness of fill). Following the Hewlett and Randolph's (1988) definition of the proportion of embankment weight carried by the pile:

Efficacy = $\frac{P_L}{A\gamma H} \times 100\%$.

Two more terms were defined to determine the degree of arching in sand fill:

Competency = $\frac{P_L}{a\gamma H}$

Stress-reduction ratio = $\frac{S_L}{(A-a)\gamma H}$

where P_L =load on cap beam; A= tributary area of one cap beam; a = area of one cap beam; γ= unit weight of the sand fill; H = thickness of the sand above the cap beam; and S_L = total load on the soft-ground area (A-a).

Results from their model tests showed that: (Figure 2.17) the efficacy increases with increasing cap beam area ratio. Competency increases with increasing cap beam spacing and likely to approach a limit value at large spacing. Stress reduction ratio decreases with increasing ratio of H/s' (s' is the clear spacing between pile cap beams). The comparison between their model test result and formulation showed reasonably good agreement. However, some discrepancies at small H/s' ratio can be found.

2.5 Pile raft Foundation

In case the shallow raft foundation can provide enough bearing capacity but the average settlement and differential settlement is excessive, piles may be introduced in order to limit settlements, according to Randolph (1994). From this feature, pile raft seems to be potentially useful for oil tank foundation.

Traditionally the pile will be designed taking all the load from the super structure and the pile group capacity is considered as the sum of all individual piles. However, the behaviour of pile in a pile group and the effective stress state in soil are quite different compared to the behaviour of a single pile. Thus it is unnecessary and uneconomical to design piles as taking the entire load and neglect the contribution of raft merely because of lack of confidence in the ability to predict the foundation deformation accurately. Figure 2.18 shows the contact pressure distributions underneath a rigid raft and a flexible raft. In order to reduce the differential settlement without necessarily reducing the average settlement significantly, a small pile group could be installed in the central region of a flexible raft. A small pile group in the central region of flexible raft can be used as design for an economic oil tank foundation.

2.6 Summary

Literature review on some aspects of oil tanks foundation reveals that the design method for such oil tank foundation can be further developed. Two factors which are most concerned to engineering are differential settlement and shape of settlement dish. To achieve the uniform base settlement is objective of a good tank foundation design. Oil tank foundation can be classified into two types which are shallow foundation and

deep foundation.

Using pile foundation to support oil tanks can be effective. However, the choice of either pile raft or pile group with a thin granular pad are very important, and then the parameters which should be used to have the most effective pile foundation system also need to be considered. However, these factors have not been investigated in detail by early researchers.

Although considerable research studies have been carried out on the load distribution and arching effect of piled embankment, relatively few studies have been carried out to investigate the performance of oil tank foundation. At present, there is generally no accepted method or criteria to design oil tank supported by either pile group or pile raft. A tank with pile group can be used to enhance the stability and reduce the settlement as well as the differential settlement. However, the thickness of the granular pad, the number of piles, the pile configuration and their load distribution to achieve the most effective foundation system is still in question. Non-uniform soil layer are commonly found in reality especially for very large tanks, but it is not easy to predict the performance of the foundation system in this kind of soil layer by any methods which were discussed in this chapter.

From the above, this research will focus on developing a design procedure in which many parameters of the pile foundation system are taken into consideration. It is hoped that this procedure can be used as a guide for the design engineers to build cost-effective pile foundation system for oil tanks.

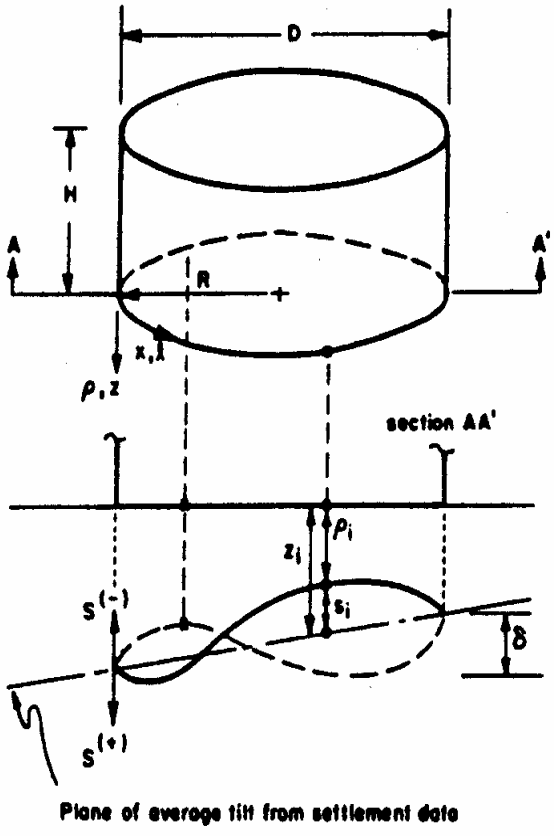

DEFINITIONS:

1. ρ_i = total measured settlement at point i with settlement measured as change in elevation of the point since end of construction of tank
2. $\Delta\rho_{i,j}$ = difference in measured settlement between points i and j
3. $\ell_{i,j}$ = circumferential distance between measurement points i and j
4. $(\Delta\rho/\ell)_{i,j}$ = angular distortion between points i and j
5. δ = difference in settlement between diametrical points
6. Z_i = component of settlement of point i due to planar tilt
7. S_i = component of settlement of point i due to out-of-plane distortions
8. $\Delta S = S_i - 0.5(S_{i+1} + S_{i-1})$
9. SAG = ΔS_{max} for quarter points
   $= \left[S_i - 0.5(S_{i+n/4} + S_{i-n/4})\right]_{max}$
10. n = number of measurement points

Figure 2.1 Settlement pattern for tank (after Marr et al., 1982)

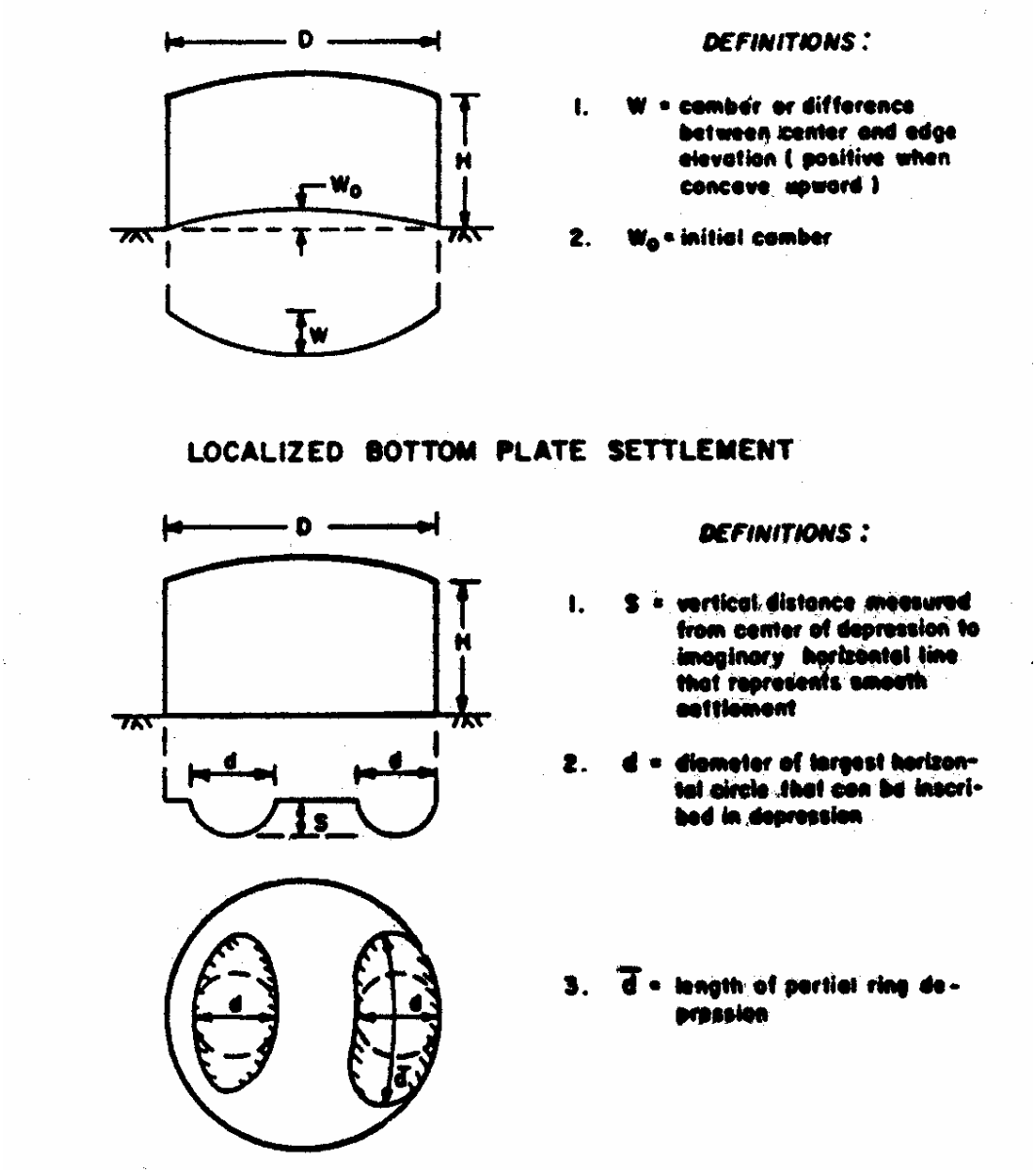

Figure 2.2 Non-planar settlement pattern of tank foundation (after Marr et al., 1982)

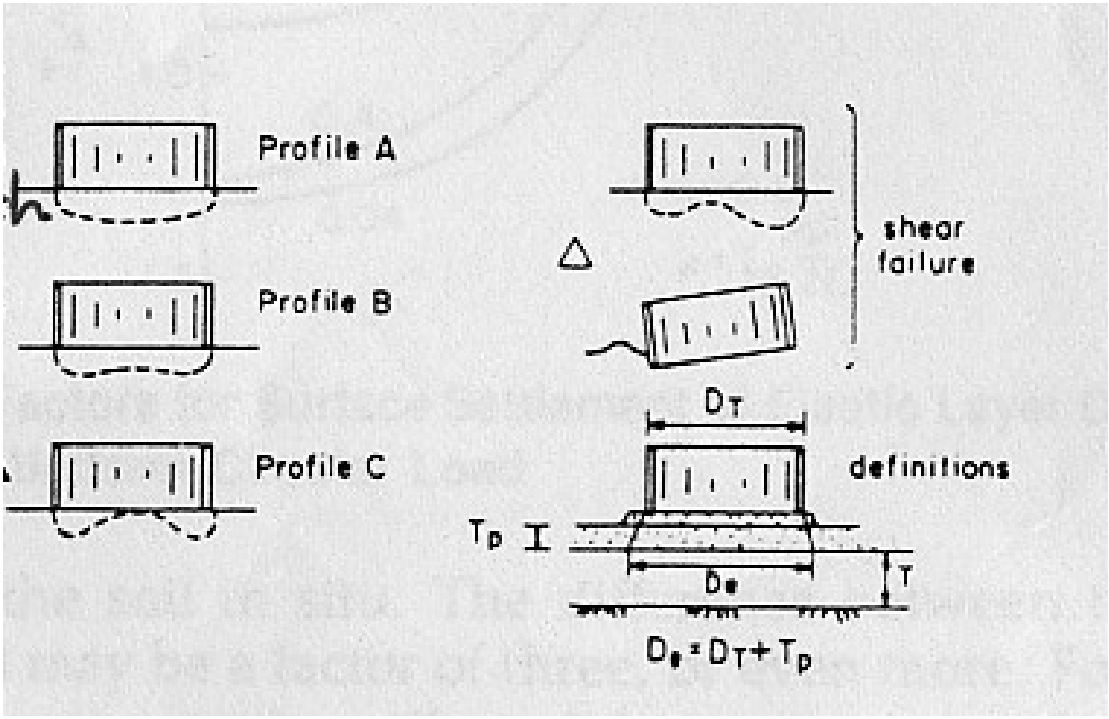

Figure 2.3 Settlement shape for Tank Studied. (after Duncan and D'Orazio, 1987)

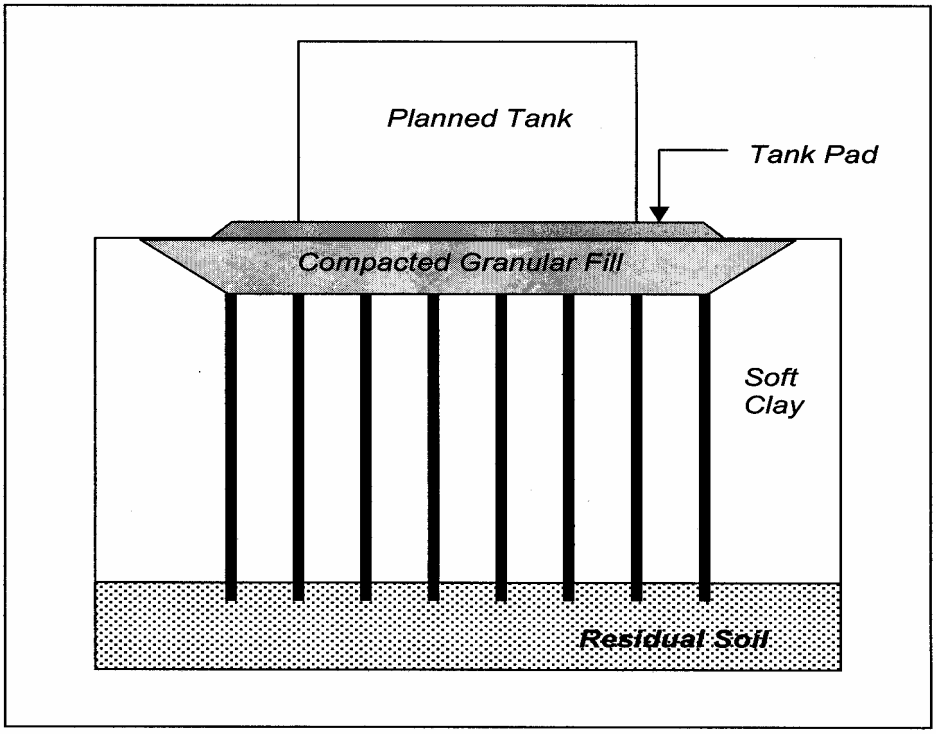

Figure 2.4 Proposed soil-pile composite system by Khoo (2001)

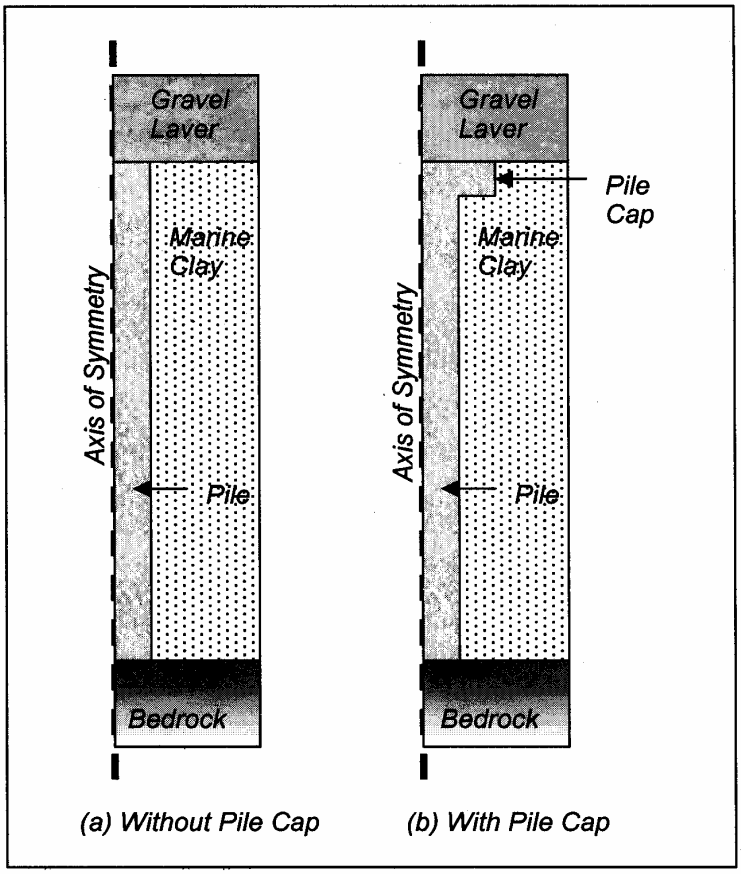

Figure 2.5 Numerical model for pile without cap and with cap (after Khoo, 2001)

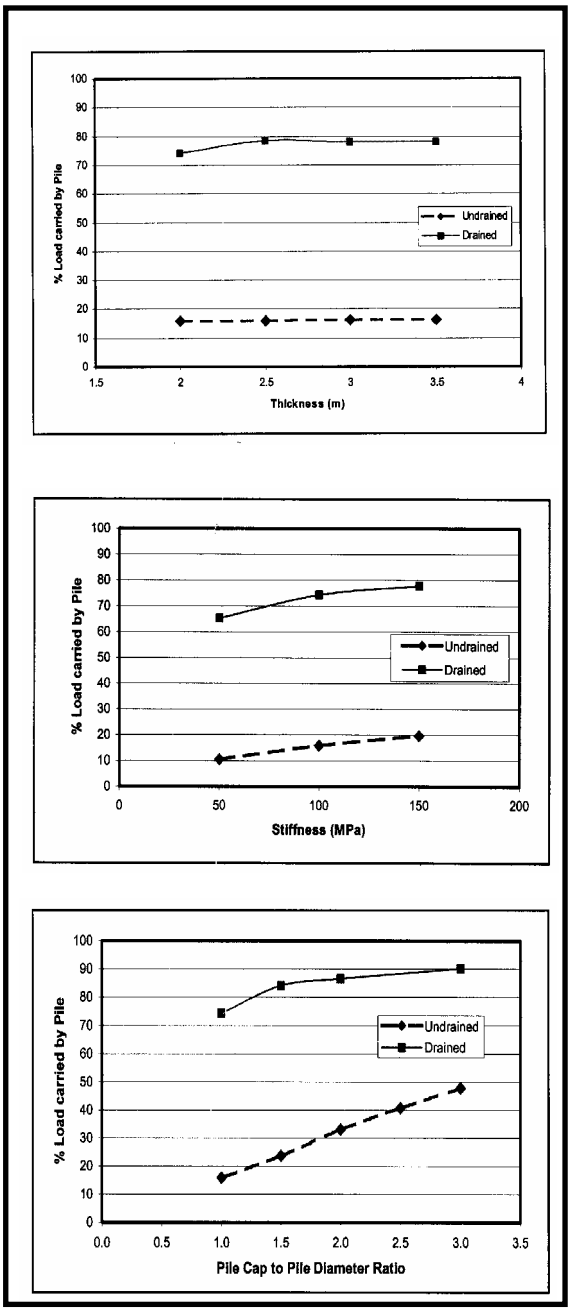

(a) Mohr-Coulomb Model Results

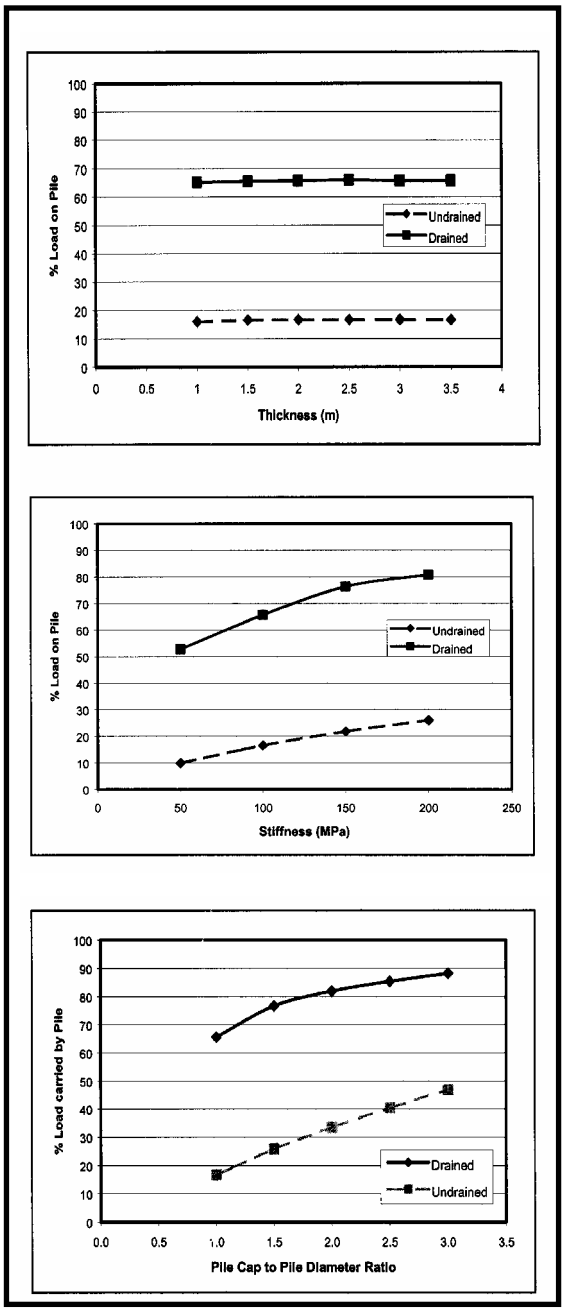

(a) Linear-Elastic Model Results

Figure 2.6 Results of percentage load on piles (after Khoo, 2001)

Figure 2.7 Experimental setup of piled embankments (after Tung, 1994)

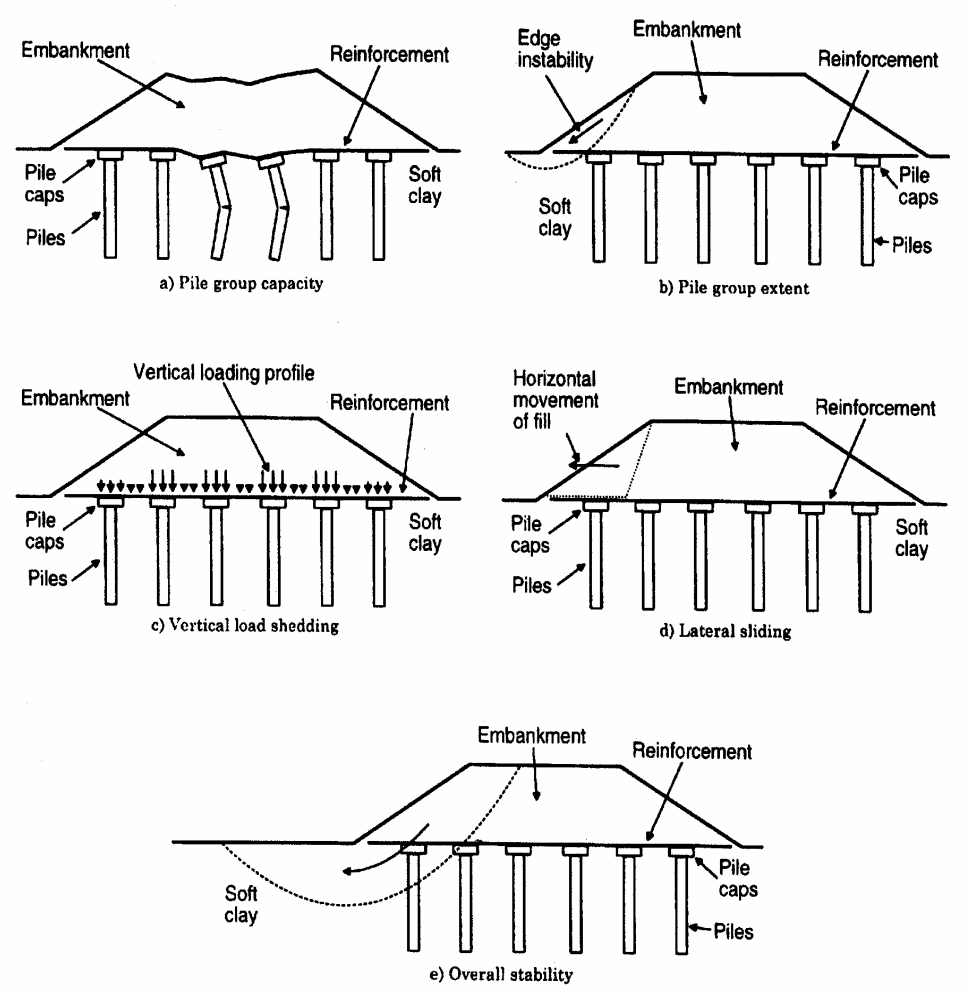

Figure 2.8 Ultimate limit state for basal reinforced piled embankment (after BS 8006, 1995)

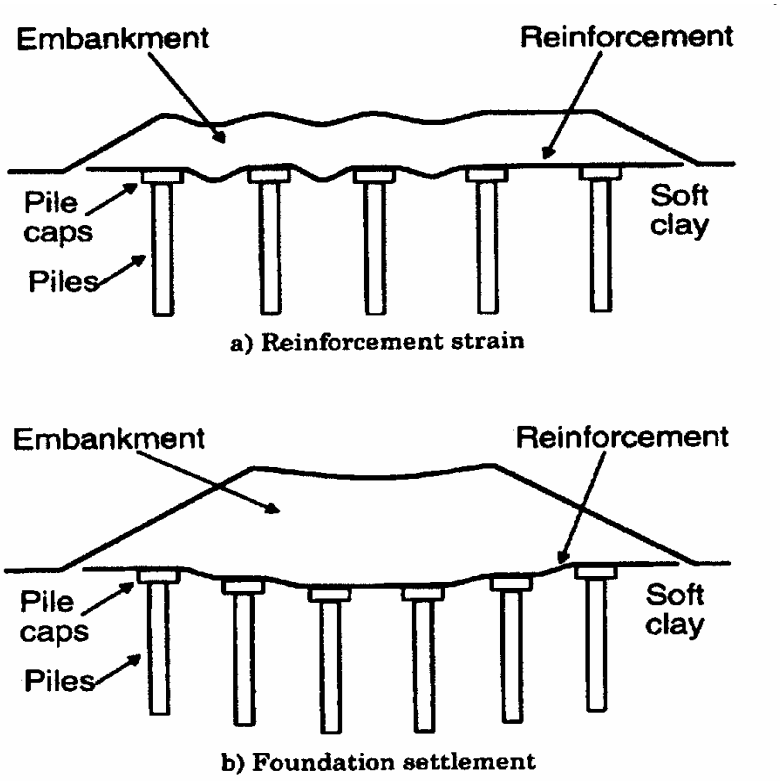

Figure 2.9 Serviceability limit state for basal reinforced piled embankment (after BS 8006, 1995)

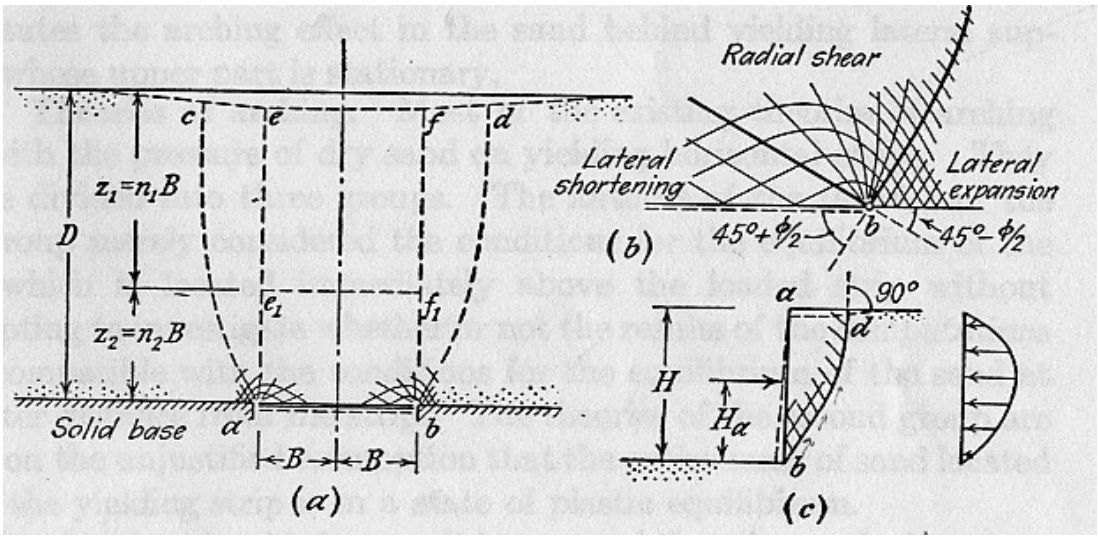

Figure 2.10 Failure in cohesionless sand preceded by arching. (a) Failure caused by downward movement of a long narrow section of the base of a layer of sand; (b) enlarged detail of diagram (a); (c) shear failure in sand due to yield of lateral support by tilting about its upper edge (after Terzaghi, 1945 and Terzaghi and Peck, 1976).

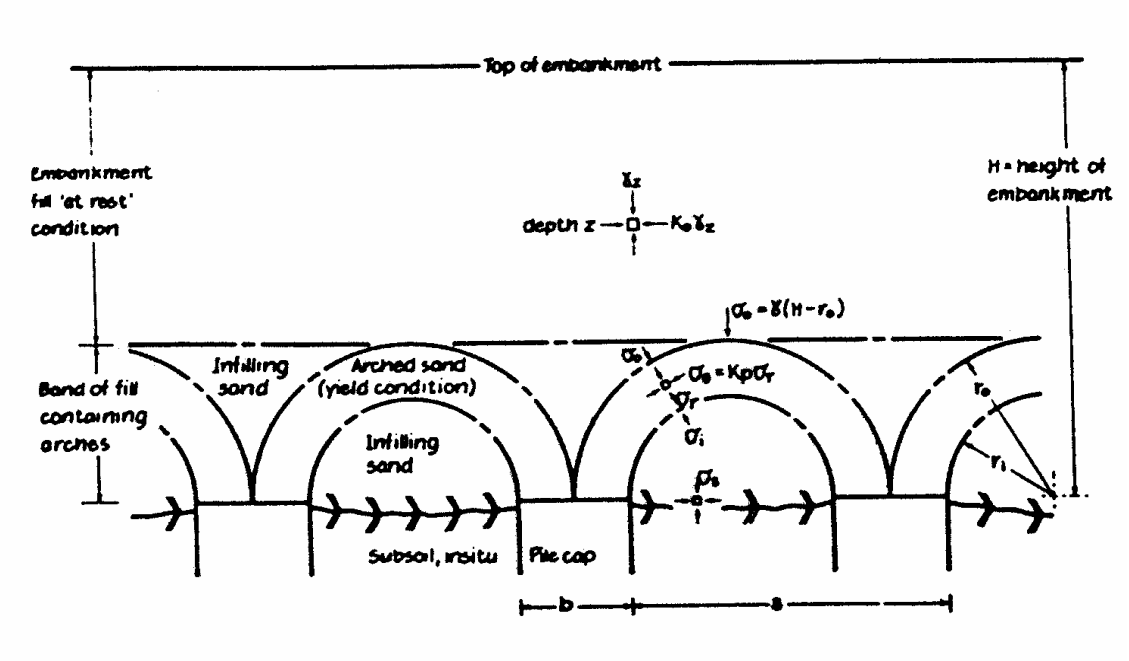

Figure 2.11 Section through a piled embankment (after Hewlett and Randolph, 1988)

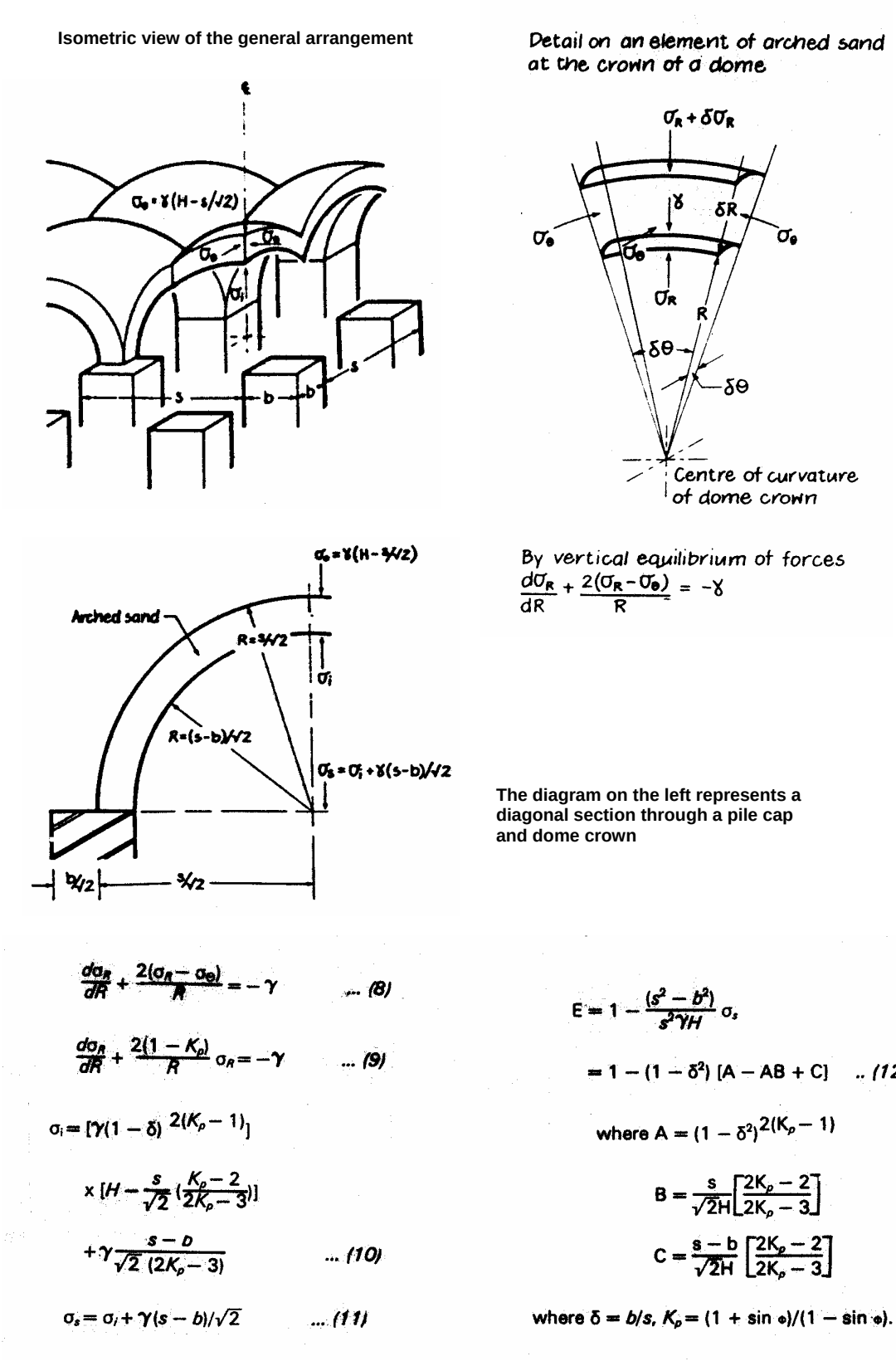

Figure 2.12 Domed analysis of crown stability in piled embankment (after Hewlett and Randolph, 1988)

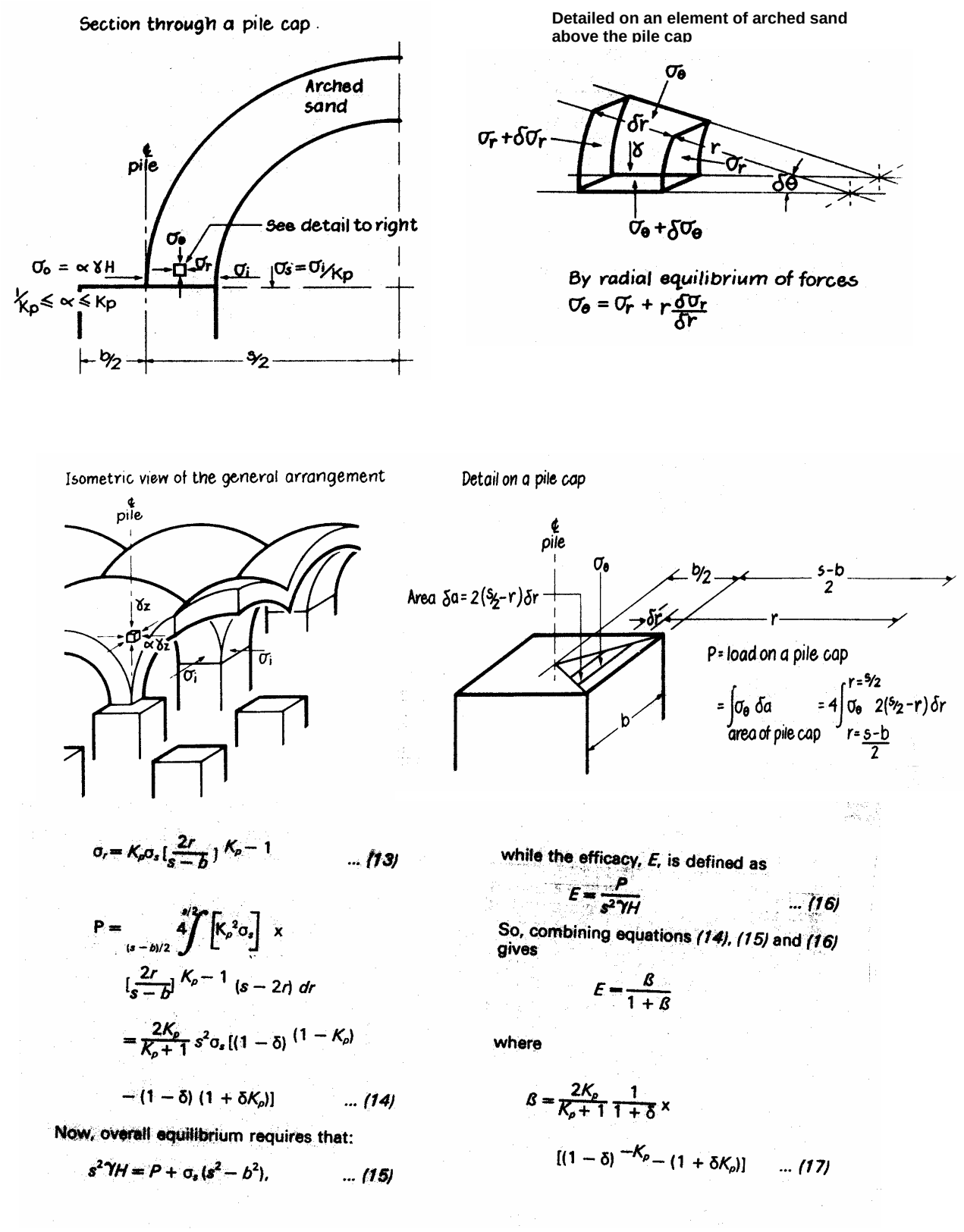

Figure 2.13 Domed analysis of cap stability in piled embankment (after Hewlett and Randolph, 1988)

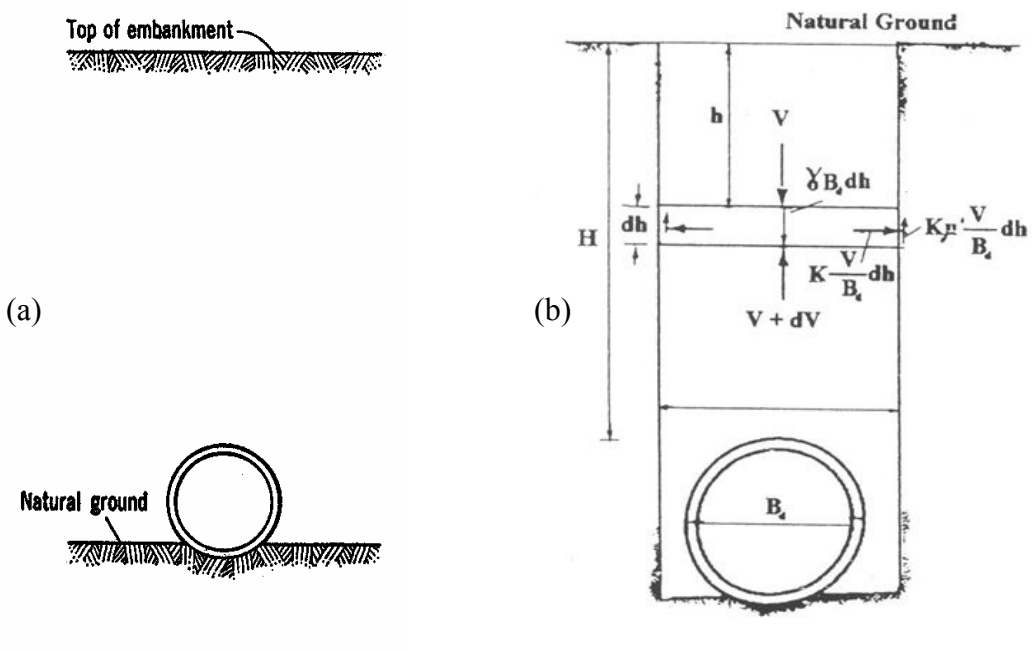

Figure 2.14(a) Positive Projecting Conduit, (b) Free body diagram for Ditch Conduit (after Spangler, 1982)

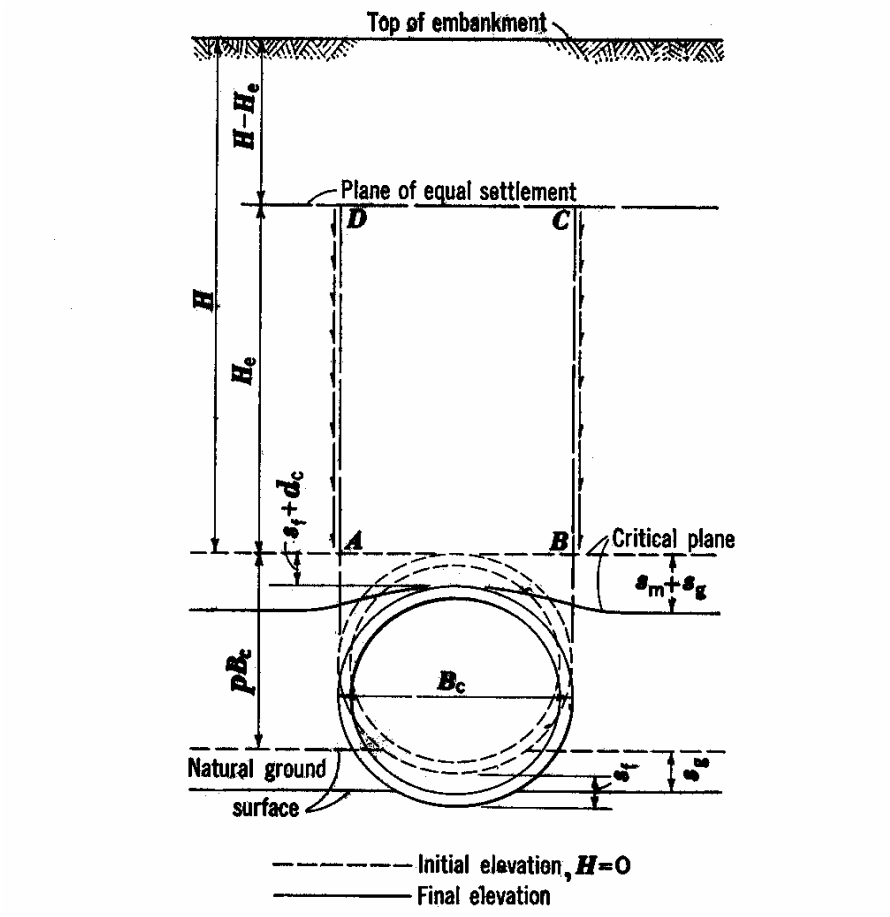

Figure 2.15 Settlements that influence loads on positive projecting conduits (after Spangler, 1982)

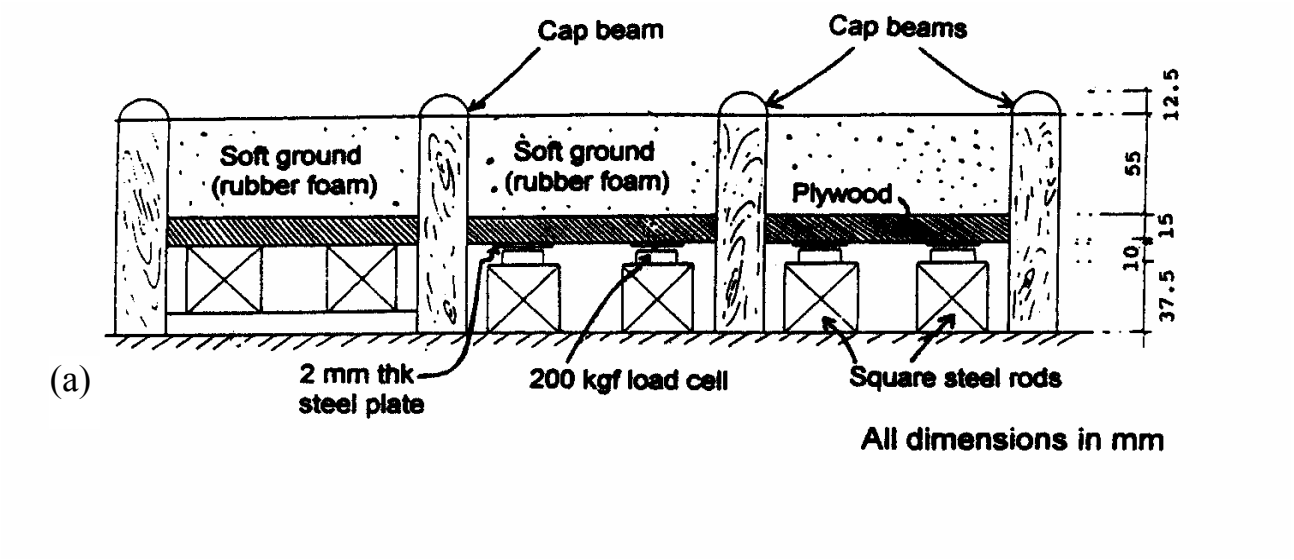

(a)

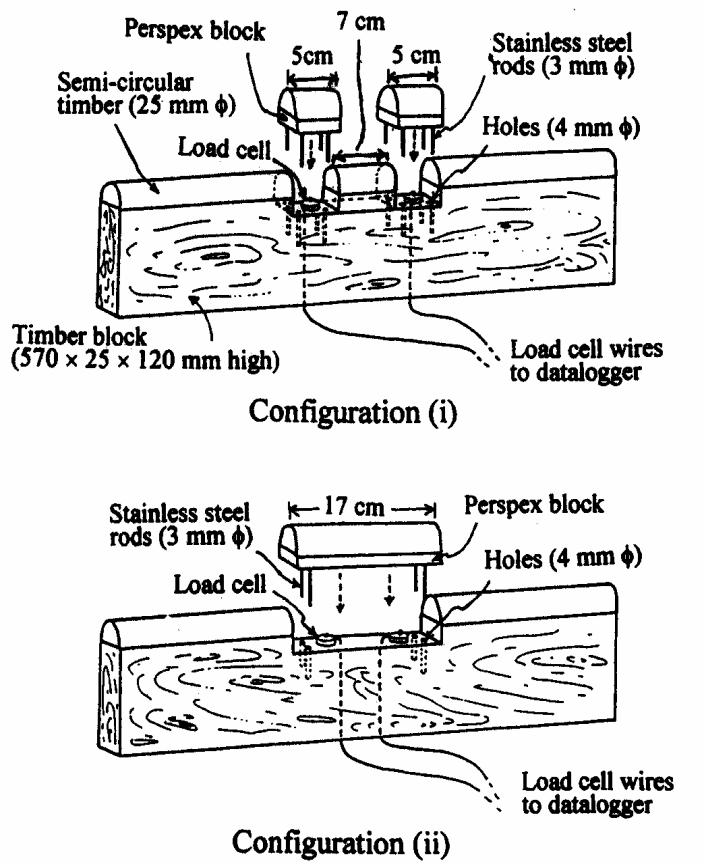

(b)

Figure 2.16 Model study by Low (a) Cross section of model soft ground and cap beams (b) Details of model cap beams (after Low et al., 1991)

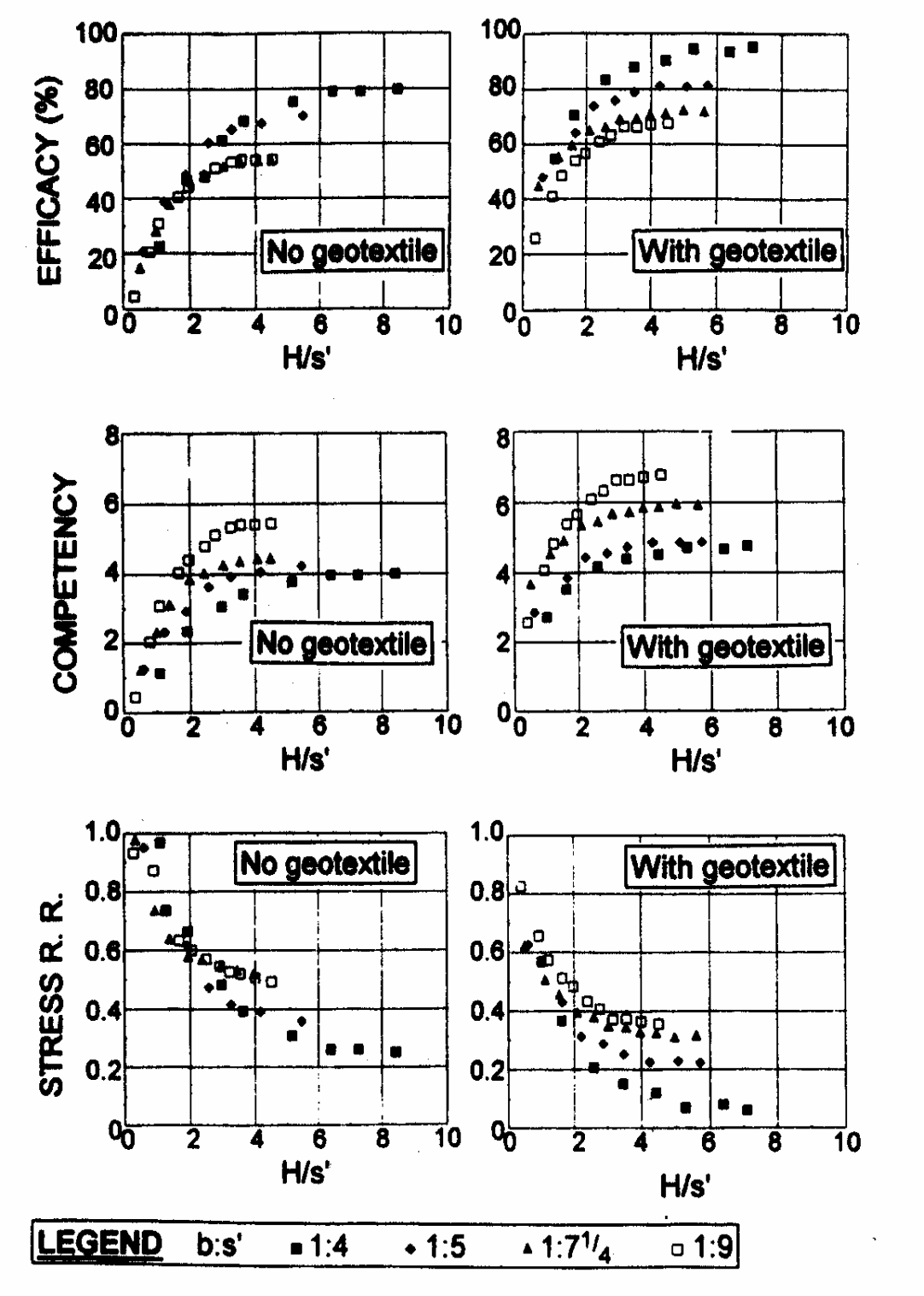

Figure 2.17 Results of model tests (after Low et al., 1991)

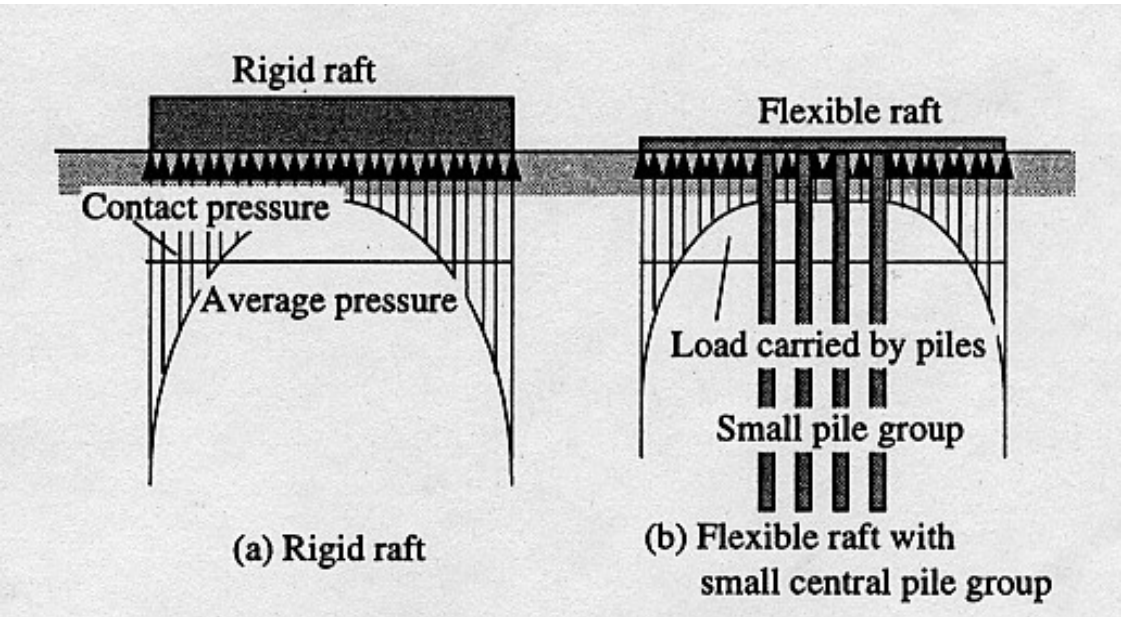

Figure 2.18 Concept of settlement reducing piles (after Randolph, 1998)

CHAPTER 3

THE INTRODUCTION OF PLAXIS AND VALIDATION

3.1 The introduction of Plaxis 2D and 3D

3.1.1 General

PLAXIS v8 and PLAXIS 3D Foundation are two finite element codes used for the numerical simulation of single pile and pile groups in this thesis.

PLAXIS 3D Foundation is the latest member of PLAXIS, which is a special purpose 3D finite element computer program used to perform deformation and stress state analyses for various types of 3D foundations in soil and rock.

3.1.2 Model

Two typical plane models are available in PLAXIS v8, plain strain model and axi-symmetry model. To analyze the problem of a single pile supporting vertical load, the axi-symmetric model which results in a 2D finite element model with only two translational degrees of freedom at each node (i.e. x- and y- direction), should be selected.

The generation of a 3D finite element model begins with the creation of geometry model. A geometry model is a composition of bore holes and horizontal work planes (xz planes). The work planes are used to define geometry lines and structures. The bore holes are used to define the local soil stratigraphy, ground surface level and pore pressure distribution.

It is recommended to start the creation of a geometry model by defining all the necessary work planes. Work planes should not only include the initial situation, but also situations that arise in the various calculation phases.

PLAXIS 3D Foundation has various special elements to model all kinds of structures, such as beam, floor, and wall elements. However, no special type of element is applied to model the pile. Representing the pile with 3D solid element limits the numbers of the piles that can be modeled due to the memory capacity of the PC.

3.1.3 Elements

In PLAXIS 8, 6-node or 15-node triangular elements are available. Six-node triangle element provides a second order interpolation for displacements. The element stiffness matrix is evaluated by numerical integration using three Gauss points. For the 15-node triangle, the order of interpolation is four and numerical integration involves twelve Gauss points.

In PLAXIS 3D Foundation, the basic soil elements of a 3D finite element mesh are the 15-node wedge elements, see Figure 3.1. These elements are generated from the 6-node triangular elements as generated in the 2D mesh. Higher order element types, for example comparable with the 15-node triangle in a 2D analysis, are not available for a 3D Foundation analysis because this will lead to large memory consumption and unacceptable long calculation times.

In addition to the soil elements, special types of elements are used to model structural behavior. For beams, 3-node line elements are used, which are compatible with the 3-noded sides of a soil element. In addition, 6-node and 8-node plate elements are used to simulate the behavior of walls and floors. Moreover, 12-node and 16-node

interface plane elements are used to simulate soil slip for soil-structure interaction problems.

3.1.4 Interfaces

Guidelines for the use of advanced numerical analysis stated that when analyzing a pile, either thin solid element or special interface elements should be placed adjacent to the pile shaft. If insufficiently thin solid elements are used, the pile/soil slip will be too stiff and the pile shaft capacity will be overestimated.

Interfaces are used when modeling soil structure interaction both in Plaxis 2D and 3D. Interfaces will be required to simulate the finite frictional resistance between the stiff structure such as pile and softer adjacent soil. It allows relative displacement slip and separation between the structure and soil mass.

When using 6-node elements for soil, the corresponding interface elements are defined by three pairs of nodes, whereas for 15-node soil elements, the corresponding interface elements are defined by five pairs of nodes.

The basic property of an interface element is the associated material data set for soil and interfaces. The roughness of the interaction is modeled by choosing a suitable value for the strength reduction factor in the interface (R_{inter}). An elasto-plastic model is used to describe the behavior of interfaces for the modeling of soil-structure interaction. The Mohr-Coulomb criterion is used to distinguish between elastic behavior, when small displacements can occur within the interface, and plastic interface behavior when permanent slip may occur.

For the interface to remain elastic the shear stress τ is given by:

$$|\tau| < \sigma_n \tan \varphi_i + c_i \qquad (3.1)$$

and for plastic behavior τ is given by:

$$|\tau| = \sigma_n \tan \varphi_i + c_i \tag{3.2}$$

where φ_i and c_i are the friction angle and cohesion (adhesion) of the interface respectively, and σ_n is the normal stress of the soil. The interface properties are calculated from the soil properties in the associated data set and the strength reduction factor by applying the following rules:

$$c_i (= R_{inter} c_{soil}) \leq c_{soil} \tag{3.3}$$

$$\tan \varphi_i (= R_{inter} \tan \varphi_{soil}) \leq \tan \varphi_{soil} \tag{3.4}$$

In addition to Coulomb's shear stress criterion, the tension cut-off criterion, as described before, also applies to interfaces (if not deactivated):

$$\sigma_n < \sigma_{t,i} = R_{inter} \sigma_{t,soil}$$

where $\sigma_{t,soil}$ is the tensile strength of the soil.

3.1.5 Material models

Linear Elastic Model

Two elastic stiffness parameters, Young's modulus, E, and Poisson's ratio, ν, are used. This model is the simplest material model in Plaxis which employs Hooke's law of isotropic linear elasticity. The linear elastic model is seldom used to simulate soil behavior. It is primarily used for stiff structural systems installed in the soil, such as the piles, floor etc in this thesis.

Mohr-Coulomb Model

The elastic perfectly-plastic Mohr-Coulomb model (Figure 3.2) is most widely used as the first approximation of soil behavior. Five parameters describing this model

are Young's modulus, E', and Poisson's ratio ν' for soil elasticity; cohesion, c', internal friction angle, ø' for soil plasticity, and dilatancy angle, ψ'. Plasticity is associated with the development of irreversible strains. A yield function, f, is introduced as a function of stress and strain in order to evaluate whether or not plasticity occurs in a calculation. A yield function is often presented as a surface in principal stress space.

Mohr-Coulomb yield condition consists of six yield functions representing six stress planes when formulated in terms of principal stresses:

$$f_{1a,b} = \frac{1}{2}\left|\sigma_2' - \sigma_3'\right| + \frac{1}{2}\left(\sigma_2' + \sigma_3'\right)\sin\varphi - c\cos\varphi \le 0 \qquad (3.5)$$

$$f_{2a,b} = \frac{1}{2}\left|\sigma_3' - \sigma_1'\right| + \frac{1}{2}\left(\sigma_3' + \sigma_1'\right)\sin\varphi - c\cos\varphi \le 0 \qquad (3.6)$$

$$f_{3a,b} = \frac{1}{2}\left|\sigma_1' - \sigma_2'\right| + \frac{1}{2}\left(\sigma_1' + \sigma_2'\right)\sin\varphi - c\cos\varphi \le 0 \qquad (3.7)$$

It can be seen that the yield surface fixed and defined by two plastic model parameters (φ and c) and is not affected by plastic straining. Six yields functions together represent a hexagonal cone in principal stress space as shown in Figure 3.3. For stress states represented by points within the yield surface, the behavior is purely elastic and obeys Hooke's law for isotropic linear elasticity with all strains reversible. The standard Mohr-Coulomb criterion allows for tension with apparent cohesion c>0.

The advanced parameters of the Mohr-Coulomb (M-C) model allow accounting for the increase of stiffness and cohesive strength with depth and the use of a tension cut-off. However, during calculations, a stiffness increasing with depth does not change as a function of the stress state.

Hardening Soil Model

The Hardening-Soil model is an advanced model developed by Schanz and

Vermeer (1998) for simulating the behavior of different types of soil, both soft soils and stiff soils. In contrast to the Mohr-Coulomb model, the yield surface of a hardening plasticity model is not fixed in principal stress space, but it can be expanded due to plastic straining. Two main types of hardening are contained in the present model namely shearing hardening and compression hardening. Shearing hardening is used to model irreversible strains due to primary deviatoric loading. Compression hardening is used to model irreversible plastic strains due to primary compression in oedometer loading and isotropic loading

The observed relationship between the axial strain and the deviatoric stress can be well approximated by a hyperbola in the special case of a drained triaxial test. Such a relationship was first formulated by Kondner (1963) and later used in the well-known hyperbolic model (Duncan & Chang, 1970). The general three-dimensional extension and implementation in PLAXIS dated back and Brinkgreve (1994).

Compared to the elastic hyperbolic model, the Hardening-Soil model has the following advantages: firstly, it employs the theory of plasticity rather than the theory of elasticity; secondly, it includes soil dilatancy and thirdly, it has a yield cap for compression loading.

As for the Mohr-Coulomb model, limiting states of stress are described by means of cohesion, c, internal friction angle, φ, and dilatancy angle, ψ. The soil stiffness however is described much more accurately by using three different input stiffnesses: the triaxial loading stiffness, E_{50}, the triaxial unloading/reloading stiffness, Eur, and the oedometer loading stiffness, E_{oed}.

The basic feature of the Hardening-Soil model is the stress-dependency of stiffness according to a power law represented by a power of exponent stress-level dependency of stiffness, m. Hence, all three stiffnesses relate to a reference stress,

usually taken as P^{ref}=100kPa.

A basic idea for the formulation of the Hardening-Soil model is the hyperbolic relationship between the vertical strain, ε_1 and the deviatoric stress, q, in primary triaxial loading. Standard drained triaxial tests tend to yield curves that can be described by:

$$-\varepsilon_1 = \frac{1}{2E_{50}} \frac{q}{1 - q/q_a} \qquad \text{For: } q < q_f \tag{3.8}$$

Where q_a is the asymptotic value of the shear strength. This relationship is plotted in Figure 3.4. The parameter E_{50} is the confining stress dependent stiffness modulus for primary loading and is given by:

$$E_{50} = E_{50}^{ref} \left(\frac{c\cos\varphi - \sigma_3^{'} \sin\varphi}{c\cos\varphi + p^{ref} \sin\varphi} \right)^m \tag{3.9}$$

where E_{50}^{ref} is a reference stiffness modulus corresponding to the reference confining pressure p^{ref}. In PLAXIS, a default setting p^{ref}=100 stress units is used, with reference to the confining stress σ_3'. The actual stiffness depends on the minor principal stress, σ_3', which is the confining pressure in a triaxial test and negative for compression. The amount of stress dependency is given by the power m, which varies in the range 0.5<m<1.0 (Von Soos, 1980), depending on soil type.

The ultimate deviatoric stress, q_f and the quantity q_a are defined as:

$$q_f = (c\cot\varphi - \sigma_3^{'}) \frac{2\sin\varphi}{1 - \sin\varphi} \quad \text{and: } q_a = \frac{q_f}{R_f} \tag{3.10}$$

The above relationship for q_f is derived from the Mohr-Coulomb failure criterion, which involves the strength parameters c and φ. As soon as $q=q_f$, the failure criterion is satisfied and perfectly plastic yielding occurs as described by the Mohr-Coulomb model. R_f is the failure ratio, defined as the ratio between q_f and q_a, to limit the failure

stress to some value smaller than the asymptote of the hyperbolic relation.

For unloading and reloading stress paths, another stress-dependent stiffness modulus is used:

$$E_{ur} = E_{ur}^{ref}\left(\frac{c\cos\varphi - \sigma_3^{'}\sin\varphi}{c\cos\varphi + p^{ref}\sin\varphi}\right)^{m} \tag{3.11}$$

where E_{ur}^{ref} is the reference Young's modulus for unloading and reloading, corresponding to the reference pressure p^{ref} of σ_3'=100 kPa. In many practical cases it is appropriate to set E_{ur}^{ref} equal to 3 E_{50}^{ref}, which is approximately correct.

In contrast to elasticity based models, the elastoplastic Hardening-Soil model does not involve a fixed relationship between the (drained) triaxial stiffness E_{50} and the oedometer stiffness E_{oed} for one dimensional compression. Instead, these stiffness can be input independently. The oedometer loading stiffness is defined as:

$$E_{oed} = E_{oed}^{ref}\left(\frac{c\cos\varphi - \sigma_1^{'}}{c\cos\varphi + p^{ref}}\right)^{m} \tag{3.12}$$

It can be seen from the formula that E_{oed}^{ref} is the tangent stiffness at a vertical stress of $-\sigma_1^{'} = p^{ref}$ =100 kPa, as shown in Figure 3.5.

In addition to all the parameters described above, the advanced parameter of the Hardening-Soil model includes:

E_{ur}^{ref} : Unloading/reloading stiffness at p^{ref} (default E_{ur}^{ref} =3 E_{50}^{ref}) (*)

v_{ur}: Poisson's ratio for unloading-reloading (default v_{ur}=0.2)

p^{ref}: Reference stress for stiffness determination (default p^{ref}=100 stress unit)

K_0^{nc} : Ko-value for normal consolidation (default K_0^{nc} =1-sinφ)

R_f: Failure ratio q_f/q_a (default R_f=0.9)

$\sigma_{tension}$: Tensile strength for tension cut off (default $\sigma_{tension}$=0 stress unit)

$c_{increment}$: As in Mohr-Coulomb model (default $c_{increment}$=0)

(*) denoted that parameter is available in basic parameter in Plaxis v8.

3.1.6 Undrained Analysis and Drained Analysis

Drained behavior

This setting is used for the case of dry soils and also for full drainage due to a high permeability (sands) and/or a very slow rate of loading in less permeable soils. This setting may also be used to simulate long-term soil behavior without the need to model the precise history of undrained loading and consolidation. Using this setting no excess pore pressures are generated.

Undrained behavior

This setting is used for a full development of excess pore pressures. Flow of pore water can sometimes be neglected due to a low permeability (clays) and/or a relatively fast rate of loading in higher permeability soils.

3.1.7 Mesh Properties

PLAXIS allows for a fully automatic generation of finite element mesh. The generation of the mesh is based on a robust triangulation procedure, which results in "unstructured" meshes.

The mesh generator requires a general meshing parameter which represents the average element size, l_e, computed based on the outer geometry dimensions (x_{min}, x_{max}, y_{min}, y_{max}) using the following relationship:

$$l_e = \sqrt{\frac{(x_{max} - x_{min})(y_{max} - y_{min})}{n_c}} \tag{3.13}$$

where n_c = 25 (very coarse mesh)

= 50 (coarse mesh)

= 100 (medium mesh)

= 200 (fine mesh)

= 400 (very fine mesh)

In PLAXIS 3D Foundation, the 3D mesh is based on a system of 2D mesh in plane view with the work planes and the soil layer boundaries as defined by the bore holes. These planes can be either horizontal or pseudo-horizontal. The horizontal planes are formed by either work plane or the boundaries of the uniform soil layer. On the other hand, the pseudo-horizontal planes are formed by the boundaries of non-uniform soil layer when using multiple bore holes. The analysis takes very much more time as compared to 2D analysis. Thus 2D meshes in the PLAXIS 3D FOUNDATION program will generally be coarser than meshes in 2D PLAXIS simulations. To create a more efficient and refined 3D finite element mesh, care should be taken to avoid creating very small or oddly shaped soil elements. If this is the case, the number of bore holes, the bore hole positions or the soil layer boundaries in the bore holes should be adjusted until a satisfactory workable 3D mesh is obtained.

3.1.8 Staged construction

PLAXIS allows for the option to change the geometrical configurations by activating and deactivating clusters or structural objects. It is convenient to simulate the installation of pile as a new material wish-in-place. No pile installation effect is simulated. The program allows for a realistic simulation of the actual construction stages such as the loading changes of the reaction system during the process of pile

loading and unloading. The material properties and pore pressure distribution can also be changed at each stage of analysis.

3.1.9 Generation of initial stresses

In PLAXIS 2D, the initial stress can be generated by either Ko-procedure or Gravity loading. The Ko-procedure is recommended for use in cases with horizontal surface for all soil layers and phreatic lines parallel to the horizontal ground surface. For all other cases, the gravity loading is recommended, as shown in Figure 3.6.
In contrast to PLAXIS 2D programs, the 3D FOUNDATION program has only one procedure to generate the initial stresses state that is gravity loading.

Gravity loading assumes that $K_o = \frac{\upsilon}{1-\upsilon}$. Therefore for settling up of the desired initial stresses, υ must be chosen to give the expected K_o. This may not be the approximate υ to use in the subsequent stress analyses.

3.2 Single pile analysis using 2D and 3D

The model was set up with a single friction pile in homogeneous soil using both 2D Axi-symmetry and 3D Foundation as shown in Figures 3.7 and 3.8. The results from 2D Axi-symmetry analysis and 3D analysis were compared. To avoid the difference from Ko proceduce due to gravity proceduce in generating initial stresses in 2D and 3D program, the medium sand with E=20 MPa, υ=0.33, c=1, φ=30^o was used in both cases so that the ratio of $\sigma'_{xx} / \sigma'_{yy}$ are the same. A concrete pile of 10m length and 0.564m diameter was simulated with interface element (R_{inter}=1). Six levels of

loading, 250 kN, 300kN, 400kN up to 700kN, were applied in the simulated pile load test.

The results from 2D axi-symmetry and 3D analysis in terms of load settlement curve are shown in Figure 3.9, in terms of load transfer curve are shown in Figure 3.10. It can be seen that both load settlement curve and load tranfer curve from 2D Axisymetry analysis and 3D analysis are slightly different, the difference being larger as the load increases. The 3D analysis gives more settlement and slightly smaller failure load than the 2D analysis. The load transfer curve from the 3D analysis gives more end bearing than 2D analysis, as shown in Figures 3.10. This may be explained as follows. Firstly, the elements used in the two programs are not identical and equivalent. The 15-node wedge element in 3D is not equivalent to the 6-node triangular element in 2D axi-symmetry. In reality, the 15-node wedge element in 3D is more like an 8-node rectangular element in 2D. Secondly, the 2D analysis can have a finer mesh than the 3D analysis so that the 2D analysis can give result more accurately especially at the region of stress concentration or the region of large stiffness changes such as at pile toe.

3.3 Pile raft comparison

In order to compare the predicted behavior of a piled raft from a number of different established methods the hypothetical example in figure 3.11 has been analyzed (after Poulos, 1994). Three cases have been analyzed:

Case A: A raft with 15 piles and a total load of 12MN.

Case B: A raft with 15 piles and a total load of 15MN.

Case C: A raft with 9 piles and a total load of 12MN.

In each case, 7 methods of analysis have been used:

1. Poulos and David (1980).

2. Randolph (1983).

3. Strip on springs approach, using the program GASP (Polous, 1991).

4. Plate on springs approach, using GARP (Poulos, 1994).

5. Finite element method of Ta and Small (1996)

6. Finite element and boundary element of Sinha (1996).

7. Plaxis 3D foundation analysis.

These models have been created in Plasix 3D Foundation as shown in Figures 3.12 and 3.13. Figures 3.14 to 3.18 show the comparison of some predicted key responses which are average settlement, differential settlement, maximum bending moment Mxx and proportion of load carried by piles from 7 above methods for case A to C respectively. It can be seen that the Plaxis 3DF can give predictions of the settlement, bending moments, differential settlement, and proportion of load carried by piles which generally agree well with other established methods.

3.4 Limitations of 3D and 2D analysis

Firstly, only gravity loading proceduce can be used to generate the initial stress. This prevents the simulation of heavily OC soils with Ko > 1. Secondly, the 15-node wedge element, which is used in Plaxis 3D is not as accurate as compared with the triangular element in Plaxis 2D. Thus the Plaxis 3D program simulation of a single pile cannot match exactly the axi-symmetry result. Thirdly, very fine big mesh cannot be used, as computational time will be very large.

On the other hand, 2D analysis cannot apply in pile group problem. The axisymetry leads to the following limitations:

- The axial load on the edge piles will be overestimated and that of center piles will be underestimated.
- The settlement of single pile cannot represent the settlement of pile group.
- The differential settlement can not be estimated.
- The settlement shape can not be investigated in 2D.

Despite the limitations of 3D Plaxis program, using it to simulate the oil tank foundation problem is still better than 2D. The Plaxis 3D programs do give a realistic simulation of pile response in a Mohr-Colomb soil continuum. In addition, the result from pile raft comparison show good agreement with other established methods. The 3D Foundation program is used to study the centrifuge model simulation of an oil tank pile foundation and extend its results to general oil tank on piles foundation.

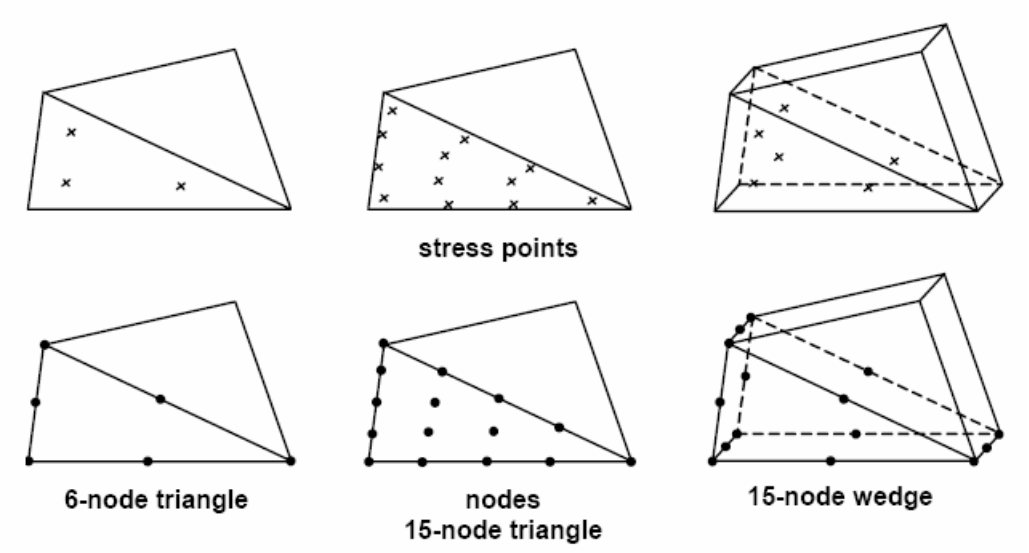

Figure 3.1 Comparison of 2D and 3D soil elements.

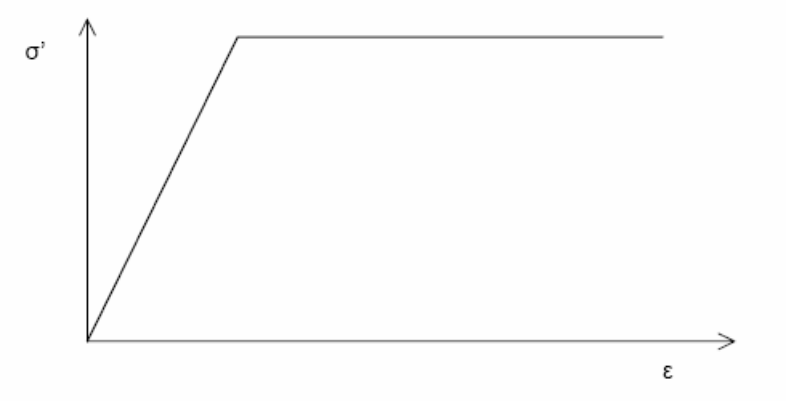

Figure 3.2 Basic ideal of an elastic perfectly plastic model.

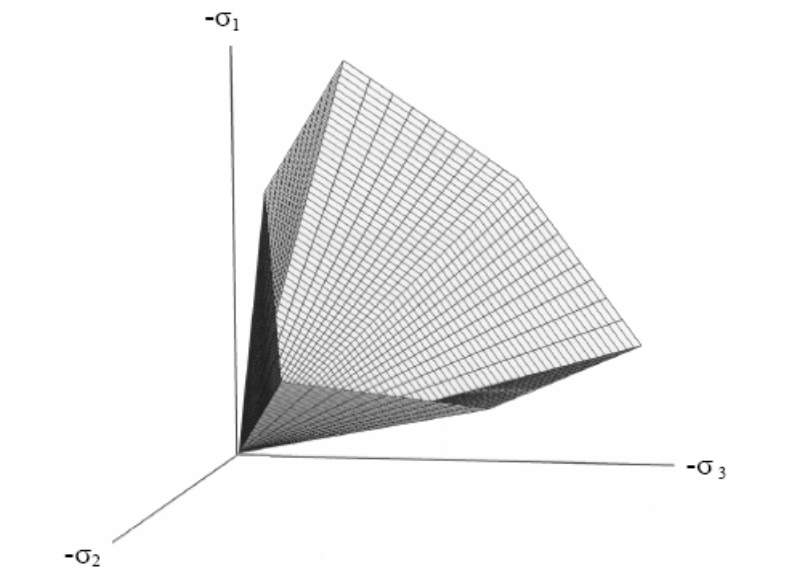

Figure 3.3 The Mohr-Coulomb yield surface in principal stress space (c=0)

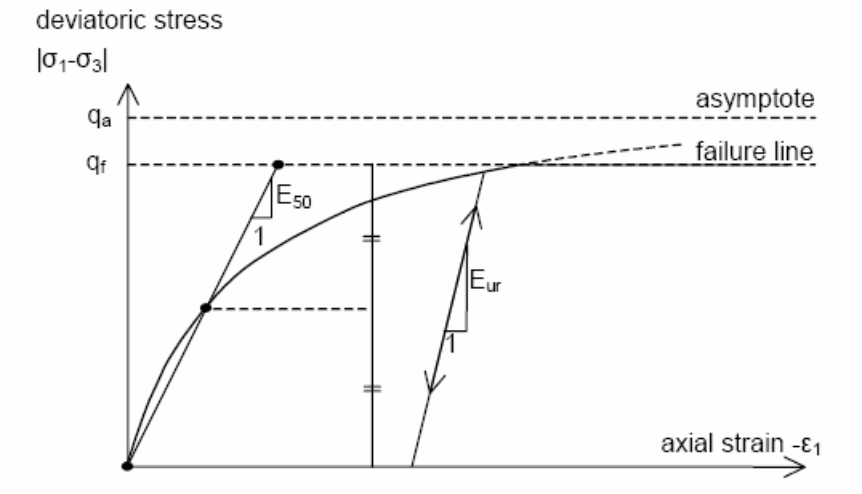

Figure 3.4 Hyperbolic stress-strain relation in primary loading for a standard drained triaxial test.

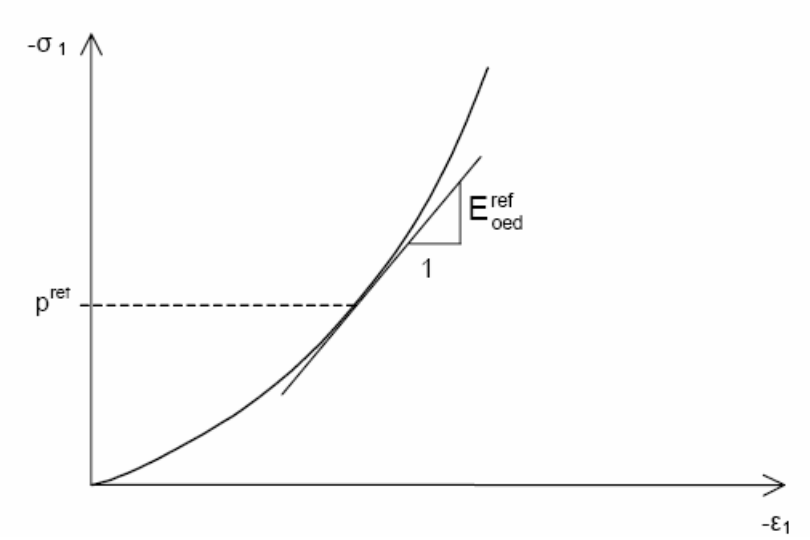

Figure 3.5 Definition of E_{oed}^{ref} in oedometer test results.

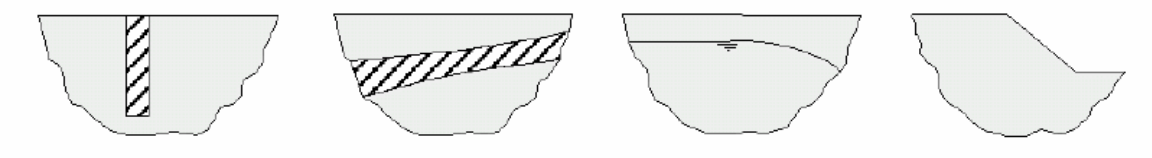

Figure 3.6 Example of non horizontal surface and non horizontal weight stratifications

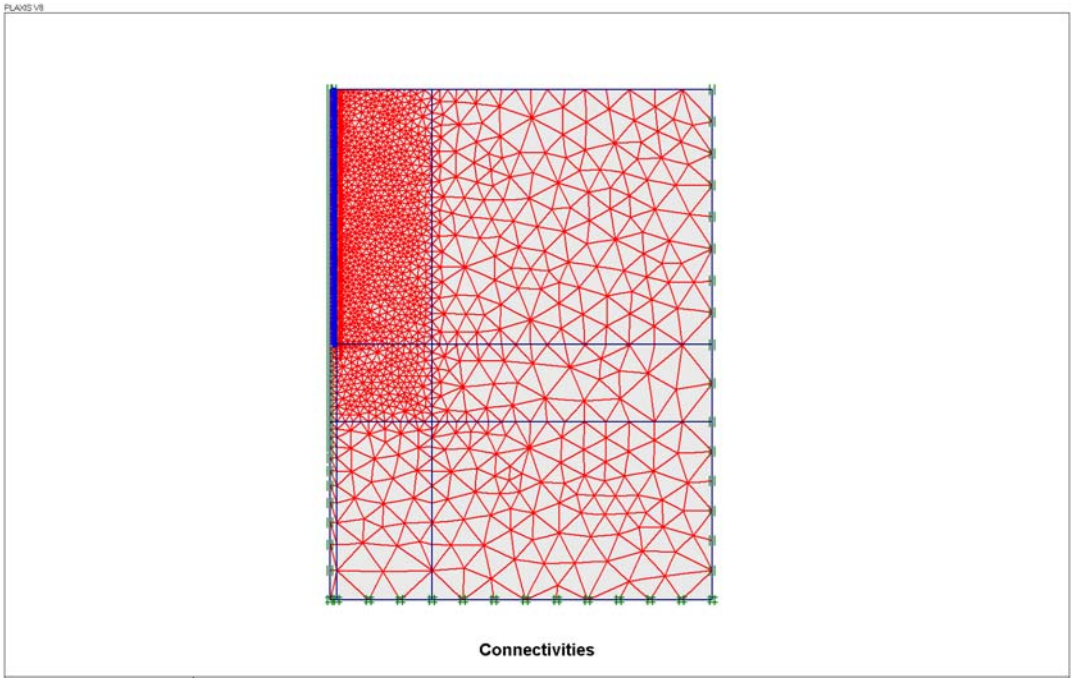

Figure 3.7 2D Axisymetry model of friction pile using Plaxis 8.0.

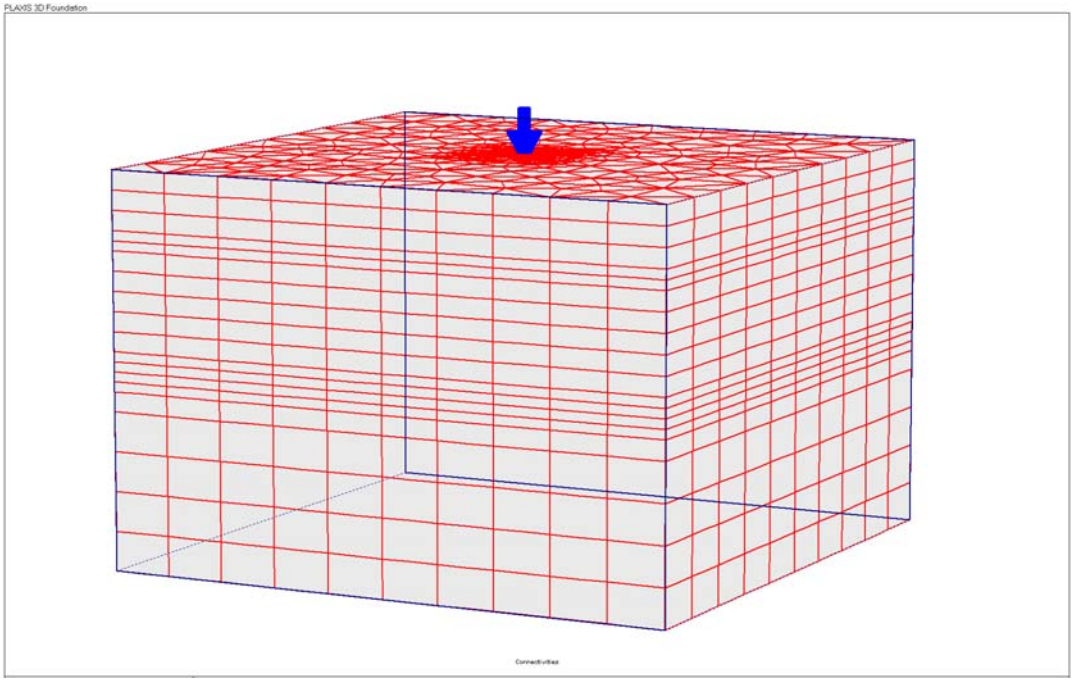

Figure 3.8 3D model of single pile using Plaxis 3D Foundation.

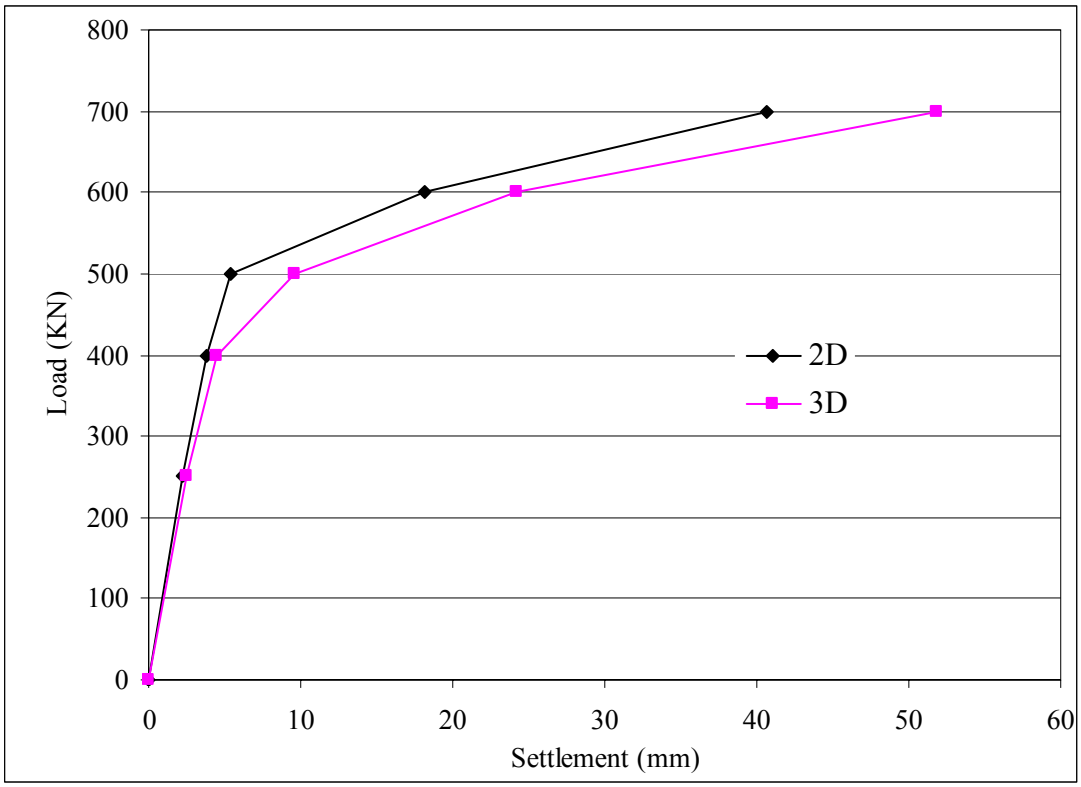

Figure 3.9 Comparison of load settlement curve from 2D axisymetry and 3D analysis in single pile.

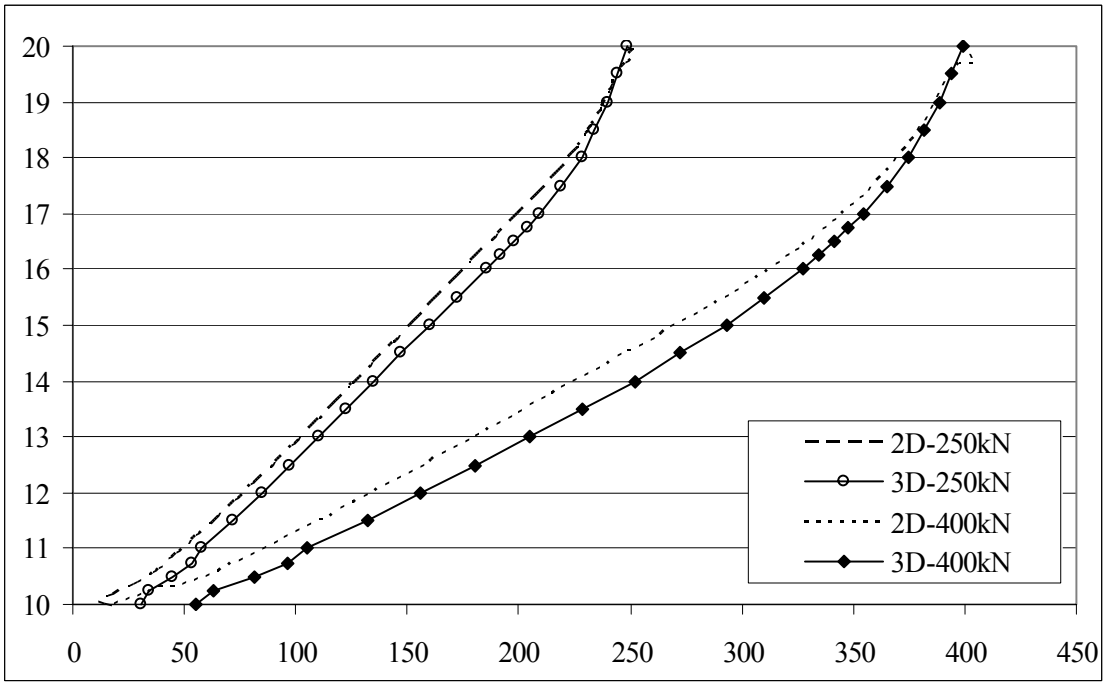

Figure 3.10 Comparison of load transfer curve from 2D axisymetry and 3D analysis in single pile.

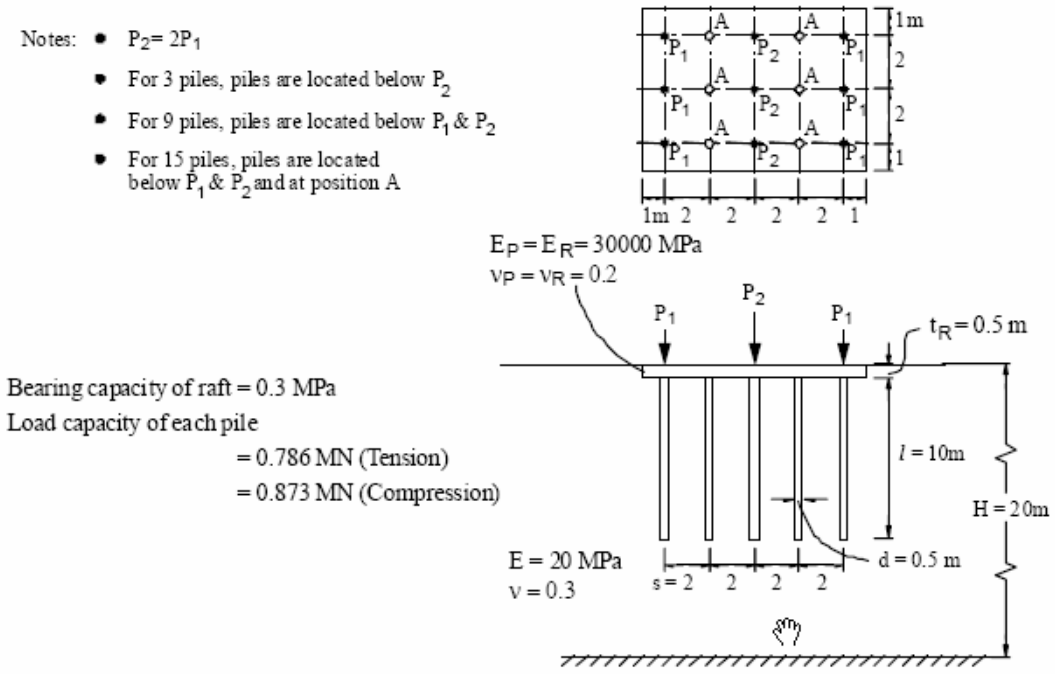

Figure 6. Simple example analysed by various methods.

Figure 3.11 Example analysed by various methods (after Poulos, 1994)

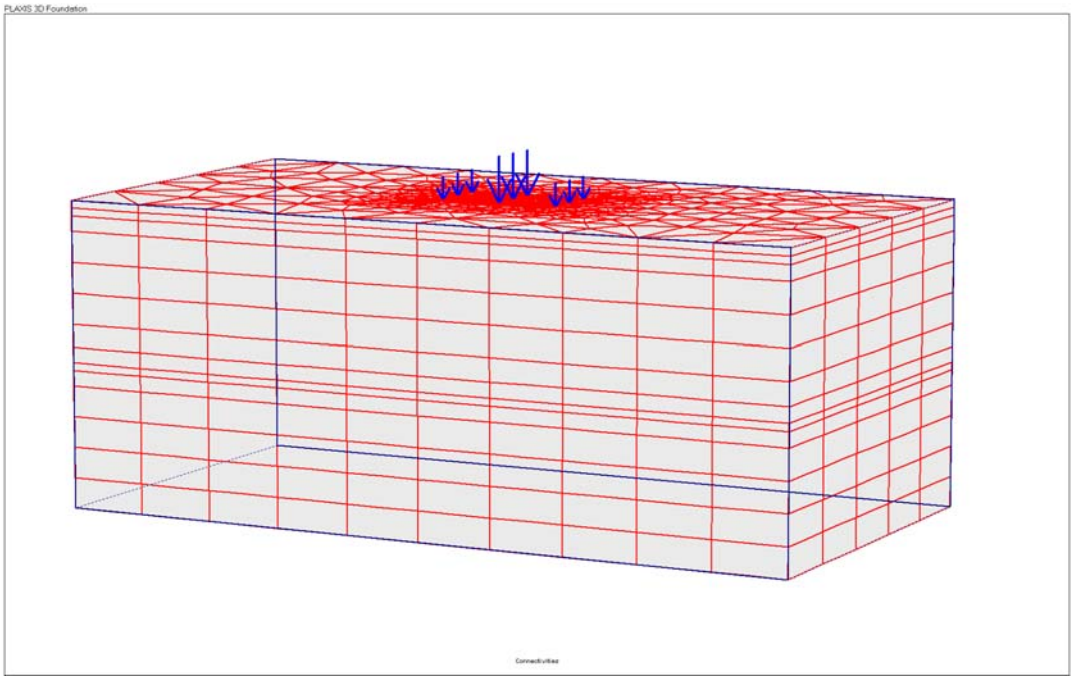

Figure 3.12 Three-dimension mesh of the model pile raft foundation in Plaxis 3D Foundation.

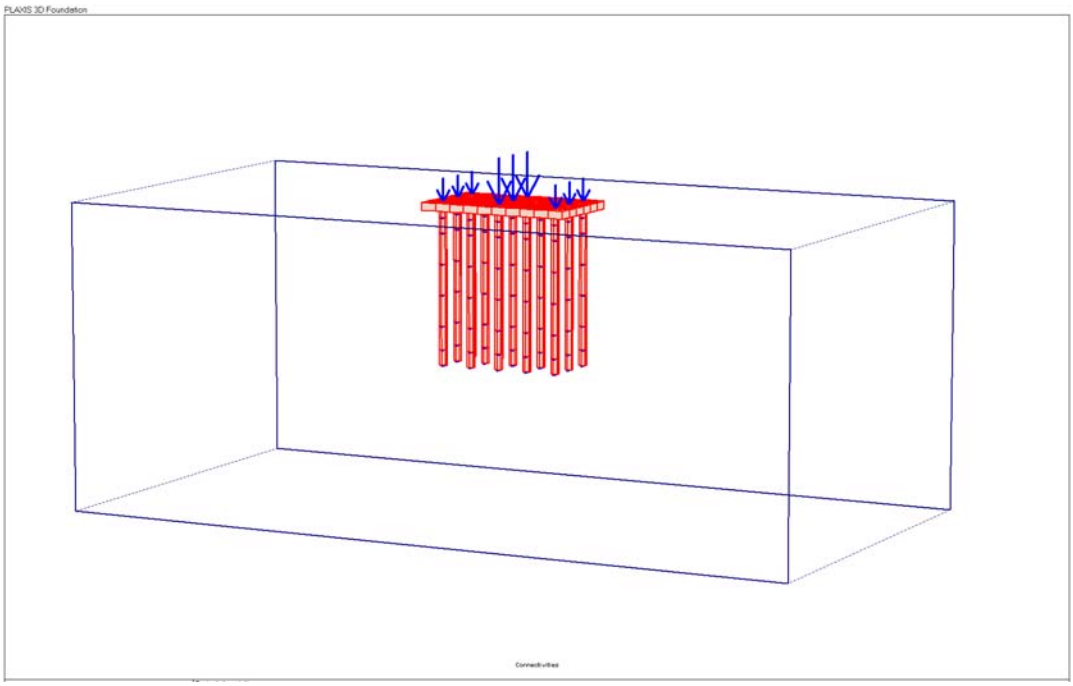

Figure 3.13 Three-dimension view of pile raft in Plaxis 3D Foundation.

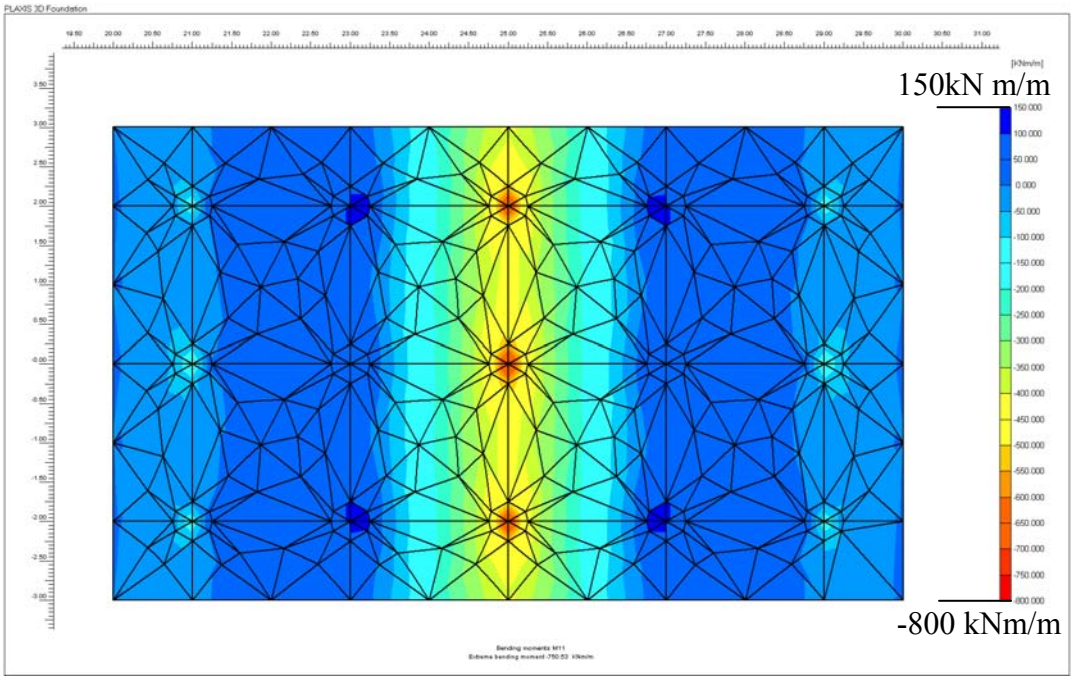

Figure 3.14 Bending moments of raft from Plaxis 3D Foundation in model case A

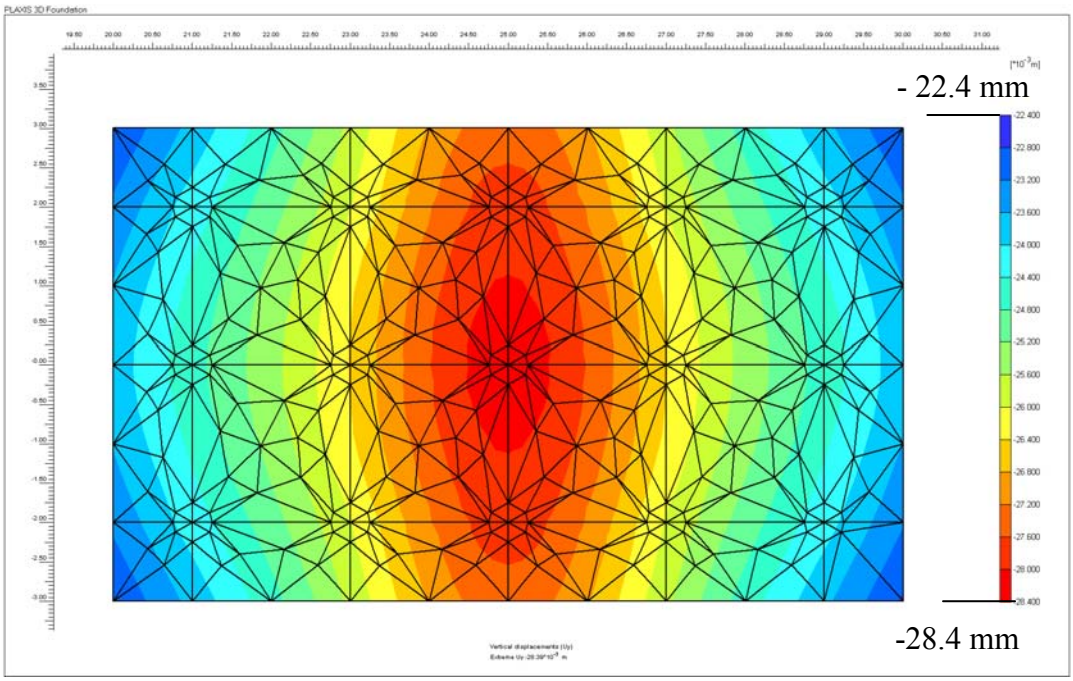

Figure 3.15 Vertical displacements from Plaxis 3D Foundation in model case A.

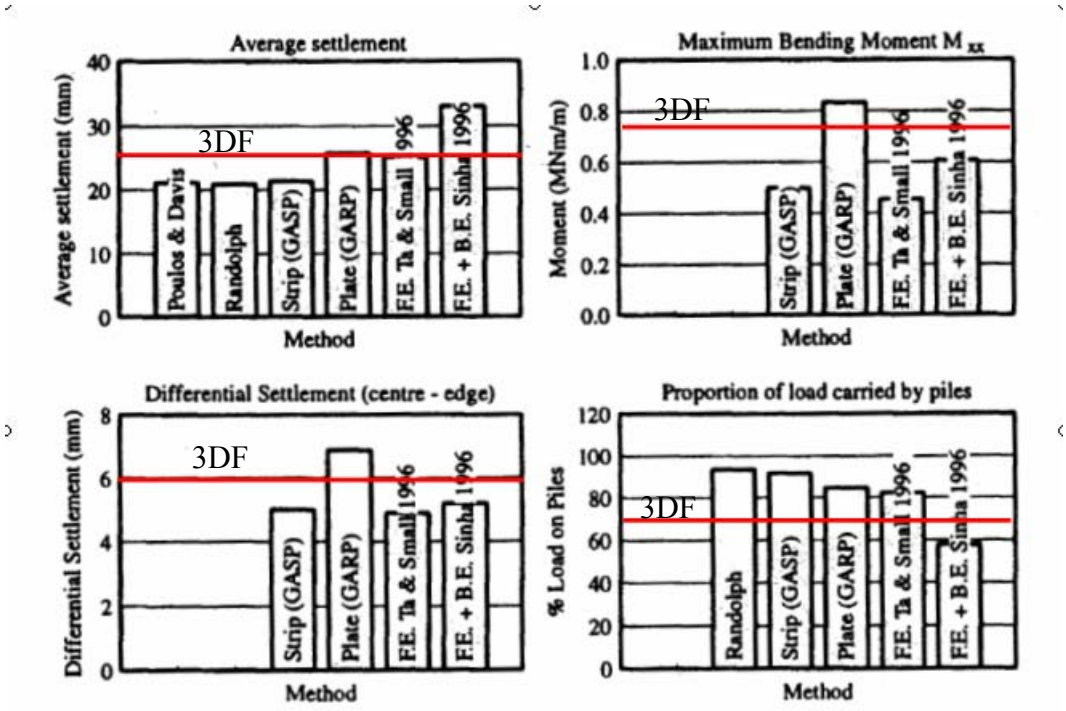

Figure 3.16 Comparison of method for Case A (Red line represent for result from Plaxis 3D Foundation)

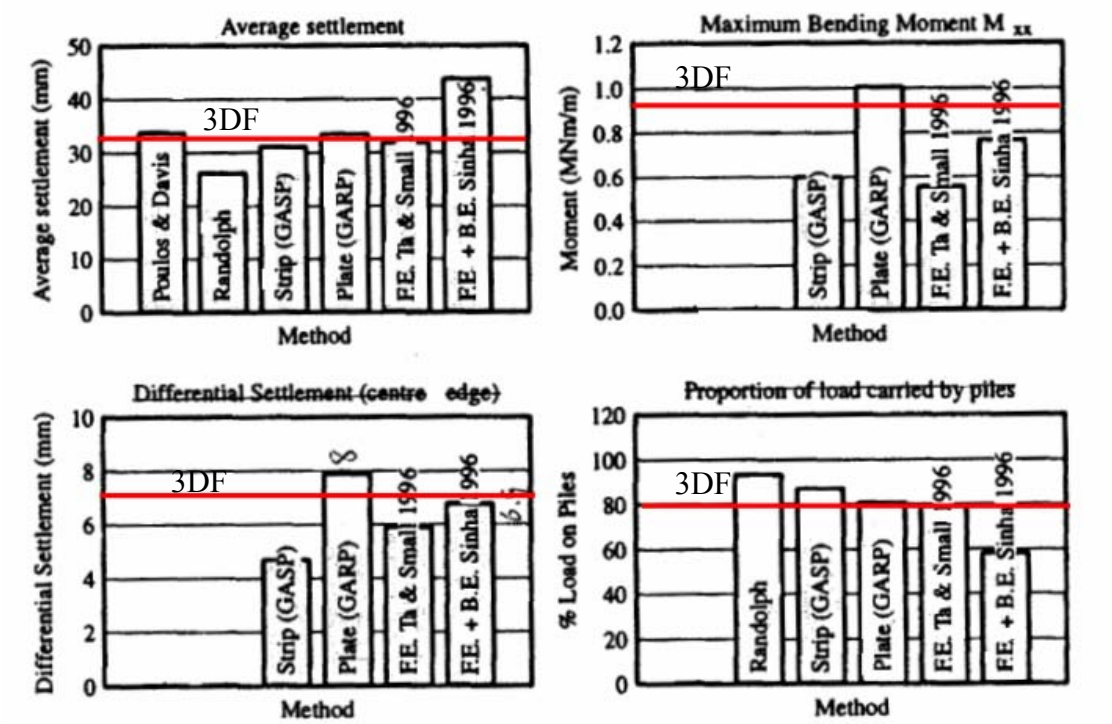

Figure 3.17 Comparison of method for Case B (Red line represents for result from Plaxis 3D Foundation)

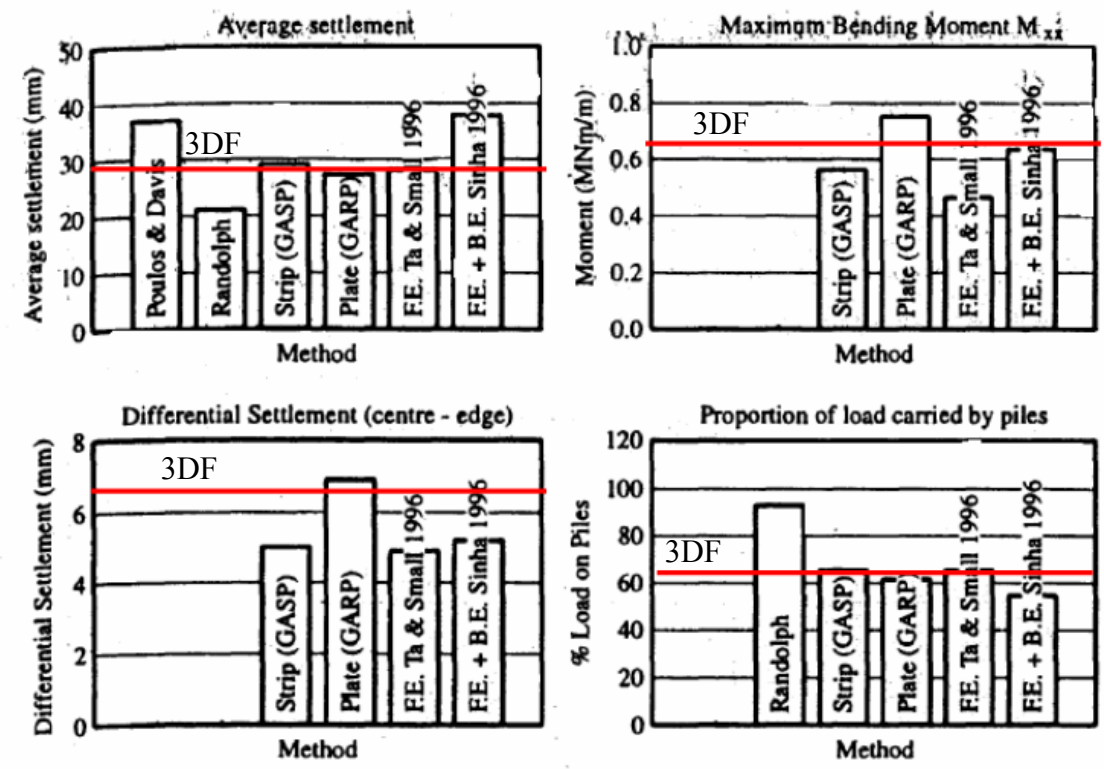

Figure 3.18: Comparison of method for Case C (Red line represents for result from Plaxis 3D Foundation)

CHAPTER 4

3D FEM ANALYSIS OF PILE GROUP FOR OIL TANK FOUNDATION ON SOFT GROUND

4.1 Introduction

This chapter presents the results of a 3D finite element study on 37 piles of the above centrifuge model study. Pile installation is wish-in-place without consideration of installation effects. The study compares the FEM results with the centrifuge test results with regards to distribution of applied loads between the piles and the soil, and distribution of loads among the piles.

In the centrifuge model, the bed layer is intended to be dense sand so that the piles should perform as end-bearing piles. However, centrifuge data in terms of the load-settlement showed quite large settlements of more than 200mm. A question arises that whether the bed layer is as stiff as dense sand or not. To look for the range of the changes of system behavior with the changes in stiffness of bed layer, two types of soil bed layer, one modeling dense sand and the other loose sand, are considered. In addition, the load transfer curve of each pile will also be assessed.

The objectives of the study are to investigate the following items:

- Efficacy of pile foundation system.
- Load sharing in the piles.
- Load transfer curves.
- Load settlement curves.
- Differential settlement.

- Settlement shape.
- Soil arching (if any).

4.2 Definitions of terms

4.2.1 Pile type

To facilitate data interpretation, the 37 piles are classified into 8 pile types: named as A, B, C, D, E, F, G and H based on symmetry of the foundation plan depicted in Figure 4.1. The center piles, henceforth, will be mentioned as pile types A, B and C, edge piles as piles D and E, outside piles as pile types F, G and H, following those defined by Lee (2004).

4.2.2 Pile cap ratio

To interpret the test results, the dimensionless pile cap area ratio, a, is introduced and defined as the ratio of one pile cap area over the tributary area of the pile as shown in Figure 4.1.

4.2.3 Sand pad thickness ratio

Following Low et al., (1993), sand pad thickness ratio is defined as H/s' where H is thickness of sand pad, and s' is clear spacing between pile cap, see Figure 4.2.

4.2.4 Efficacy

Following Hewlett and Randolph's (1988) definition, the proportion of the load

carried by the pile is represented by efficacy which is defined as:

$$\text{Efficacy} = \frac{P_L}{P_T} \times 100\%$$

where P_L = Load on pile top, and

P_T = Total load at pile cap level.

The total load at pile cap level is the sum of the load from the oil tank, the self weight of the bottom plate of the oil tank, and the self weight of the overlying dense sand layer. In the early results, the load spread in the dense sand layer is considered as 1:1. Hence, the load of the self weight of overlying dense sand layer is taken as a mass 2m high and 12m in diameter. After further study, this load was adjusted according to the findings on the extent of load spread in the dense sand layer.

Low et al. (1993) reported that the efficacy increases with applied load. Hence, the proportion of load, due to self weight of overlying dense sand layer, taken by piles will be different for different magnitudes of loading. Therefore, it will be unfair if the efficacy is taken as a ratio of (axial load on piles at the last stage - axial load on piles in initial stage) to the applied tank load. For this reason, the efficacy in this study is not defined in the same manner as the centrifuge study by Lee (2004).

4.3 Centrifuge Model

The centrifuge test model was set up with piles in a rectangular grid of 2 m center-to- center spacing. In all analysis except test series 2, the thickness of overlying sand layer is 2m. The number of piles is 37 in all models except the test series 3 as shown in Figures 4.3 and 4.4

The centrifuge test procedure basically consists of 4 stages: that is (a) soil pre-consolidation under self-weight, (b) pile installation and sand layer preparation at 1g,

(c) soil re-consolidation under self-weight and (d) application of loading up to 220kPa.

4.4 FEM Model

To compare the calculations with centrifuge model results, the FEM model study is the same as the centrifuge model except the oil tank diameter, which is 9.5m in the centrifuge model, was 16 - sided - polygons with mean diameter of 9.9m in the FEM model due to the nature of mesh generation in Plaxis 3DF.

Table 4.1 summarizes the configuration of all FEM models analyzed in this chapter. In model series 1, similar to centrifuge model, five FEM models with different sizes of pile cap named A1, A2, A3, A4 and A5 were analyzed to study the effect of pile cap size on distribution of tank load, load transfer, arching and tank settlement. Model series 2 consists of 5 tests with the same pile cap area ratio of 0.25 but five different thicknesses of dense sand (N1, N2, A4, N3, N4) corresponding to the dense sand thickness ratio of 1, 1.5, 2, 2.5 and 3. This series of FEM model tests aims to investigate the effect of thickness of dense sand layer to efficacy of the pile foundation system, load distribution in pile group, load transfer to soft soil, maximum settlement, differential settlement and arching of the oil tank foundation system. In model series 3, another 2 FEM models (S2, S3) with a reduced number of piles were analyzed. In these two models, the pile cap area ratio was kept at 0.25. All the above models were performed with two different kinds of soil bed layer of dense sand and loose sand. To distinguish the model in different bed layer, the prefix DS will be added to the name of model with dense sand bed layer and prefix LS will be added to the name of model with loose sand bed layer.

4.4.1 General setting

The numerical simulation of the 37-pile group supporting the oil tank foundation was performed using Plaxis 3D foundation. The following settings were assigned and with some assumptions made:

- Mohr-Coulomb model with 15 node tetrahedral elements was used for all soil types.
- The dense sand layer overlying the soft soil and the bed layer is assumed as drained material while the soft soil layer is assumed as an undrained material.
- The model is analyzed perfectly undrained with no soil consolidation under the short term load test.
- The pile is modeled as solid element with outside interface elements connected to the soil elements.
- Some series of wall element with stiffness of 10^{-6} time the real pile are installed along 8 pile types to obtain the axial load distribution along the piles.
- To avoid difficulties in mesh generation of the FEM model, the 9.5m diameter oil tank was modeled as 9.9m diameter polygon with 16 short sides.
- Floor element was used for the bottom of oil tank simulating 50mm thickness of steel.
- In the centrifuge model, the size of the model is 500x500 mm. This is equivalent to 25x25m in prototype scale at 50g. The boundary can be considered as on rollers. Because the standard boundary condition in Plaxis 3D is fixed, the size of the FEM model is taken as 40x40m.

A finite element mesh including 37 square piles (300x300mm) in a cross-section layout is shown in Figures 4.5 to 4.7. In 13 pile locations, wall elements were installed and labeled as A, B, C, D, E, F, G, H, B1, D1, E1, F1, G1, H1 to determine the load distribution and load transfer to the piles. Approximate 44000 nodes and 13000

elements are included in the 37-pile group model. The number of nodes and elements are slightly different in different models.

The elastic perfectly-plastic Mohr-Coulomb constitutive model is used to simulate the non-linear elasto-plastic material behavior of the soil layers shown in Figure 4.6. Although more advanced elasto-plastic constitutive models such as Hardening-Soil model exist, which can combine the shear failure surface with a cap surface to simulate soil dilation or compression; but for load transfer study, the well-known and simpler Mohr-Coulomb model with interface element is adequate. The interface properties are calculated from the soil properties in the associated data set and the strength reduction factor R_{inter}=1.

4.4.2 Soil profile.

According to Biarez & Hicher (1994) for Kaolin with the value Liquid limit of 79.8%, the soil parameter can be estimated as follows:

c'=0; φ'=22; m=1; p_{ref}=100kPa; $E_{50}^{ref} = 1.3MPa$

$$E_{50} = E_{50}^{ref}(\frac{\sigma_y^{'}}{p_{ref}})^m$$

$\sigma_y^{'}$=Load from oil tank foundation + load from sand pad

In preliminary test, the maximum pressure of 103kPa

$\rightarrow \sigma_y^{'}$=103+20×2=143kPa $\quad \rightarrow E_{50} = 1.3(\frac{143}{100}) = 1.86MPa$

It is well known that the stiffness of soil increases with the increasing of effective stress. In this saturated soil, γ'=6 kN/m^3

$$\Delta c_u = \frac{1}{2}(K_o + 1)\sin\phi' \Delta\sigma_v = \frac{1}{2}(0.625 + 1)\sin 22^o \times 6 = 1.824\,\text{kPa}$$

$\Delta E = 200\Delta c_u \approx 350kPa$

The soil properties of the four soil types are shown in Table 4.2. The structural element properties are shown in Table 4.3.

4.4.3 Construction Stages

Loading increment in the centrifuge model is 20kPa up to pressure of 220kPa except for the preliminary test tank load without piles which was loaded up to 103kPa. To check the appropriateness of soil parameter used in the FEM model compared to the real soil used in the centrifuge model, the FEM model test of P1 was done for the same load increment as in the centrifuge model. For the purpose of study beyond the centrifuge model data, most of the FEM models were loaded to a maximum pressure of 400 kPa with loading increment of 50kPa. Some cases showed failure before reaching 400kPa; others needed refinement of the loading increment because the maximum number of iterations is not enough for convergence. To compare with the centrifuge test results, all the load distribution and load transfer curves were evaluated at the loading of 220 kPa.

The detail loading steps used for all FEM models are listed in Table 4.4.

4.4.4 Initial stage

The initial phase represents the gravity loading phase in the finite element calculation in which the soil weight is applied by means of gravity loading. This is to produce the correct initial stresses in the model. However, deformations calculated in the initial phase are not considered to be relevant for further calculations. Therefore,

these displacements are, by default, reset to zero at the beginning of the next calculation phase.

4.4.5 Pile and tank installation stage

In this stage, all piles are installed by replacing the soil at location of piles and caps by concrete as wish-in-place, where pile installation effects are not modeled. To determine the load distribution in the pile group and load transfer for each pile type, Eight walls (plate elements) along 8 piles (corresponding to pile types A, B to H) will be installed. The stiffness of the plate is taken as 10^{-6} times as the real piles. The axial force in each wall will represent about 10^{-6} time the axial forces in piles. These plate elements with very small stiffness values will not affect the system behavior. The plate elements are activated at the same phase as the pile installation.

The bottom plate of the steel tank is represented by the floor elements, which is activated together with the pile/cap elements.

4.4.6 Loading stage

All models were loaded up to 400 kPa with increments of 50kPa and one stage loading of 220kPa was added in order to compare with the centrifuge model test results.

4.5 Preliminary Test without Piles

A model of preliminary test (P1) was made to evaluate the performance of tank supported by dense sand overlying soft clay without piles. The model of this test basically follows all the procedures above, except for the absence of piles. This model aims to check the soil parameters chosen to represent the soil used in the centrifuge test.

Figure 4.9 portrays the loading pressure vs. maximum tank settlement. It can be observed that the tank settlement increases significantly during the application of loading. To compare with the centrifuge test results, the loading was taken up to 110kPa with increments of 20kPa. It can be seen that the FEM results and the centrifuge model results are in good agreement. Thus the chosen parameters represent realistically the soil used in the centrifuge model.

4.6 Boundary Effect

4.6.1 Model

The finer the mesh, the more accurate the result we can achieve but computation time increases significantly especially in 3D model as mentioned in chapter 3. Consequently, this section will study the mesh size which can be used to get the accurate answer with minimal computation time. Firstly, the global setting will be set to coarse mesh in models DS-A4-Coarse Mesh (see Figure 4.10). Secondly the global setting will be set to medium mesh in models DS-A4-Medium Mesh (see Figure 4.6). Thirdly, number of element will be doubled by doubling number of elements of work plan in the model DS-A4-Fine Mesh (see Figure 4.11). Finally the global setting will be set to fine mesh in the model DS-A4-Very Fine Mesh (see Figure 4.12). The load settlement curve and will be compared to seek the best mesh configuration for efficient computation.

4.6.2 Load-settlement comparison

The load settlement curves are compared in Figures 4.13. It can be seen that the settlement is larger in the model with more refine mesh. The difference is quite big

from the point of view of the load settlement curve using coarser mesh compared to that of the medium mesh. The difference becomes smaller in model DS-A4-fine mesh and DS-A4-very fine mesh.

4.6.3 Conclusion

The computation time increases 5 times from the model with medium mesh to the model with Fine mesh and more than 10 times for very Fine mesh but the answer showed little difference so that the model with medium mesh seems good enough for accuracy to cost return.

4.7 Typical model results (Test A4)

The results of model test A4 in test series 1 are presented next in greater detail to compare the FEM result with the centrifuge test results.

4.7.1 Efficacy

The calculation in 3D foundation reveals that the efficacy is dependent on the applied pressure. At 220kPa applied pressure, about 81% of the tank loads have been transmitted to the piles based on dense sand as the founding layer, see Figure 4.14. The centrifuge test showed that, the piles take about 82% of axial load (see Table 4.5). The FEM result is in good agreement with the centrifuge result.

It can be seen that the efficacy is also dependent on the bed layer stiffness. For a stiff bed layer like dense sand, 81% of tank load was carried by the piles. On the other hand only 71% of tank load was carried by piles when the bed layer is loose sand.

The relationship between pressure and efficacy are shown in Figure 4.14. It can be seen that the load carried by the pile increases with increasing of tank load but the rate of increase decreases as the load increases. After the tank load exceeds 200kPa, the percentage of load carried by the piles is around 80% for the case of dense sand bed layer and 70% for the case of loose sand bed layer. The applied load can be represented by an equivalent "embankment" height. The phenomenon of increasing efficacy of the pile support with increasing embankment height has been reported by Tung (1994). On the other hand when the equivalent embankment height is large enough for arching to be fully mobilized, the proportion of load taken by the piles will not increase. This is the reason why efficacy tends to reach a constant after the tank load exceeds 200kPa.

4.7.2 Load distribution among pile group

Figure 4.15 shows the load distribution among the 8 piles for the case DS-A4 under 220kPa applied pressure. The axial forces carried by the center piles (A, B, C) are much higher when compared to the corner piles (D, E). The axial forces in the piles outside the tank (F, G, and H) are quite small, which is less than 10% center pile. This characteristic is in agreement with the centrifuge observations. Nine piles in the center (type A, B and C) take 38% load.

It can be seen that the stiffness of the bed layer played an important role on the behavior of pile system. All pile types in the model with dense sand bed layer carried more load than that in the model of loose sand bed layer, this finding agrees well with Khoo (2001).

4.7.3 Load transfer

The load transfer curves for dense sand bed layer is shown in Figures 4.15, it can be seen that the soft soil layer does not carry much load in friction, the piles work like end-bearing piles. The gradient of load transfer curve changes sharply at levels near the pile toe. This does not mean that the soft soil layer skin friction is more effectively mobilized near the pile toe. The friction near the pile toe is mobilized from a mass of soil near pile toe, some distance above and below the pile toe, (this may be inferred from stress trajectories near the pile toe) which is significantly influenced by the stiffer end-bearing layer.

Figures 4.16 show the development of loads carried by each pile top with loading pressure. The Figure suggests that as the load increases, the rate of load distribution to the center piles increases faster than the load transfer to the edge and outside piles. The rate of increase about 10:6.5:1 corresponding to the increase of center piles, edge piles and outside piles.

4.7.4 Settlement

Figure 4.17 shows the load settlement curve for different pile types in model test DS-A4. It can be seen that the pile top settlements of each pile type is proportional to the load taken by that pile type (see Figure 4.16). Result also reveals fairly uniform tank settlements at the elevation of 0m (ground level) for both cases of bed layer. At 220kPa loading pressure, the model with dense sand bed layer gives a settlement of 30 to 31.57mm as shown in Figure 4.18 and the model with loose sand bed layer gives settlement of 80 to 105mm as shown in Figure 4.19.

Figures 4.18 to 4.21 showed that there are some differences in the location of maximum settlement depending on the magnitude of pressure applied and the stiffness

of bed layer. For loading below 100kPa both models show the maximum settlement is at the center of tank. When the load increases to 150kPa and above; the maximum settlement of model with loose sand bed layer is located at the center of tank, but the maximum settlement of model with dense sand bed layer is located about two third of the radius from the center of tank. The reason for this characteristic will be explained later in the settlement result of model test series 1.

4.7.5 Arching

Figure 4.22 shows the total normal stresses by shading and contour. It can be seen that the normal total stress at the region above the pile cap is much higher than that between pile caps. However, the difference ceases at about 0.6m below the ground level. As discussed in Chapter 2, the difference in vertical pressure caused by arching could affect the load redistribution between the piles and the soil zones between pile caps.

4.8 Model of Test series 1 – Pile cap area ratio

Ten FEM models labeled as A1, A2, A3, A4 and A5 in two different types of bed layer with five different pile cap sizes of 0.5m×0.5m (Test A1), 0.7m×0.7m (Test A2), 0.9m×0.9m (Test A3), 1.0m×1.0m (A4) and 1.1m×1.1m (Test A5) were used to study the effects of pile cap size on efficacy, load distribution, load transfer, settlement and arching of system. A comparison will be made with the results of five centrifuge model tests by Lee (2004). The performance of the system at 220kPa pressure is calculated and compared in detail.

4.8.1 Efficacy

The results in Table 4.6 show that the proportion of tank load carried by the piles, as given by the efficacy, depends on the stiffness of the bed layer. Since the bed layer is loose sand, the efficacy for all the models of tests LS-A2 to LS-A5 is around 71%, 72% while it is around 80%, 81% in models with dense sand bed layer. The model of test A1 can not reach to the maximum loading of 220kPa.

The efficacy does not change when the pile cap ratio increases from 12% to 30%. This can be explained by two possible reasons. Firstly, according to Hewlett and Randolph (1988), arching above a grid of pile is considered as a series of domes, the crown of each dome being approximate to a hemisphere. Using this theory to look at series test 1, s' varies from 0.9m to 1.5m, arching can only be fully developed when the thickness of dense sand layer is greater than 0.75m. Hence, with 2m of overlying dense sand layer, the arching will be fully developed in all this series. Secondly, Marston stated that if the embankment is sufficiently high, the shear force may terminate at some horizontal plane so that soil arching will develop to its maximum for a certain thickness of soil (see Figure 4.23). Using this concept to look at the system with tank pressure of 220kPa, the equivalent height will be about 11m added to 2m of dense sand; this provides sufficient equivalent height for arching to be fully developed. From these two reasons discussed above, it can be stated that the arching in pile grid system is fully developed at 220kPa of pressure with 2m of overlying dense sand layer. Therefore, the efficacy remains the same for the above tests.

Model of test DS-A1 gives an efficacy of 72% at pressure of 180kPa compared to that of model test DS-A4 at 76%. It can be seen that the efficacy is slightly smaller. Also in model LS-A1, the efficacy is 61% at a pressure of 160kPa compared to 66% of model LS-A4.

In addition, the FEM results from Table 4.6 showed that the axial forces on each pile type in model test DS-A2 to DS-A5 are not the same but the difference is not significant to the total loads taken by piles so the values of efficacy are not much different. Thus, it can be stated that, when the pile cap area ratio increases from 0.12 to 0.3, the efficacy is relatively unchanged, but some small difference is shown when the pile cap area ratio drops to 0.06.

4.8.2 Load distribution on pile group

The load distribution in pile group and load transfer curve of piles with different model tests DS-A1, DS-A2, DS-A3 and DS-A5 are shown in Figures 4.24 to 4.27.

It can be seen that the load distribution and load transfer of all the piles from tests DS-A2 to DS-A5 in both cases of bed layer, loose sand and dense sand, are the same as test DS-A4 respectively. The reason for this characteristic is also the same as reason for the same efficacy above.

It also reveals that when the pile cap ratio increases, the center pile axial load seems to decrease a bit and the edge piles seem to slightly increase. It is possible because the bigger pile cap ratio the better the load spread to each pile.

If we consider the bottom of the tank and the dense sand layer as a raft in a pile raft foundation, the smaller the pile cap, the more flexible the raft. It is clear that the more flexible raft, the more load will be taken by the center piles and the less load will be taken by the edge piles.

4.8.3 Load transfer

Figures 4.28 to 4.37 showed the comparison of the load transfer curves for each pile type in different models. It can be seen that the load transfer curves of all pile types in model tests A3 to A5 are similar while the load transfer curves of the pile in model of test A2 shows that the load is transferred more to the soft soil than that of model A3 to A5. It is reasonable since the model A2 gives more settlement as it can mobilize more skin friction.

4.8.4 Settlement of tank

Figures 4.38 and 4.39 show the load settlement curve of the tank. It can be seen that the tank settlement decreases with increasing pile cap area ratio, as illustrated in Figure 4.38 for models with dense sand bed layer and in Figure 4.39 for models with loose sand bed layer. However, it also reveals that the rate of decrease in tank settlement will reduce when the pile cap area ratio increases. There are significant differences in maximum tank settlement when pile cap area ratio increases from 6% to 12%. The difference reduces when pile cap area ratio changes from 12% to 20% and the difference in tank settlement is fairly small when pile cap area ratio changes from 20% to 30%. The relative difference in settlements is in fair agreement with centrifuge test results but the absolute values are not the same.

In the centrifuge model, the bed layer is supposed to be dense sand so that the pile should perform as end bearing piles. However, the data from centrifuge shows large settlements, model of test A4 shows 250mm of settlement at applied pressure of 220 kPa, and this result is out of range for either settlement from the case of dense sand bed layer of loose sand bed layer. The explanation for this data could be some of the following reasons:

- The difference of g-scale in pile installation and overall model may affect the result significantly.
- The piles are not always installed fully seated in bed layer leading to soft toe phenomenon. A small seating error in the centrifuge model is large in prototypes scale.

For dense sand bed layer, model test DS-A1 with pile cap area ratio of 0.06 gives the largest settlement of 69.6 mm when the applied pressure is 180kPa (Figure 4.40). The soil collapses when applied pressure increases to 190kPa. When pile cap area ratio is 0.12 in model of test DS-A2, the maximum settlement reduces to 48 mm at pressure of 220kPa (Figure 4.41) and the soil collapses when applied pressure increases to 300kPa. Models of test DS-A3, DS-A4 and DS-A5 are taken to applied pressure of 400kPa. At applied pressure of 220kPa, the maximum settlements are 35.8mm, 31.6mm, 28.5mm respectively (Figure 4.42, 4.18 and 4.43 respectively). Clearly, the settlement obtained in these three models is fairly similar.

For loose sand bed layer, the differences among the models of tests LS-A1 to LS-A5 are fairly similar to that of model with dense sand bed layer. At 160kPa pressure, the model of test LS-A1 gives 134.2mm settlement (Figure 4.44) and the soil collapses when applied pressure increases to 180kPa. Model of test LS-A2 can be analyzed up to pressure of 250kPa and soil collapse when applied pressure increases to 300kPa. The maximum settlement at pressure of 220kPa is 135.9mm (Figure 4.45). Three other models LS-A3, LS-A4 and LS-A5 are analyzed up to pressure of 400kPa. The maximum settlement given at 220kPa pressure is 115.0mm; 105.4mm and 100.3mm, respectively (Figure 4.46, 4.19 and 4.47 respectively).

It is interesting that the location of maximum settlement is dependent on the pile cap area ratio, the magnitude of loading and stiffness of bed layer (see Figures 4.18 to 4.19 and 4.40 to 4.51). In all the models with loose sand bed layer, the

maximum settlement always occurs near the center of the oil tank. On the other hand, the results are markedly different in the models with dense sand bed layer. The location of maximum settlement in model of test DS-A1 and DS-A2 (Figure 4.40 and 4.41 respectively) is near to the center of oil tank for all loading levels. The models of tests DS-A3 to DS-A5 perform quite differently. With a pressure lower than 150kPa, the maximum settlement location is still near the center of oil tank. However, when the pressure increases to 200kPa and above, the location of maximum settlement changes to about two third of the radius from the center of oil tank (Figure 4.42 and 4.43).

The differential settlement obtained from models with dense sand bed layer and loose sand bed layer is different. The differential settlement in loose sand model is much higher than that of dense sand bed layer. The pile cap area ratio also plays an important role in reducing the differential settlements. The bigger the pile cap size, the smaller the differential settlement. The comparison at level of loading 220kPa shows that the differential settlement from model tests DS-A2 to DS-A5 are 13mm, 10mm, 8mm and 6.5mm, respectively, while that from model test LS-A2 to LS-A5 are 36mm, 25mm, 20mm and 18mm, respectively. The differential settlement in model test DS-A1 is 19mm at 180kPa pressure while in model test LS-A1, it is 34mm at 160kPa of pressure.

This characteristic can also be explained by the reasons given in load distribution section. If we consider the tank bottom together with the dense sand layer behaving as a raft in pile raft foundation, the smaller the pile cap, the more flexible the raft. It is clear that in a stiffer raft, the magnitude of settlement and the differential settlement is small. This is the main reason why the maximum settlement and the differential settlement decrease with increasing pile cap ratio.

4.8.5 Summary of test series 1

The findings of test series 1 can be summarized as follows:

- The proportion of tank loads carried by the pile cap, as given by efficacy, increases with increasing tank load. However, the rate of increase in efficacy decreases as the load increases.
- The efficacy depends on the stiffness of bed layer. In model of test A4, the results show that with a pressure above 200kPa, the efficacy is around 80% for stiff bed layer like dense sand, and 70% for softer bed layer like loose sand.
- When the condition of arching reaches its full development, the efficacy does not depend on the pile cap ratio.
- The greater the pile cap ratio, the better the load spread to the piles.
- The maximum settlement and differential settlement of the tank decreases with increasing pile cap area ratio. When the bed layer is dense sand, the maximum tank settlement is reduced by half when the pile cap area ratio increases from 0.06 (Test DS-A1) to 0.12 (Test DS-A2). However, in loose sand bed layer, the maximum settlement is almost half reduced when the pile cap ratio increases form 0.06 (model test LS-A1) to 0.20 (model test LS-A3).
- The gradient of the load-settlement response of the tank decreases with increasing pile cap area ratios.
- The location of maximum settlement also depends on the bed layer stiffness, pile cap ratio and magnitude of loading.

4.9 Test series 2 – Thickness of overlying dense sand

Test series 2 consists of two model series, named as Test N1, N2, N3, N4 and A4 in two different bed layers of dense sand and loose sand. In this series, the pile cap area ratio is kept unchanged at 25%, but the sand pad thickness ratio is changed from 1 in model test N1, to 1.5 in model test N2, to 2 in model test A4, to 2.5 in model test N3, and to 3 in model test N4. The results showed that the thickness of sand pad may have different effects depending on stiffness of bed layer.

4.9.1 Efficacy

The result shows in models of series test 1 that the load was not spread at 45 degree in the overlying dense sand. Hence, from this series onward, the load from the dense sand layer will be taken as the prism of 9.9m diameter. The result show that the load carried by pile decreases when the thickness of the dense sand layer increases either in loose sand bed layer or dense sand bed layer as shown in Figure 4.52.

In the model with dense sand bed layer, the efficacy in model test SS-N1 is largest at 93%. It reduces to 89% in model test SS-N2, the model of test SS-A4 and SS-N3 reports quite the same efficacy at 86% and 85% respectively, the efficacy is lowest at model of test SS-N4 at 82%. The relative difference was similar in models with loose sand bed layer. The largest efficacy is 83% in model test LS-N1; it reduces to 80% in model test LS-N2. The lower efficacy in model test LS-A4 and LS-N3 was found to be 76% and 74% respectively and the lowest efficacy is 69% in model test LS-N4.

It can be explained that the thicker of dense sand layer, the lower the pressure at the sand-clay interface which leads to the lower efficacy, see Figure 4.52.

4.9.2 Axial force on piles

Figures 4.53 and 4.54 showed the load transfer curves of piles in models DS-N1 and DS-N4 respectively. The development of axial load with thickness of sand pad for each pile type is further scrutinized and shown in Figures 4.55 and 4.56. It can be seen that the load distribution in pile group performs differently in model with dense sand bed layer compared to that of loose bed layer

a. Dense sand bed layer.

It can be observed from Figure 4.55 that when the thickness of sand pad increases, the axial load transfer to the outside piles increases. This performance is reasonable on two accounts. The thicker the sand pad, the better the degree of load spreading. Also, the thicker the sand pad layer, the more load from sand pad will act on the outside piles.

Contrary to the outside piles, the edge piles (pile type C, D and E) carry less load from the system when the thickness of sand pad increases.

The load transfer to pile type A and B tends not to show the same trend. When the sand pad thickness increases from 1m to 2.5m the axial load in piles type A and B increases. However, the axial load in piles type A and B decreases when the thickness of sand pad increases from 2.5m to 3m. This is due to a lower pressure from load spreading effects on the deeper sand-clay interface, resulting in smaller axial loads on the piles. This characteristic is the same as the centrifuge results.

Looking at the system as a combination of two components which are sand pad and the combination of piles and sand bed layer, it can be seen that the stiffness of the sand pad is less than that of the combination of piles and sand bed layer. So that if we consider the tank bottom and the sand pad layer as a raft in pile

raft foundation, the thicker the sand pad layer, the more flexible the raft. It is clear that for a more flexible raft, more load will act on the center pile and less load on edge piles. This explains why the axial force on pile type C, D, E decreases while that of pile type A and B increases with increasing sand pad thickness.

b. Loose sand bed layer

It can be seen from Figure 4.56 that the axial load on outside piles increases and that of both the edge piles and the center piles decreases with increase in sand pad thickness.

The reason for the increase of axial force in outside piles with the increase of sand pad thickness is similar to the dense sand bed case. The thicker the sand pad, the better is the load spreading and also more load from weight of the sand pad will act on the piles.

Numerical study of the single pile (Khoo, 2002) shows that percentage of load taken by pile does not change with the changing of the sand thickness (see Figure 2.6). However, It can be seen clearly in this study that the performance of piles in group are much different; single pile can not represent piles in group.

4.9.4 Settlement of tank

Figures 4.57 and 4.58 show the load-settlement curve for models N1 to N4 and A4. It can be seen that the effect of thickness of the sand pad layer on tank settlement is different for the model with a loose sand bed layer and with a dense sand bed layer. When the bed layer is dense sand, the thicker the sand pad, the larger the tank settlement at the pressure of 220kPa. The maximum tank settlement of 39.2mm is higher in model test DS-N4 with 3-m sand thickness compared with 44.5mm from

model test DS-N3 (2.5m thickness of sand pad). The maximum tank settlement for models DS-A4 and DS-N2 is 31.6mm and 28.9mm, respectively. The smallest maximum settlement is 25.3 mm for model DS-N1 (1m thick sand). It can be explained that the pile group performs as a frame to transfer the load from the sand pad to dense sand bed layer. Moreover the dense sand bed layer is too hard so the tank settlement is mainly contributed by the compression of sand pad. This point reveals that the thicker the sand pad, the larger is the tank settlement.

This characteristic performance is different in model with loose sand bed layer. The maximum tank settlement is similar for models LS-N1 to LS-N4 and LS-A4 (around 100mm). This result can be explained that the loose sand affects the settlement considerably. It is this reason why the maximum vertical settlement is not effected by the changing of sand pad thickness.

The thickness of sand pad layer plays an important role in the differential settlement and the location of maximum settlement, see Figures 4.59 to 4.62. The results show that, when the bed layer is dense sand, the differential settlement in model DS-N1, DS-N2 is 5mm and 6mm respectively while that of test DS-A4 is 8mm and that of test DS-N3 and DS-N4 is 10mm and 12mm. The location of maximum settlement also changes. It can also be seen for the load distribution in the pile group. The load carried by pile types C, D and E increases with increasing sand pad thickness. It can be explained that the thicker the sand pad means large compressions of the sand layer.

4.9.5 Summary of test series 2

The results of test series 2 can be summarized as follows:

- Axial force in outside piles increases and that of pile C, D, E decreases with increasing sand pad thickness for both models.
- The axial force in pile type A and B in model of loose sand bed layer decreases with increasing sand pad thickness while that of dense sand bed layer changes differently. The axial force in pile types A and B increases since the thickness of sand pad increase from 1m to 2.5m, and it decreases when the sand pad thickness increases to 3m.
- The models with dense sand bed layer reveal an increasing maximum and differential tank settlement when the thickness of sand pad increases. The results are similar for loose sand bed layer.
- The location of maximum settlement depends on the thickness of sand pad, stiffness of bed layer and also the level of loading.

4.10 Model of Tests with reduced numbers of piles (Tests S2 and S3)

As discussed in the results of model tests series 1 that outside piles of the tank seem to carry very little load. This depends on pile cap size and the stiffness of bed layer, varying from 10% to 15% of center pile axial forces. Thus the load spread ratio in the dense sand layer may not be 1:1. Two centrifuge models were performed with reduced number of piles under and outside the tank corner by Lee (2004). The configuration of pile layout for tests S2 and S3 is shown in Figures 4.63(a) and (b), respectively. The pile cap size remains the same as test A4.

4.10.1 Efficacy

The results show that the proportion of load taken by the pile increases with the

number of pile. For the dense sand bed layer, the efficacy increases from 75% to 86% when the number of pile increases from 15 (model of test DS-S3) to 37 (model of test DS-A4). For the loose sand bed layer, the efficacy is smallest for model LS-S3 (58%), larger for model LS-S2 (67%) and largest for model test LS-A4 (76%), see Table 4.6. The centrifuge test results reveal that the efficacy in model test S2 is 79%, which is in fairly good agreement with FEM results of model test DS-S2 (81%), see Table 4.5.

4.10.2 Load distribution in pile group

Figures 4.64 to 4.67 showed the load transfer curve of piles in the models of tests S2 and S3. Comparing results model S2 with A4, it can be observed that all the piles in model S2 carry more load than that of model A4 but the change is not significant. For the dense sand bed layer, the increase in axial load for the edge piles is larger than that of center piles. The axial force in pile types E and D increases 12% and 6% respectively while that of piles A, B and C are 2%, 4% and 3% respectively. Results from loose sand bed layer models showed slight difference with that of dense sand bed layer, the increase in axial force for all pile types ranges from 3% to 6%. The reason for this characteristic is the omission of outside piles near the edge pile than to center pile, thus the effect of this omission for edge piles is larger.

The axial force changes considerably when number of pile reduces form 21 (model S2) to 15 (model S3). The increase in axial force in the edge piles is higher than that of center piles in both dense sand and loose sand bed layers. The stiffness of bed layer does not influence the axial force of the center piles while it does on the edge piles. The increase of axial force in the edge piles in dense sand bed layer models is higher than that of loose sand bed layer. For the dense sand bed layer, the axial force in pile types E and D increase 30% and 38%, respectively while that of other pile types is

around 15%. Similarly for loose sand bed layer, the axial force in pile types E and D increases by 22% and 26%, respectively while that of other pile types is around 16%.

4.10.3 Settlement

Figures 4.68 and 4.69 illustrate the comparison in development of settlement with pressure in models S2, S3 and A4 for the two different bed layers. It seems that there is a slight increase in maximum settlement when the number of pile reduces form 37 (model of test A4) to 21 (model of test S2), but that increase is greater when the number of pile reduces from 21 (model test S2) to 15 (model test S3).

In addition, the differential settlement between models A4 and S2 is quite comparable but it increases more in model S3. The location of maximum settlement also changes with the number of piles, see Figures 4.70 to 4.75. For the dense sand bed layer, the location of maximum settlement in model DS-A4 moves to about two-third of the radius from the center of oil tank at 150kPa pressure while this happens in models DS-S2 and DS-S3 at 50kPa pressure. For model LS-S3, the location of maximum settlement is located at two-third of the radius from the center of oil tank due to omission of pile type D.

It can be stated that the outside piles do not play significant roles to support the oil tank system but the edge piles do. Thus the omission of outside pile does not affect to the load-settlement response and the load distribution of the pile foundation system significantly. In addition, it is fairly obvious that when a pile is omitted, the effect is more significant on adjacent piles.

4.10.4 Summary of test series 3

- The efficacy increases with increasing of number of piles.

- The axial force in edge piles increases faster than that of center piles with the decreasing number of piles but the change is small when the number of piles reduces from 37 to 21 and much larger when the number of pile reduces from 21 to 15.
- The stiffer the bed layer, the larger the increase in axial load in the edge piles.
- The maximum settlement and differential settlement increase with decreasing number of piles but the change is small when the number of pile reduces from 37 to 21 and much bigger when the number of pile reduces from 21 to 15.
- For the dense sand bed layer, the location of maximum settlement moves to the tank edge.
- The FEM results in this section are in fair agreement with centrifuge results.

4.11 Conclusion

In this chapter, FEM was used to back analyze the centrifuge test results to study the efficacy of pile foundation system, the load sharing in the piles, the load transfer curves and soil arching with various of the pile cap area ratio, the thickness of the dense sand layer, the number of piles and the stiffness bedding layer. The results are compared to the centrifuge model results. The following conclusions can be deduced:

- The FEM model results report a lower settlement in comparison with the results from the centrifuge model.
- The magnitude of axial load on center pile after loading from centrifuge model result and FEM analysis result are similar.
- In model series with several pile cap ratios, centrifuge model results and FEM analysis results are similar in terms of the trend of reduced settlements when the pile cap ratios increase but the absolute values are not the same.

- The trend of reduced settlement with the increase of overlying dense sand thickness layer from centrifuge model result and FEM analysis result are not alike.
- In the model series with reduced number of piles, the results are in good agreement in term of the trend but the absolute value of settlement are not the same.
- The effected arching seems not to be a major factor affecting the changes of axial load distribution between the piles in these models because the arching seems to be fully mobilized in all the models which are done in this chapter, see section 4.7.1.

From all above finding, it can be seen that the FEM described not only load settlement but also the shape of the settlement; not only the load distribution between the piles but also the load transfer from pile to each soil layer. In addition the soil arching and stress state can be shown in detail.

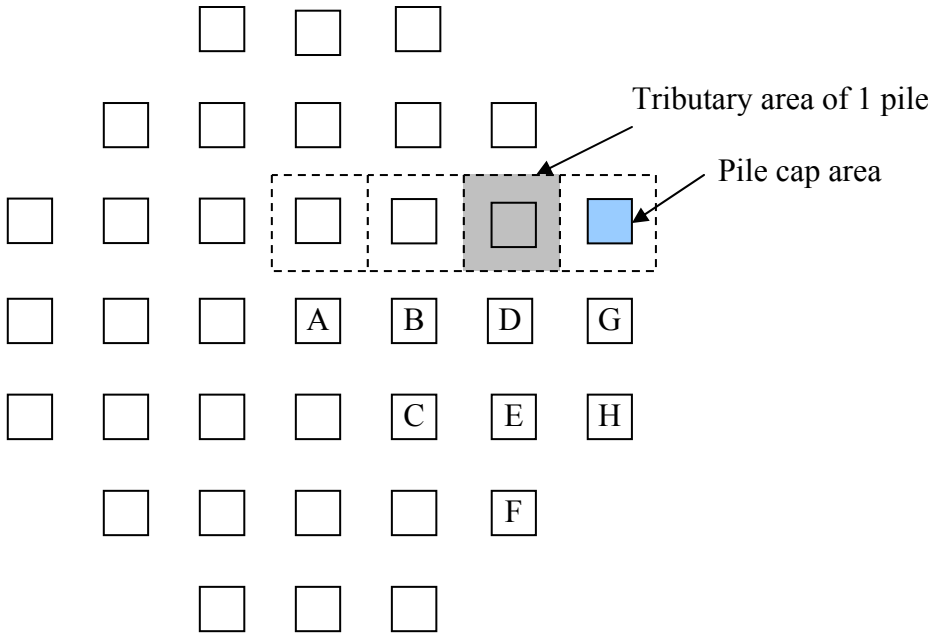

Figure 4.1 Classification of piles (after Lee, 2004)

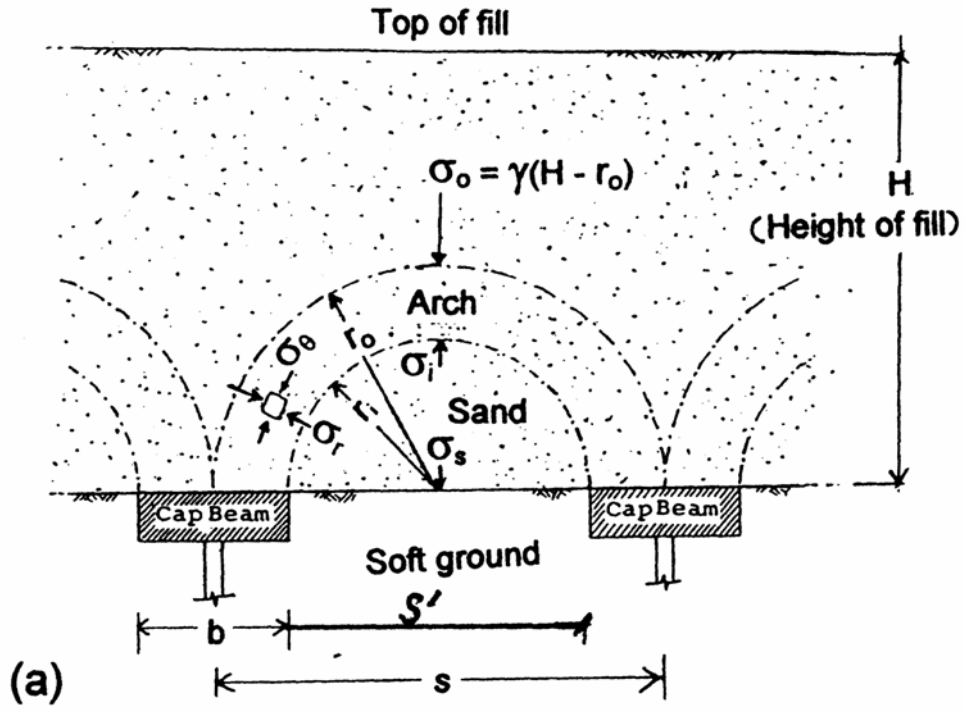

Figure 4.2 Definition of s' (after Low et al., 1991)

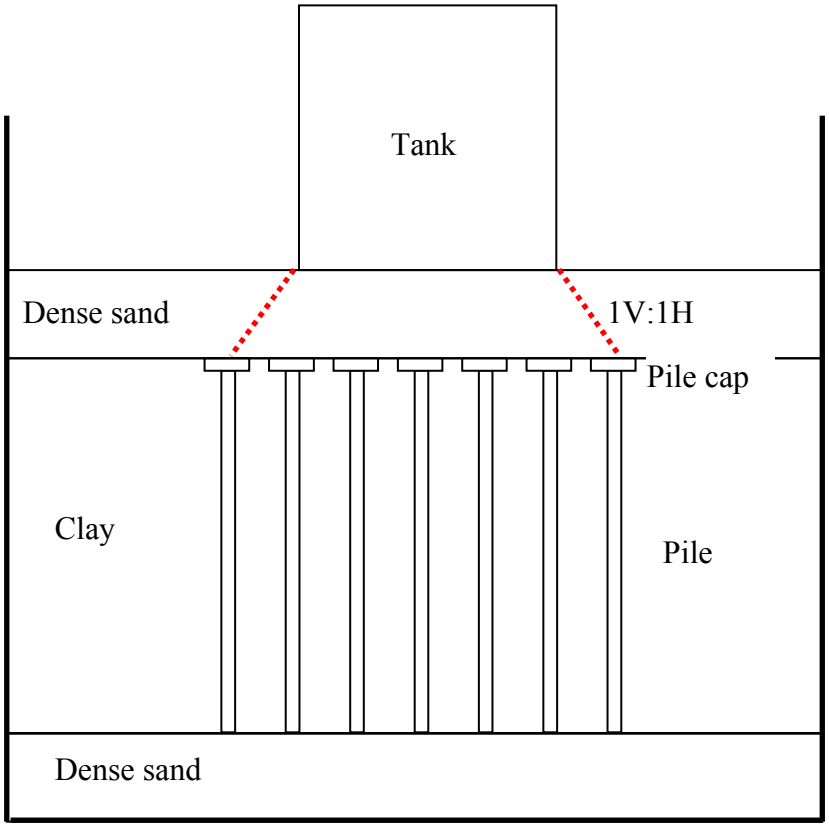

Figure 4.3 Cross-section view of model using in centrifuge test (after Lee, 2004)

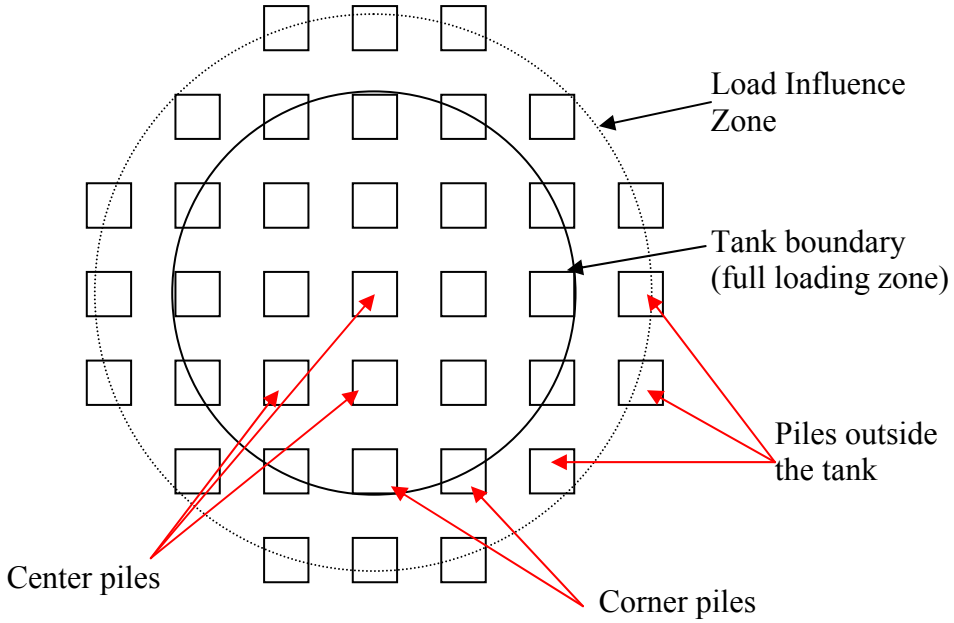

Figure 4.4 Plan view of model using in centrifuge test (after Lee, 2004)

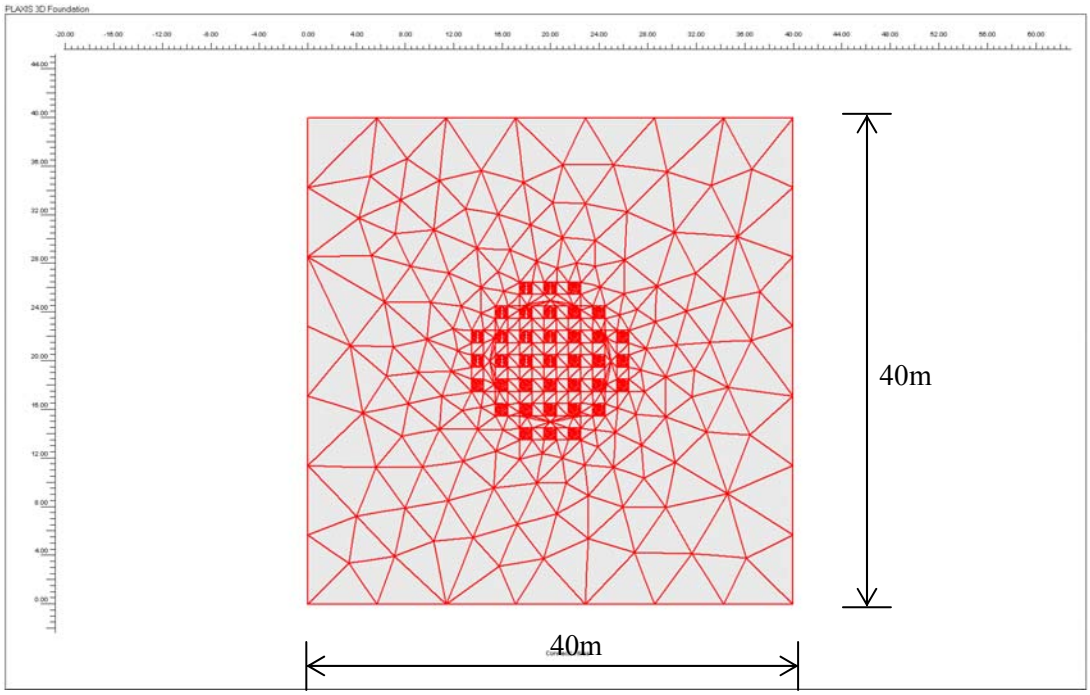

Figure 4.5 Two-dimension mesh of the model.

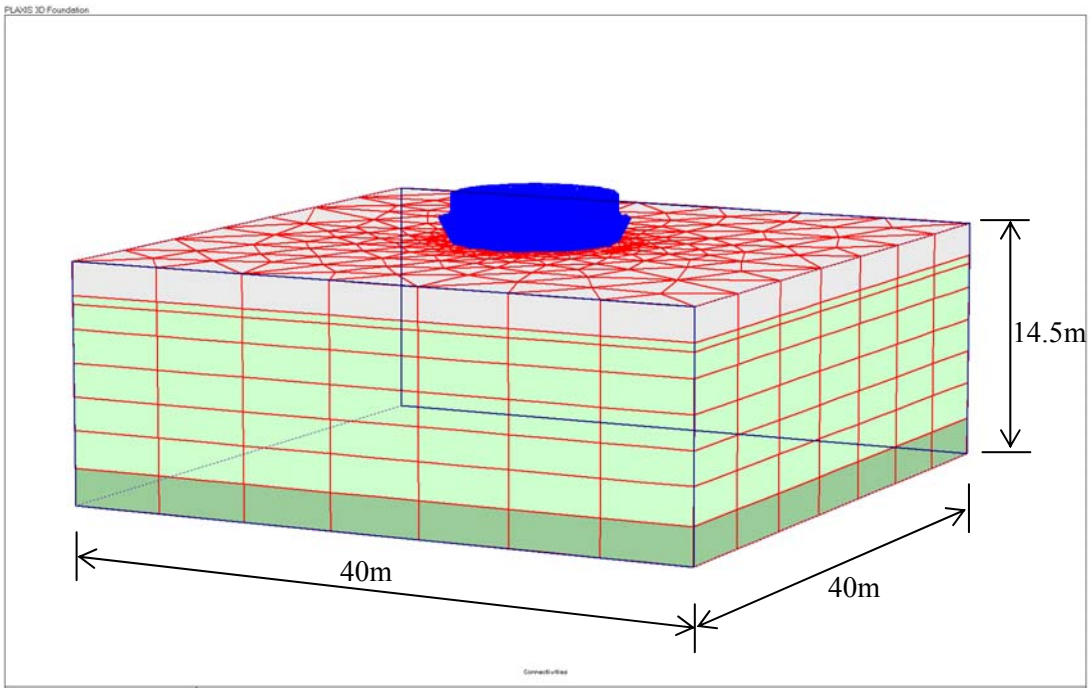

Figure 4.6 Three-dimension mesh of the model.

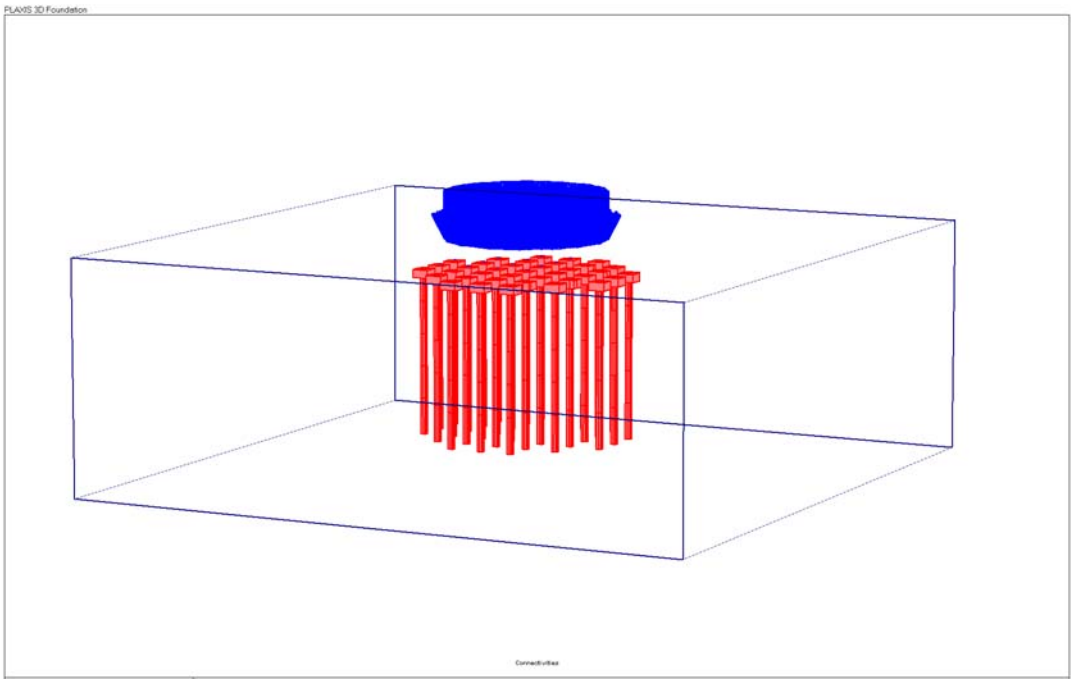

Figure 4.7 Three-dimension view of pile group in FEM

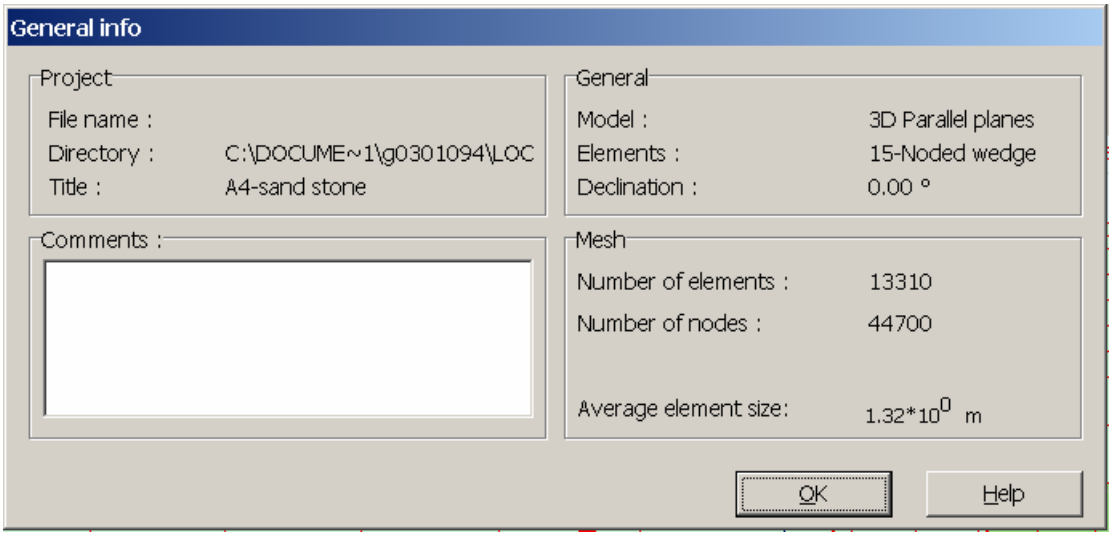

Figure 4.8 General information for FEM model.

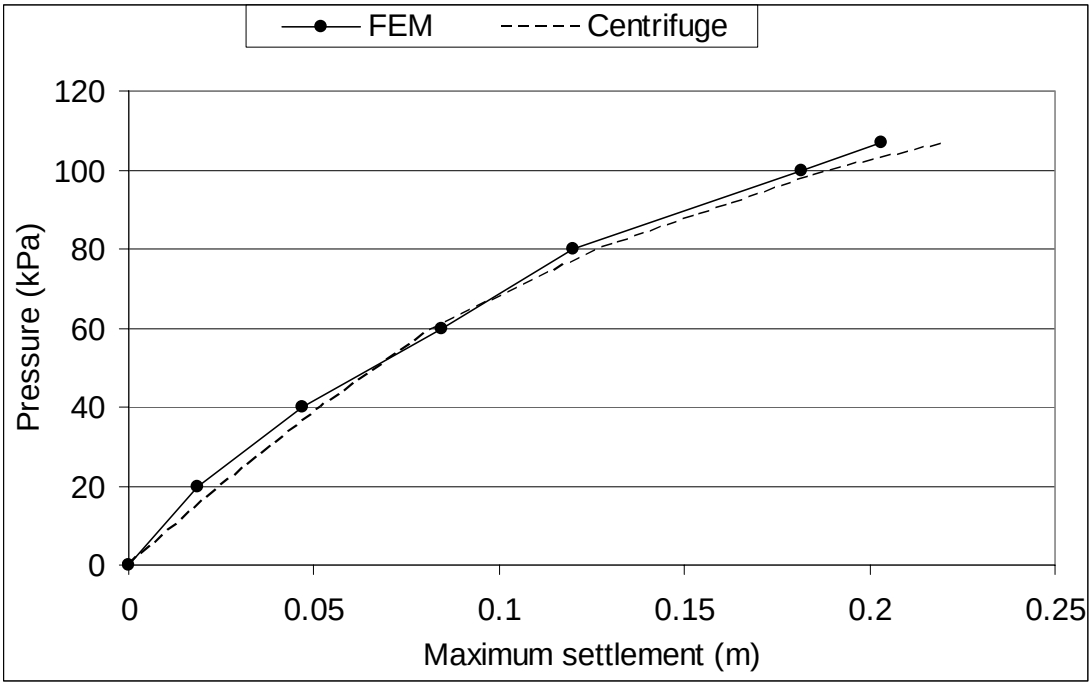

Figure 4.9 Development of maximum tank settlement with pressure (Test P1)

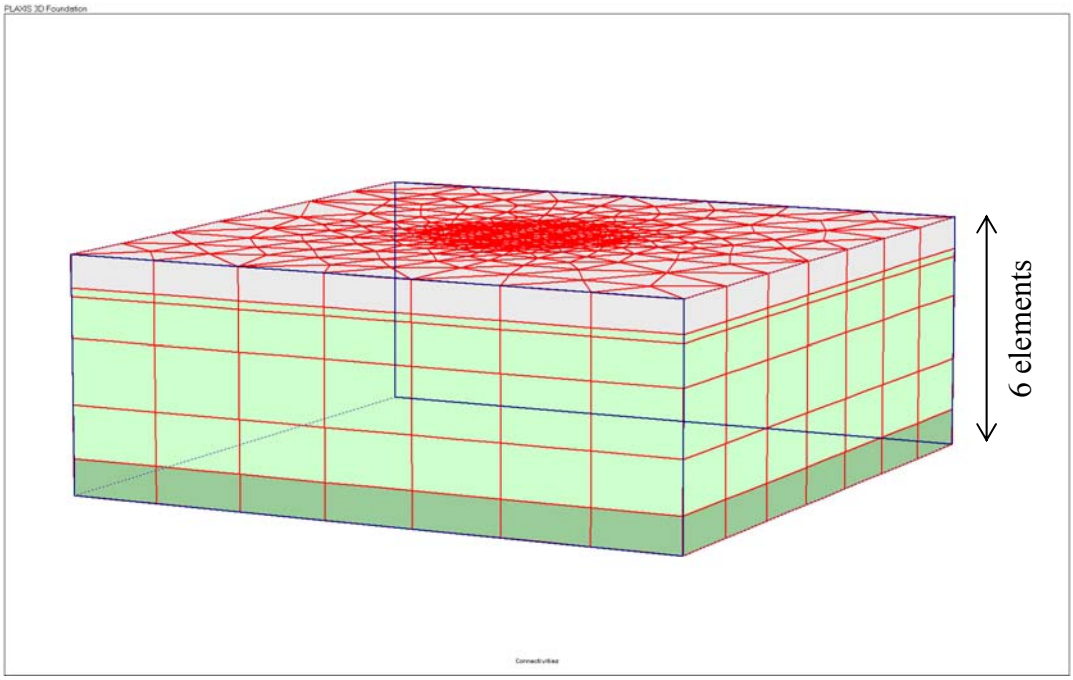

Figure 4.10 Three-dimension mesh of the model A4-Coarse mesh.
(Approximation number of elements: 8500; Approximation number of nodes: 28000)

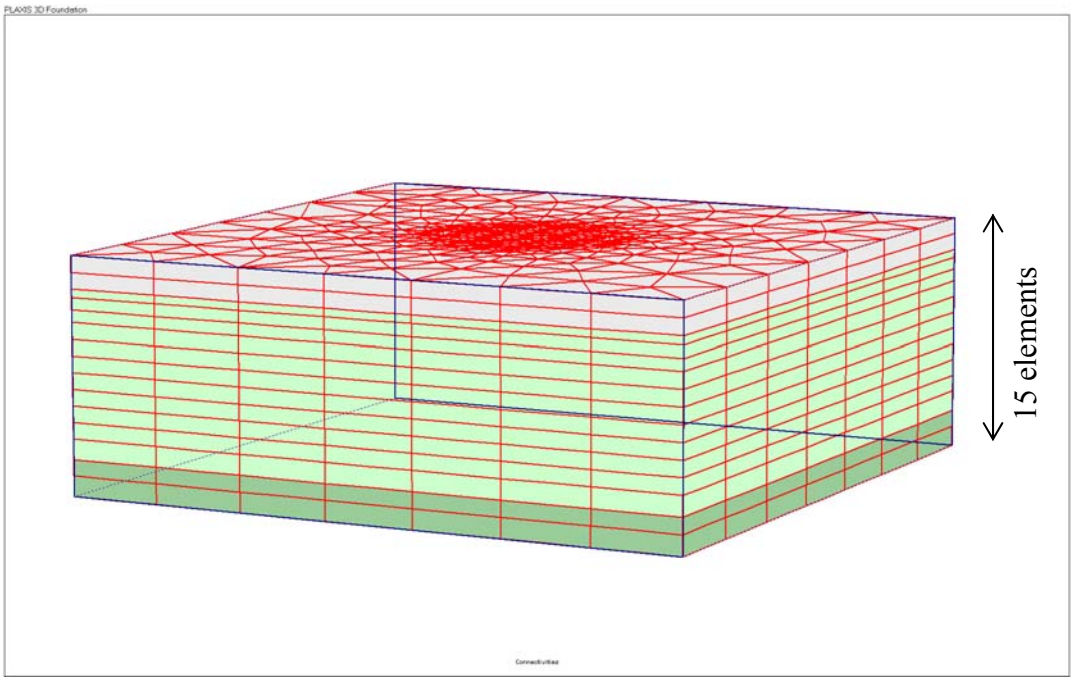

Figure 4.11 Three-dimension mesh of the model A4-Fine mesh.
(Approximate number of elements: 18000; approximate number of nodes: 58000)

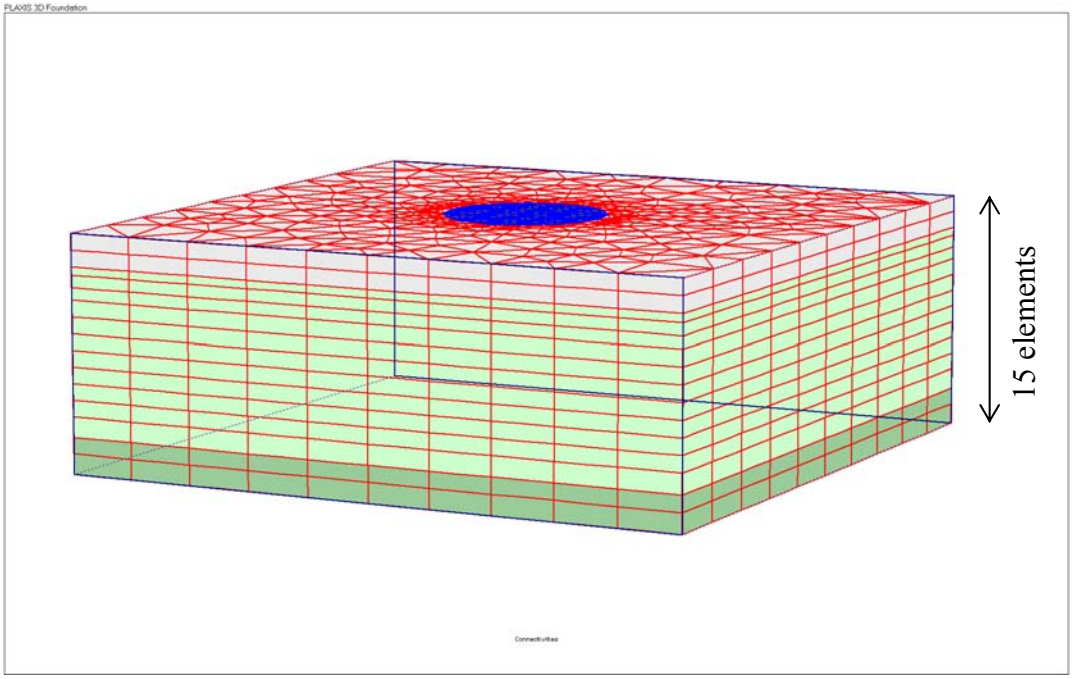

Figure 4.12 Three-dimension mesh of the model A4-Very Fine mesh.
(Approximation number of elements: 24000; Approximation number of nodes: 77000)

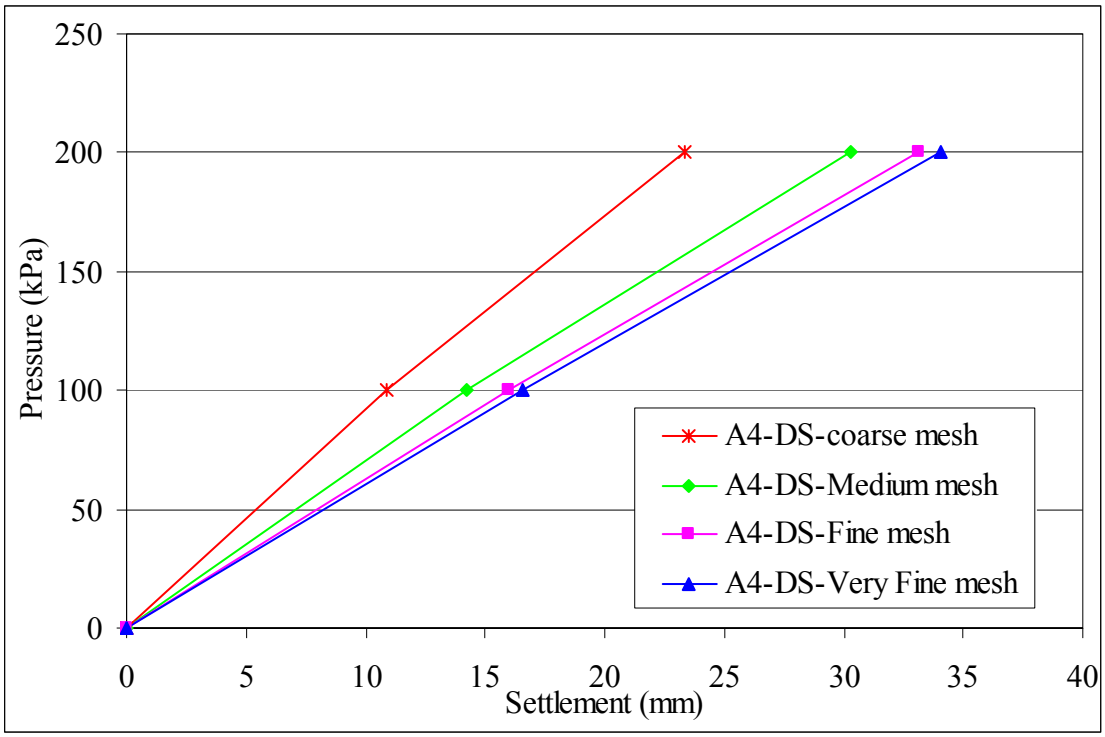

Figure 4.13 Development of maximum tank settlement with pressure from tank for model of test series 4 (dense sand bed layer).

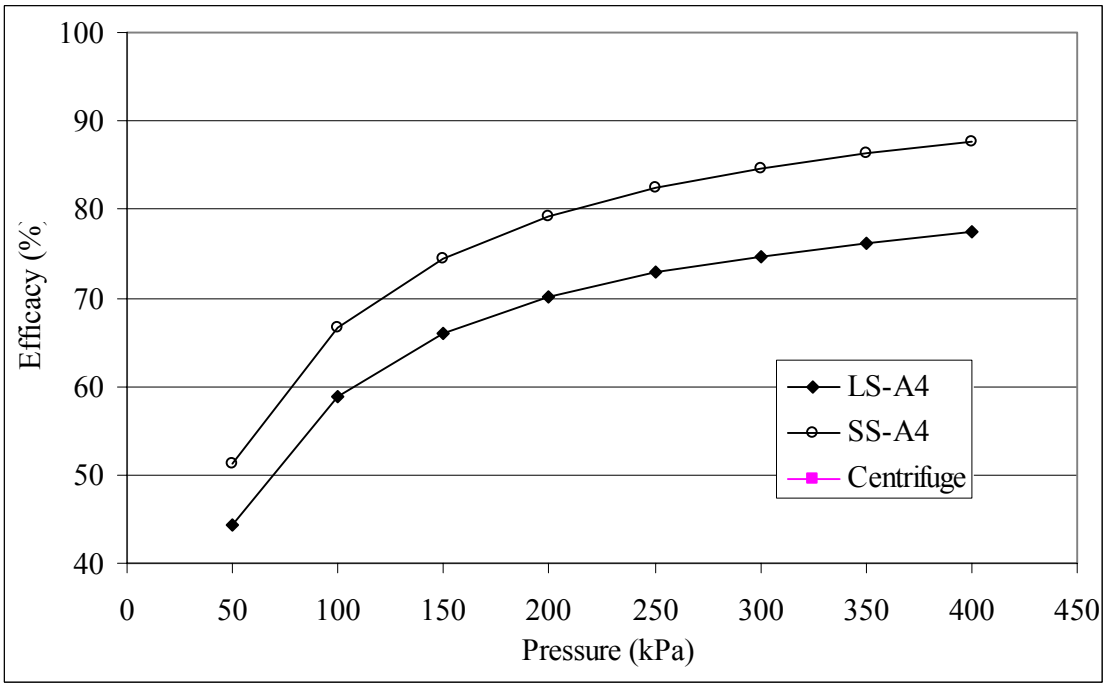

Figure 4.14 Development of efficacy with pressure

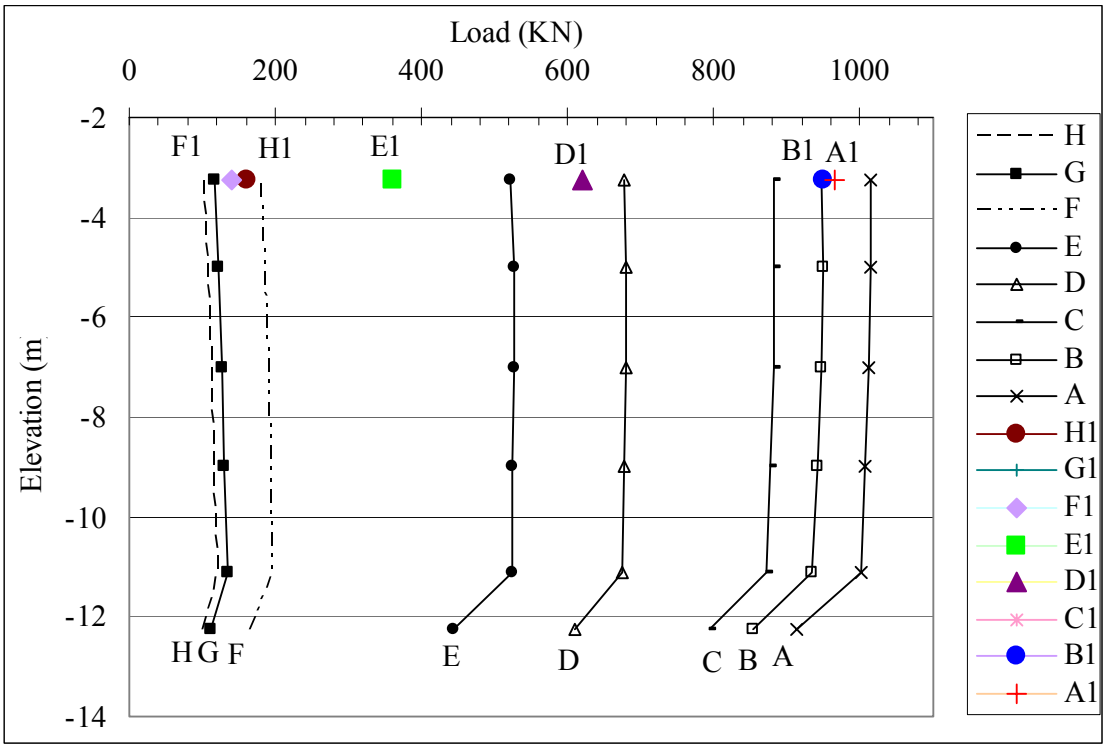

Figure 4.15 Load transfer curves in model of test DS-A4, 220kPa pressure (Black lines present load transfer curve from FEM analysis; Color dots present load distribution from Centrifuge observation)

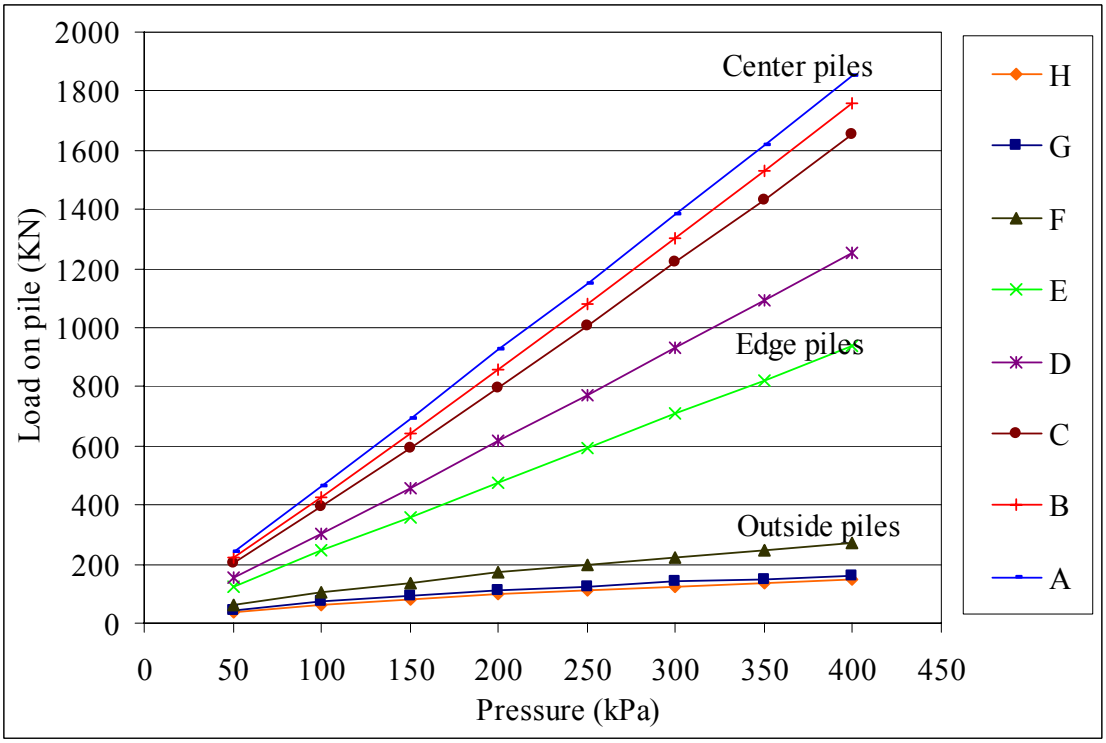

Figure 4.16 Comparision of load distribution among pile when load increasing (DS-A4)

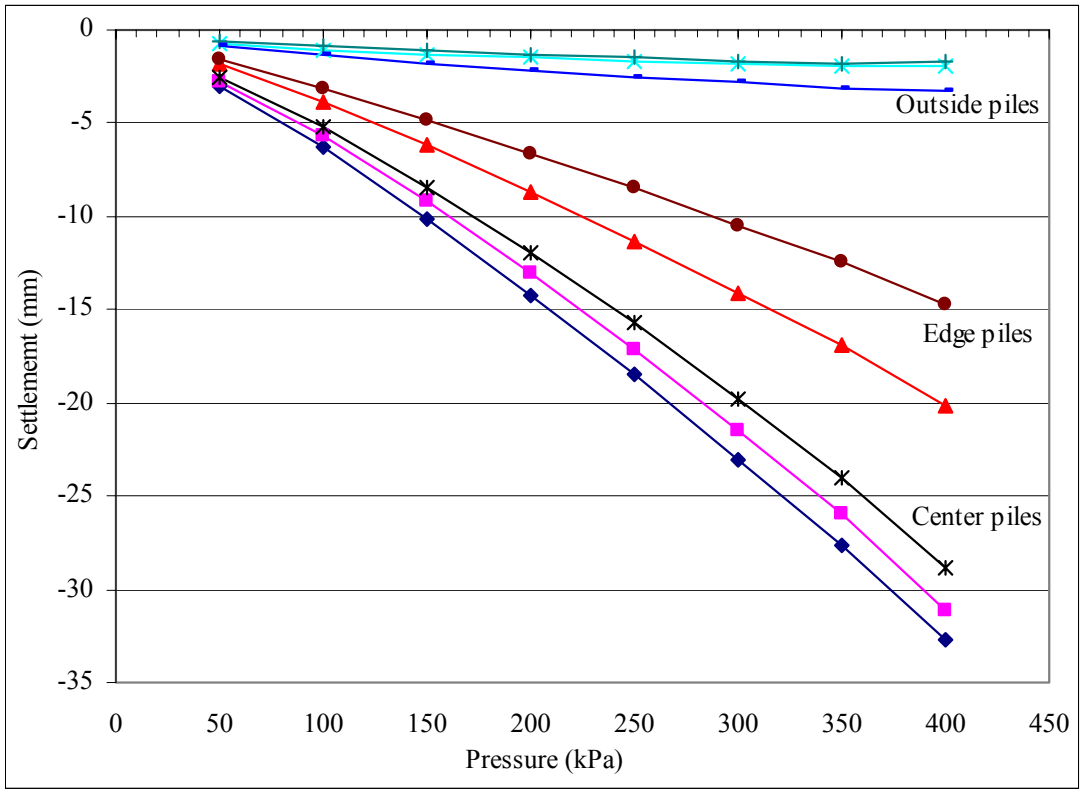

Figure 4.17 Comparision of load settlement curve among pile when load increasing (DS-A4)

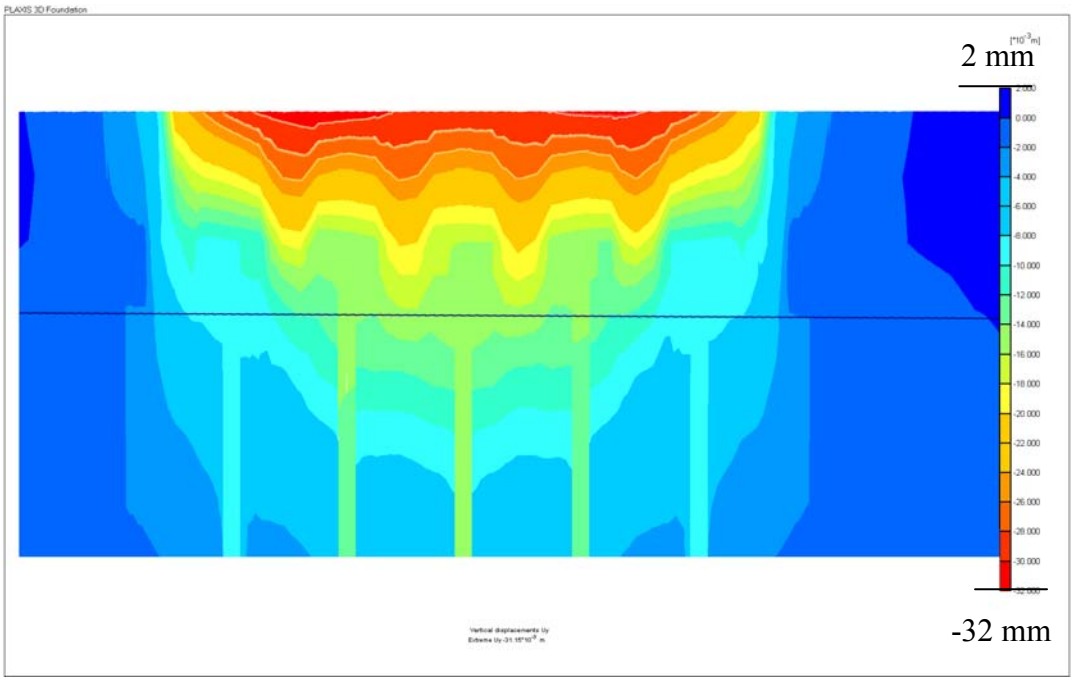

Figure 4.18 Vertical displacements at pressure of 220kPa (DS-A4) – cross section.

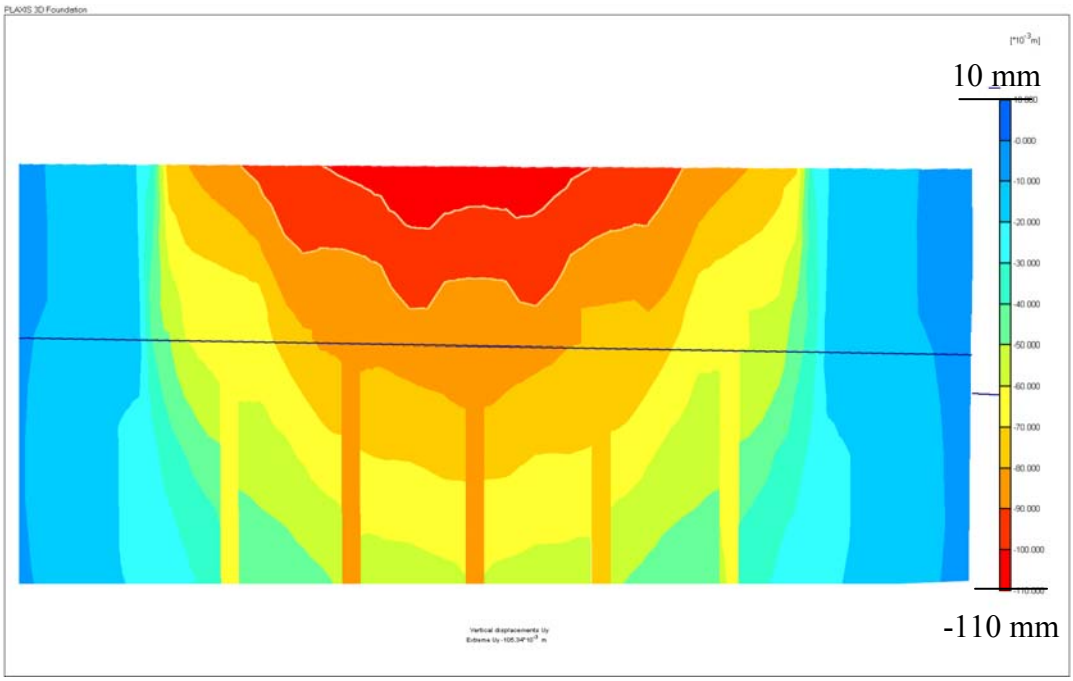

Figure 4.19 Vertical displacements at pressure of 220kPa (LS-A4) – cross section.

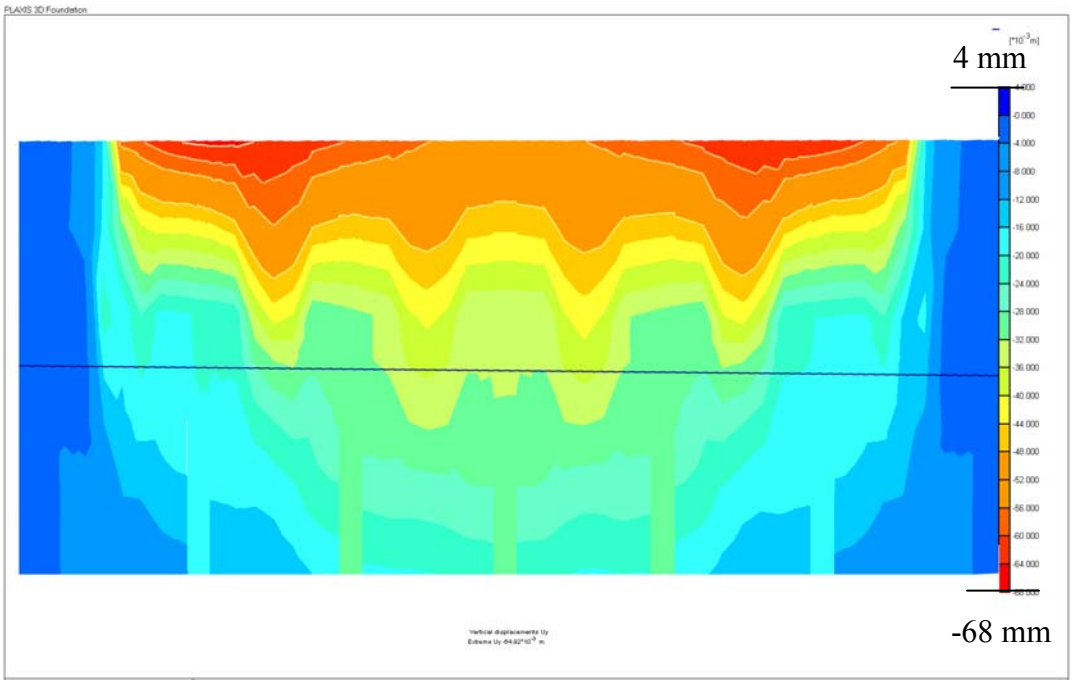

Figure 4.20 Vertical displacements at pressure of 400kPa (DS-A4) – cross section.

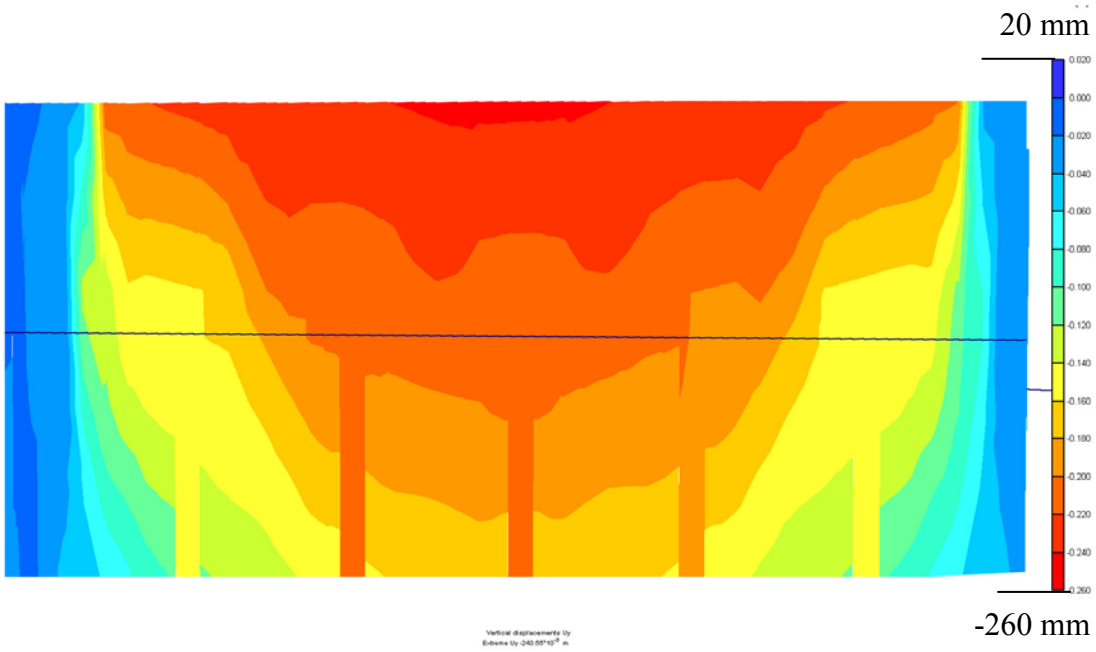

Figure 4.21 Vertical displacements at pressure of 400kPa (LS-A4) – cross section.

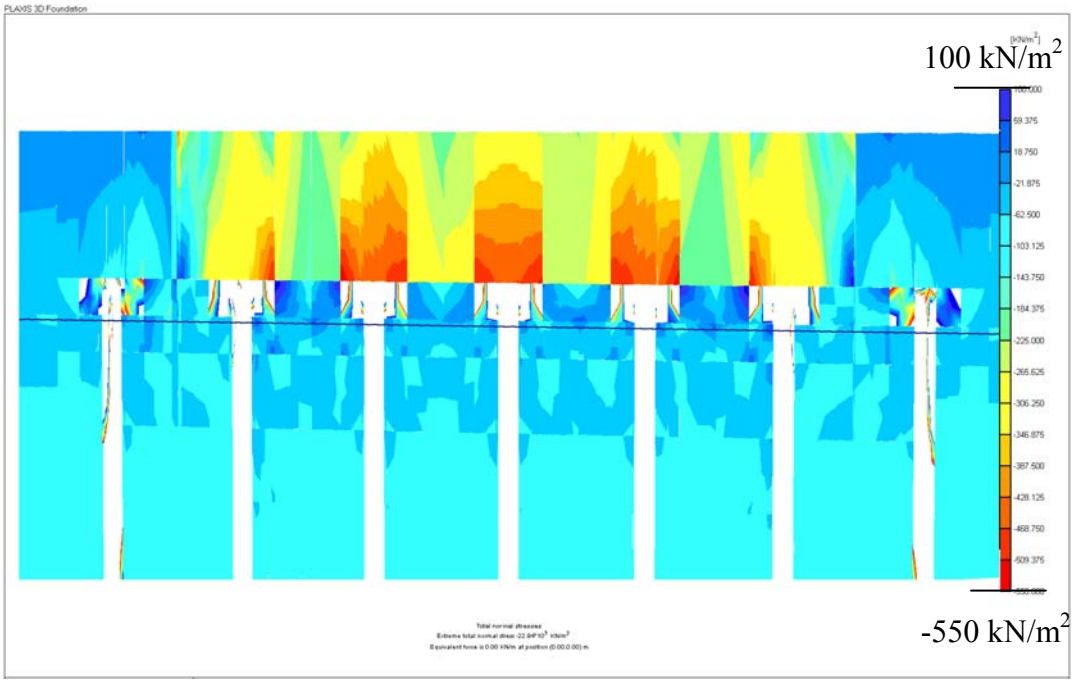

Figure 4.22 Total normal stresses at pressure of 220kPa (DS-A4) – cross section.

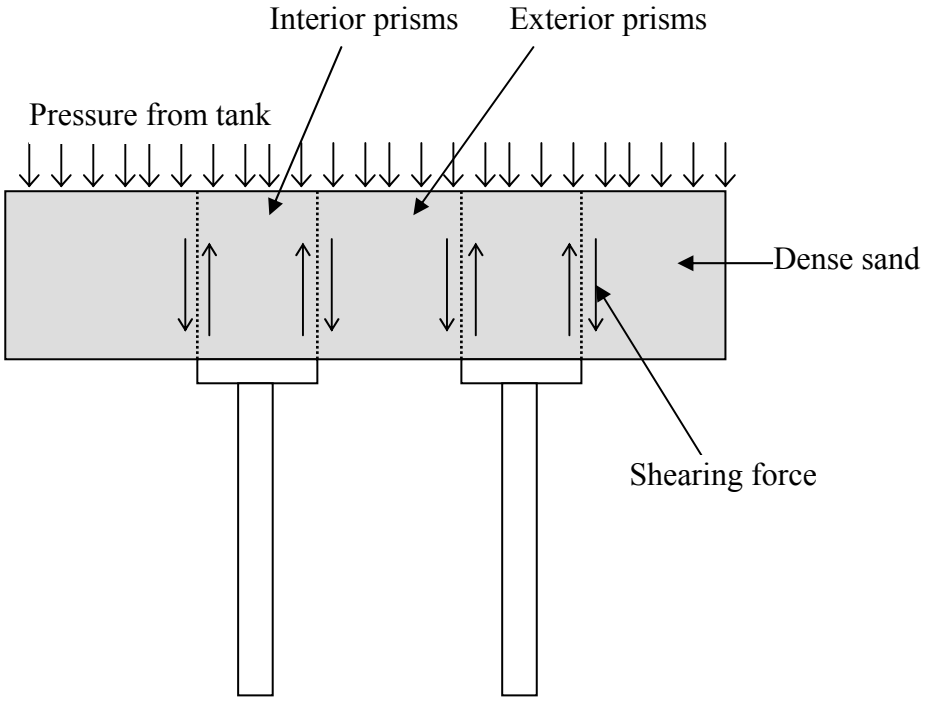

Figure 4.23 Shearing forces between interior prisms and exterior prisms (after S.C. Lee, 2004)

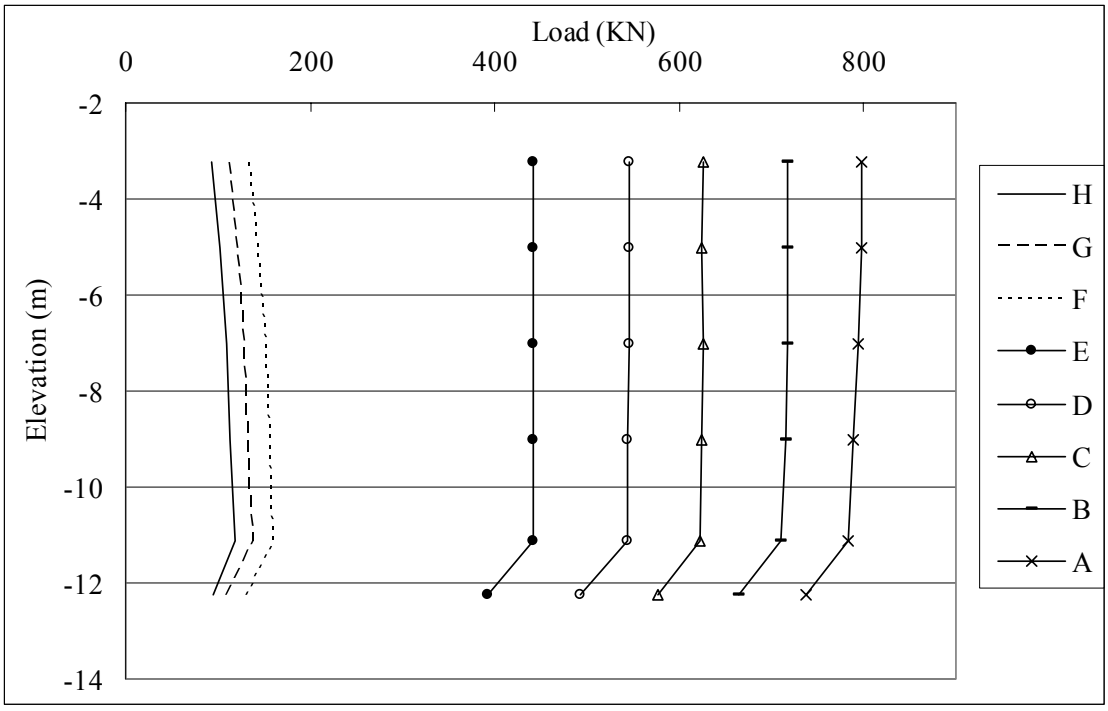

Figure 4.24 Load transfer curves in model of test DS-A1, 180kPa pressure.

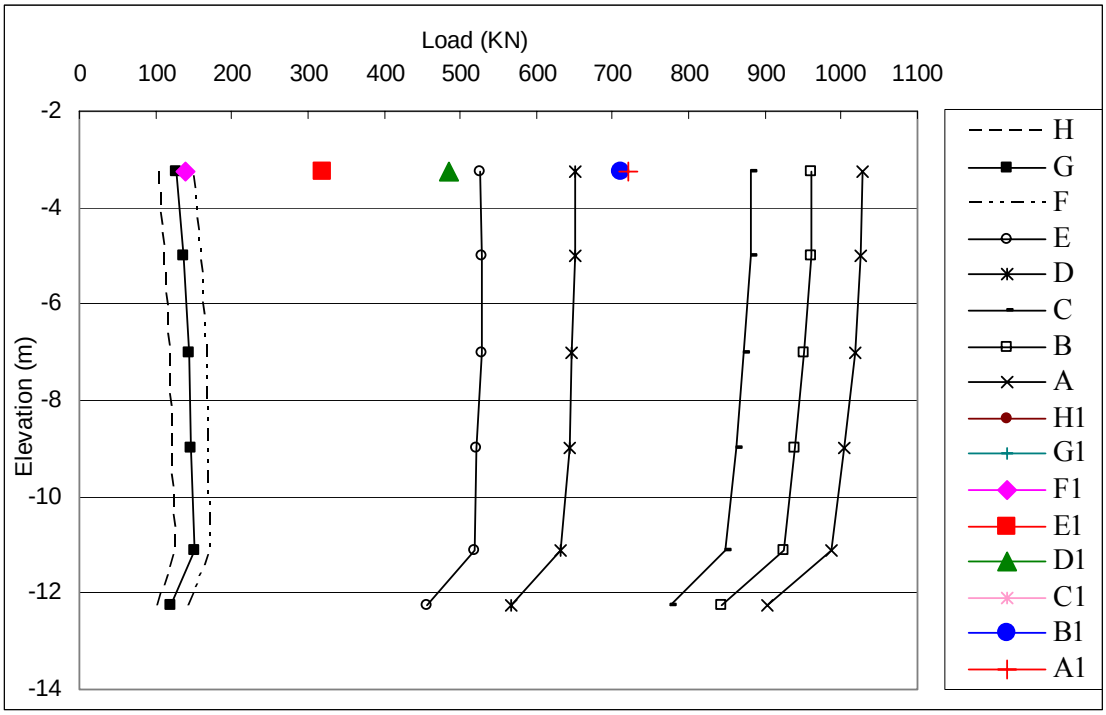

Figure 4.25 Load transfer curves in model of test DS-A2, 220kPa pressure. (Black lines present load transfer curve from FEM analysis; Color dots present load distribution from Centrifuge observation)

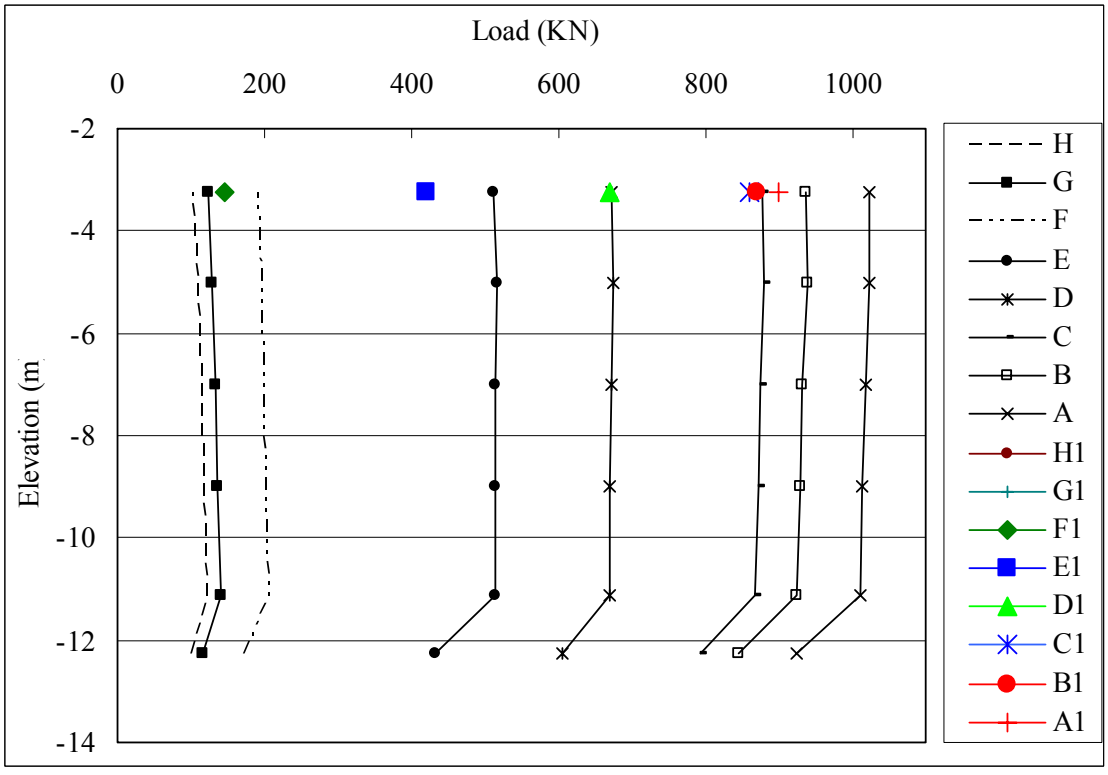

Figure 4.26 Load transfer curves in model of test DS-A3, 220kPa pressure. (Black lines present load transfer curve from FEM analysis; Color dots present load distribution from Centrifuge observation)

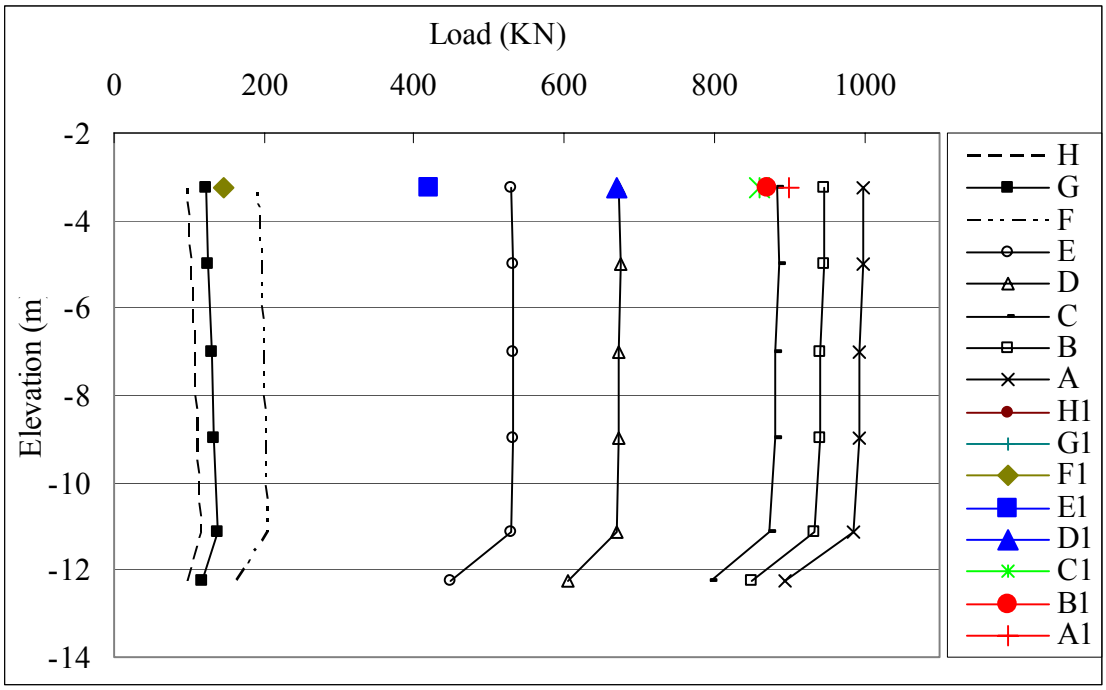

Figure 4.27 Load transfer curves in model of test DS-A5, 220kPa pressure (Black lines present load transfer curve from FEM analysis; Color dots present load distribution from Centrifuge observation)

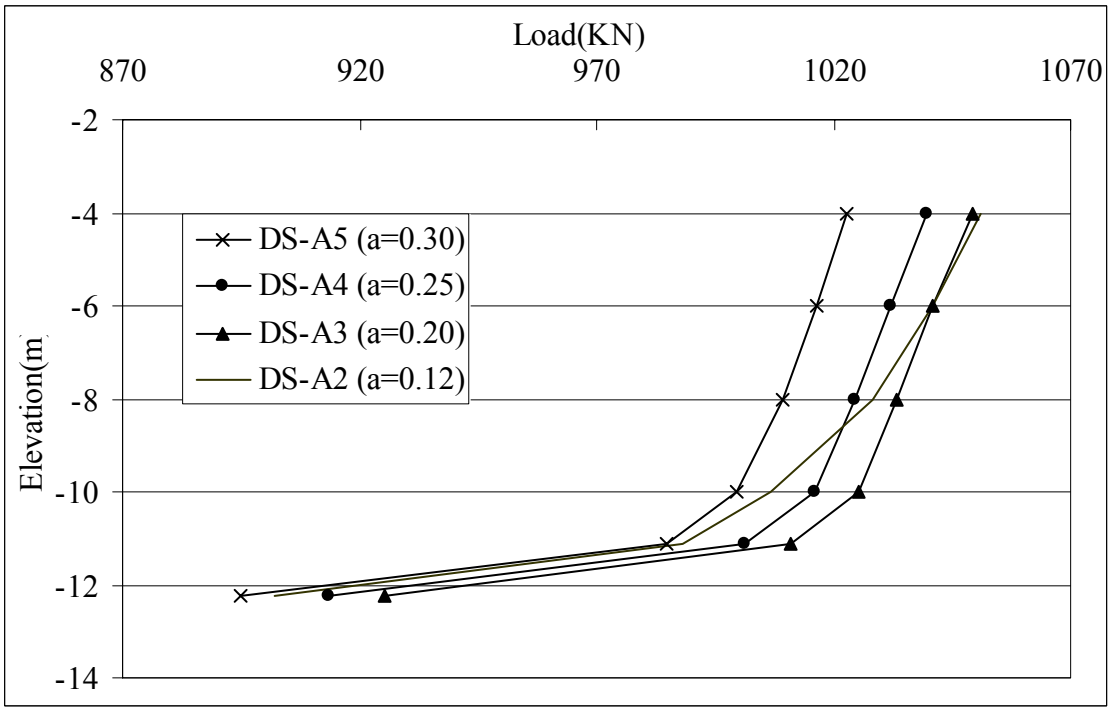

Figure 4.28 Comparision of load transfer curve of pile type A (dense sand bed layer).

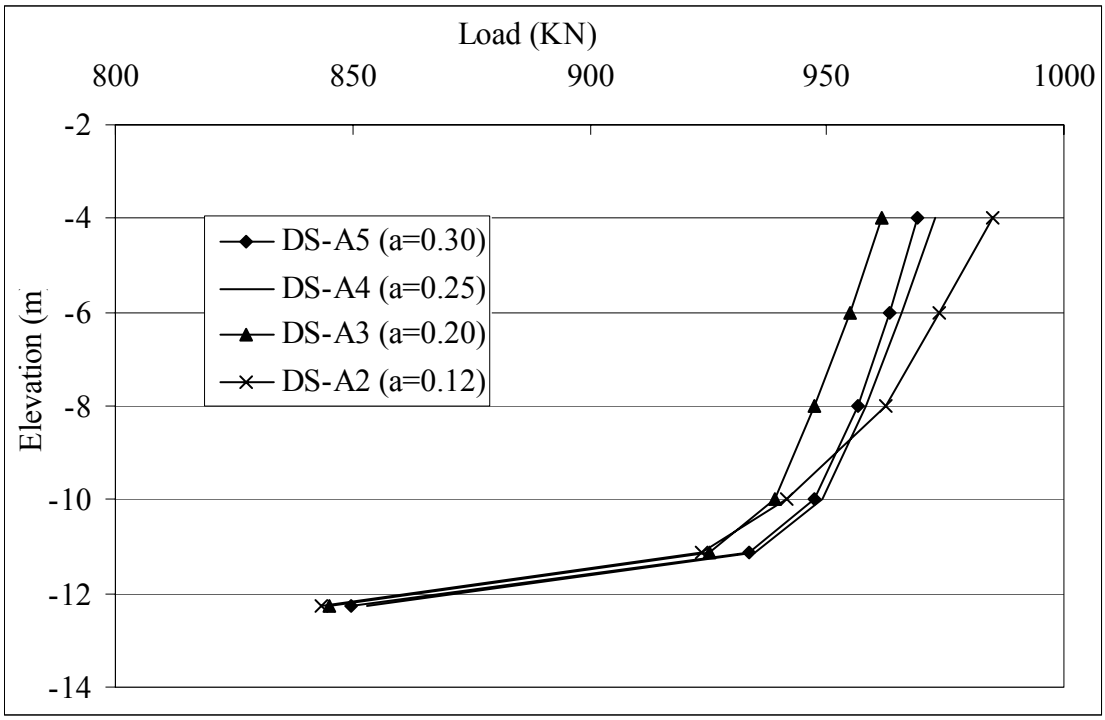

Figure 4.29 Comparision of load transfer curve of pile type B (dense sand bed layer).

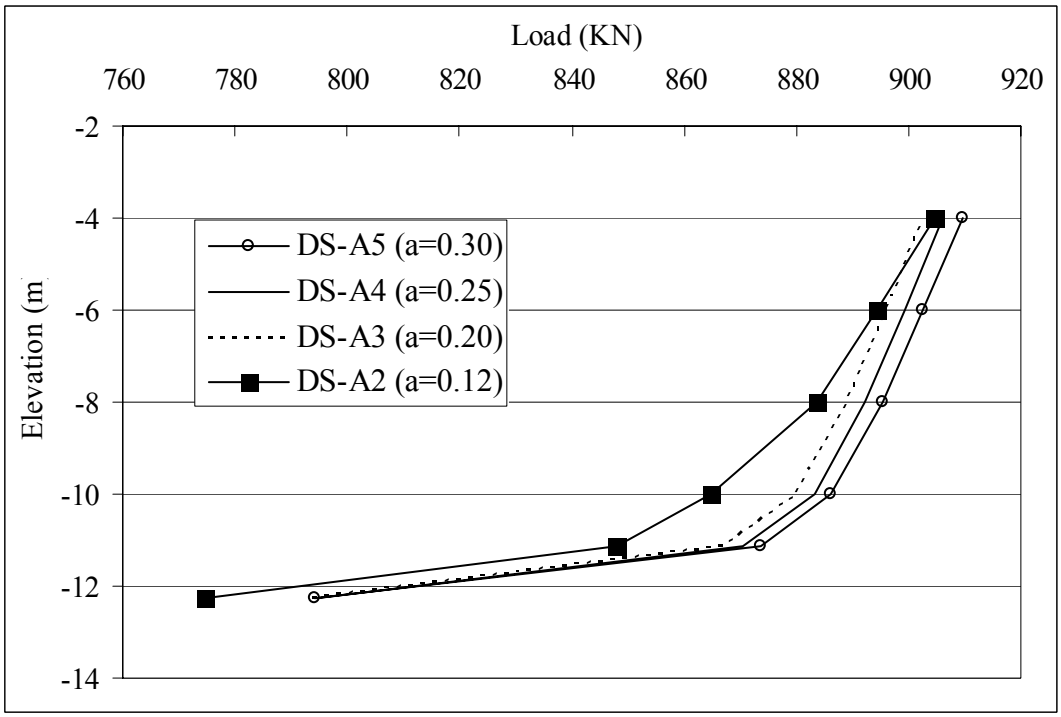

Figure 4.30 Comparision of load transfer curve of pile type C (dense sand bed layer).

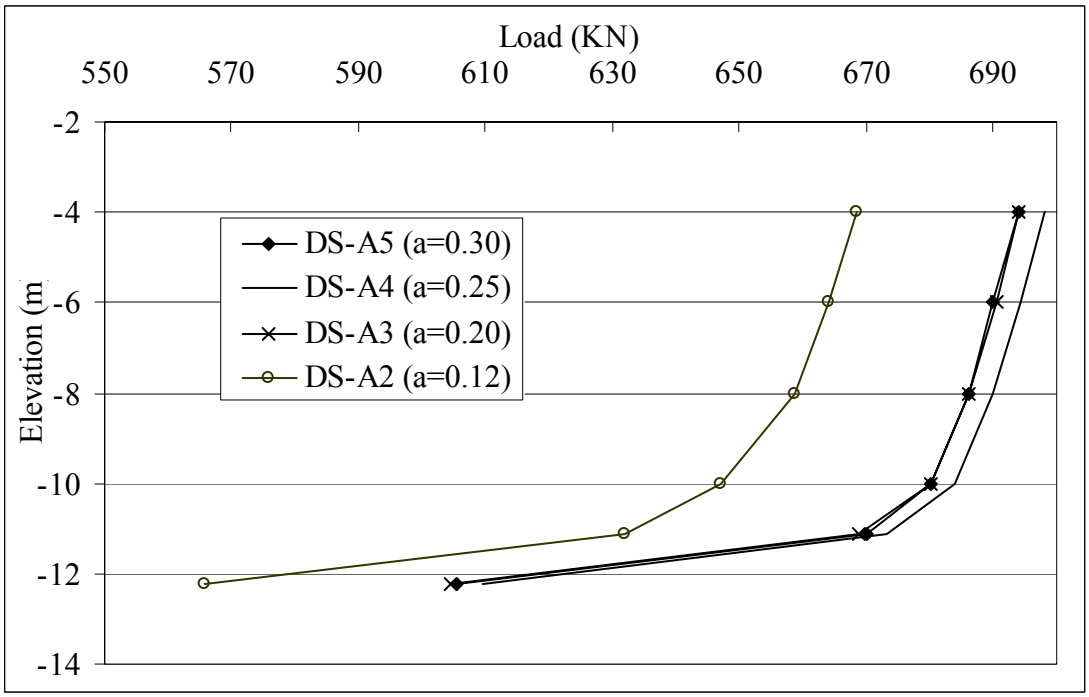

Figure 4.31 Comparision of load transfer curve of pile type D (dense sand bed layer).

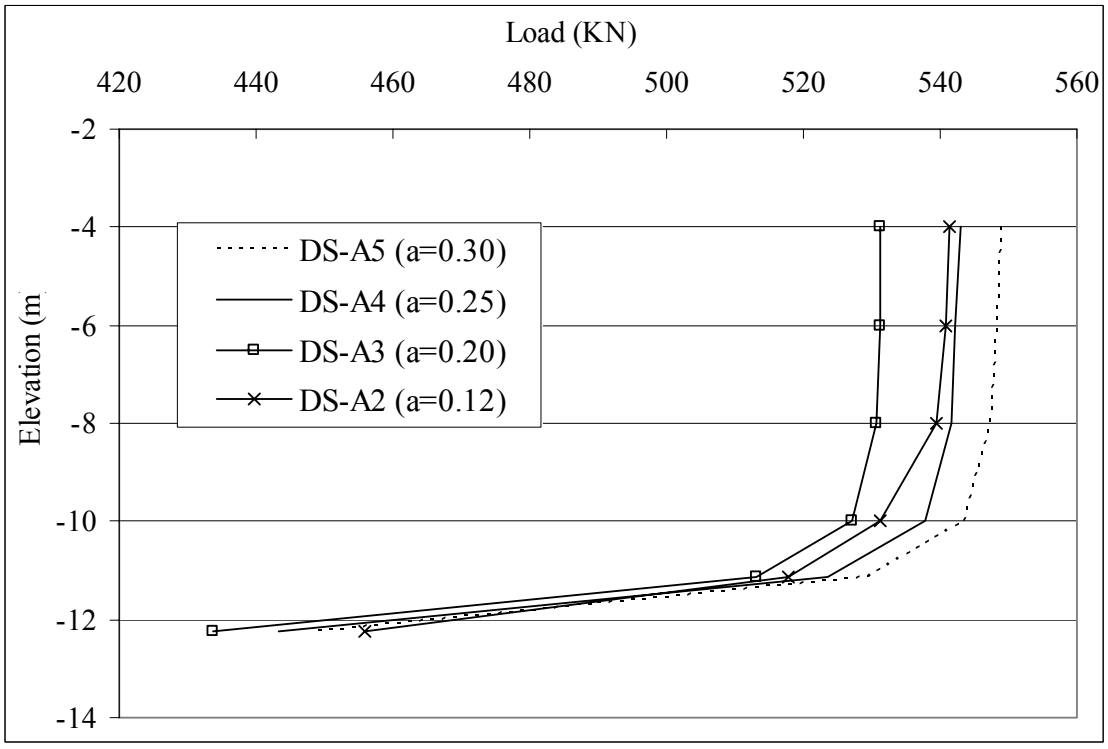

Figure 4.32 Comparision of load transfer curve of pile type E (dense sand bed layer).

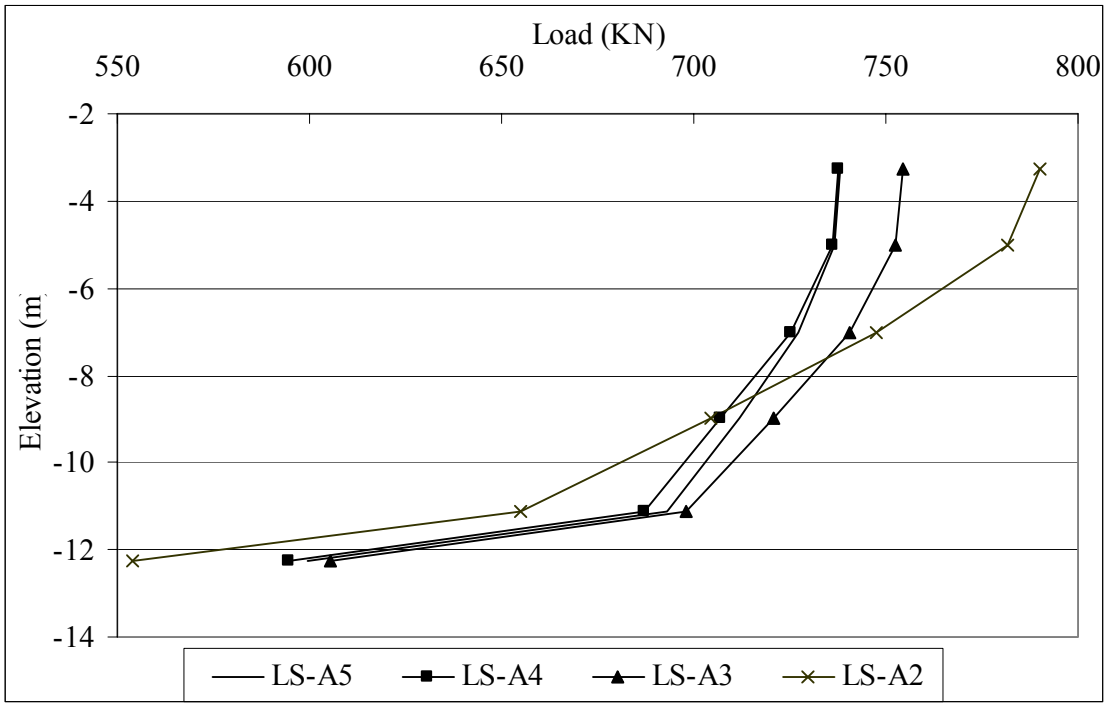

Figure 4.33 Comparision of load transfer curve of pile type A (loose sand bed layer).

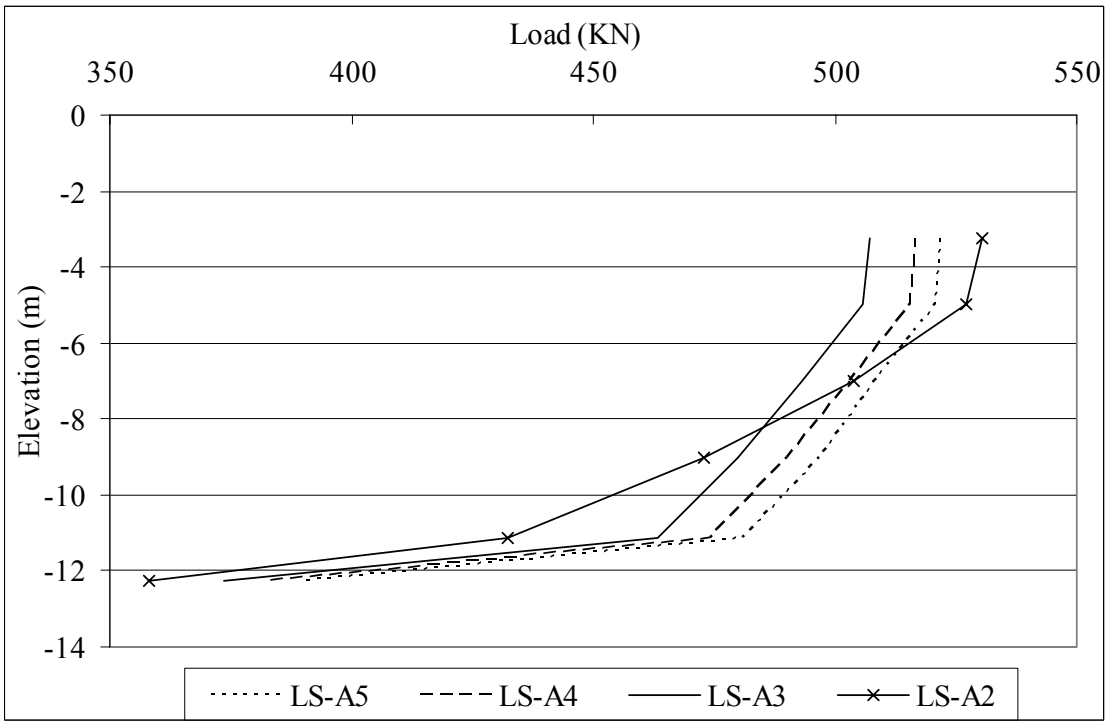

Figure 4.34 Comparision of load transfer curve of pile type B (loose sand bed layer).

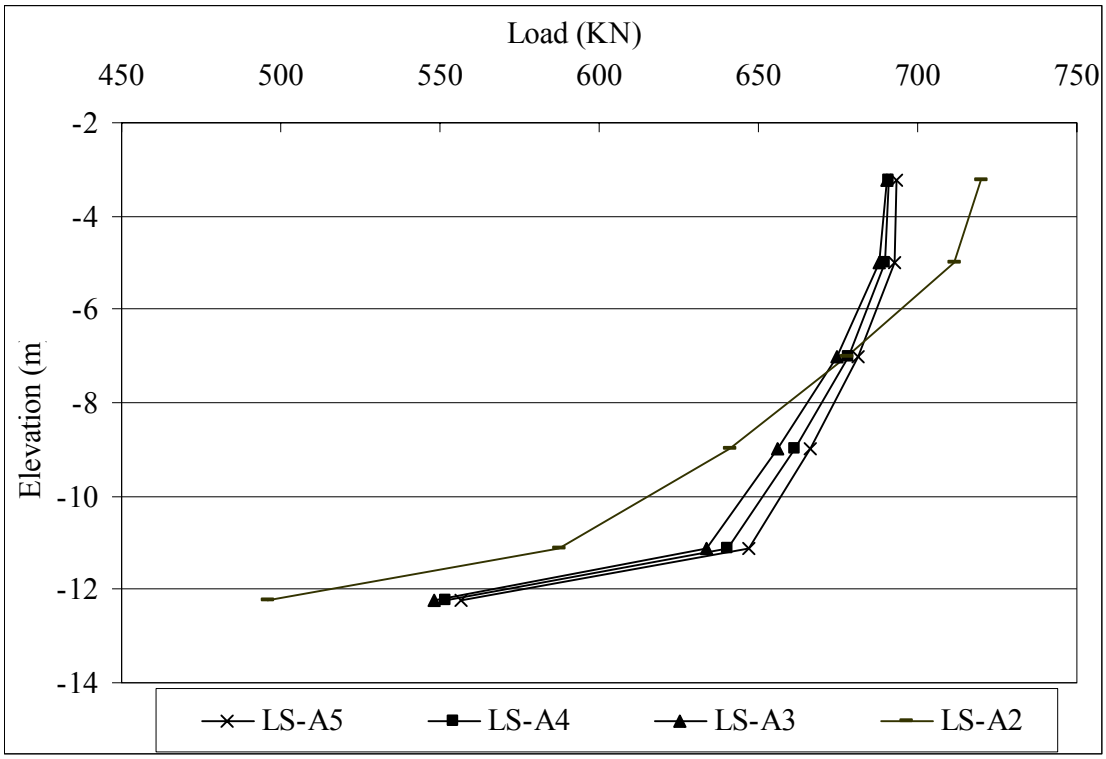

Figure 4.35 Comparision of load transfer curve of pile type C (loose sand bed layer).

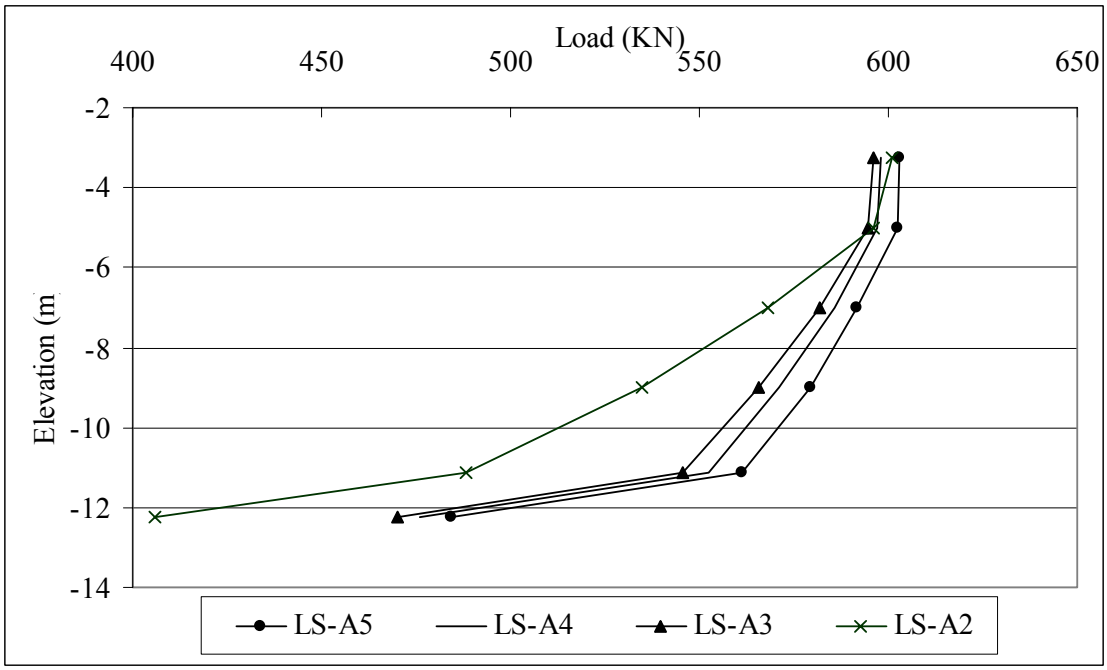

Figure 4.36 Comparision of load transfer curve of pile type D (loose sand bed layer).

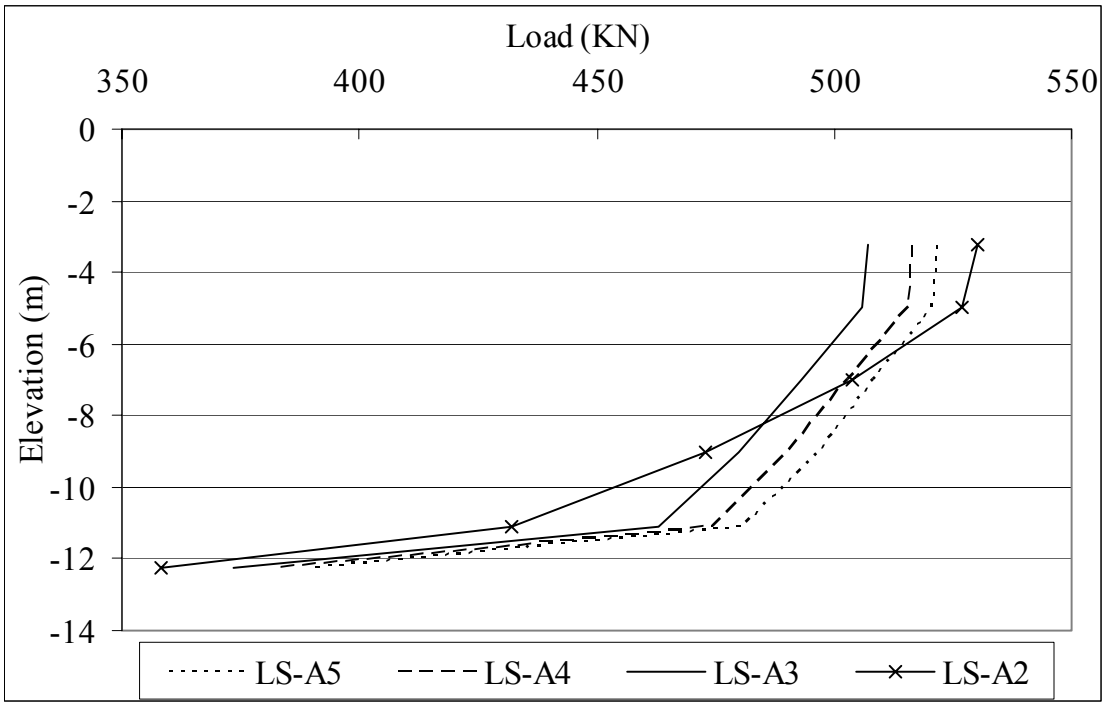

Figure 4.37 Comparision of load transfer curve of pile type E (loose sand bed layer).

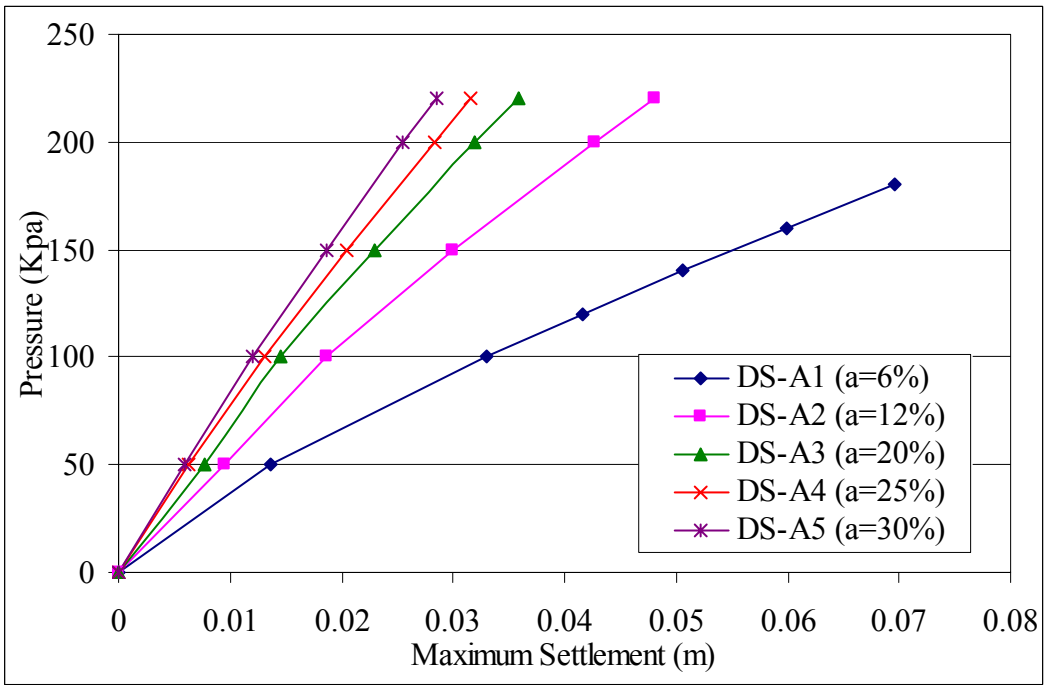

Figure 4.38 Development of maximum tank settlement with pressure from tank for model of test series 1 (dense sand bed layer).

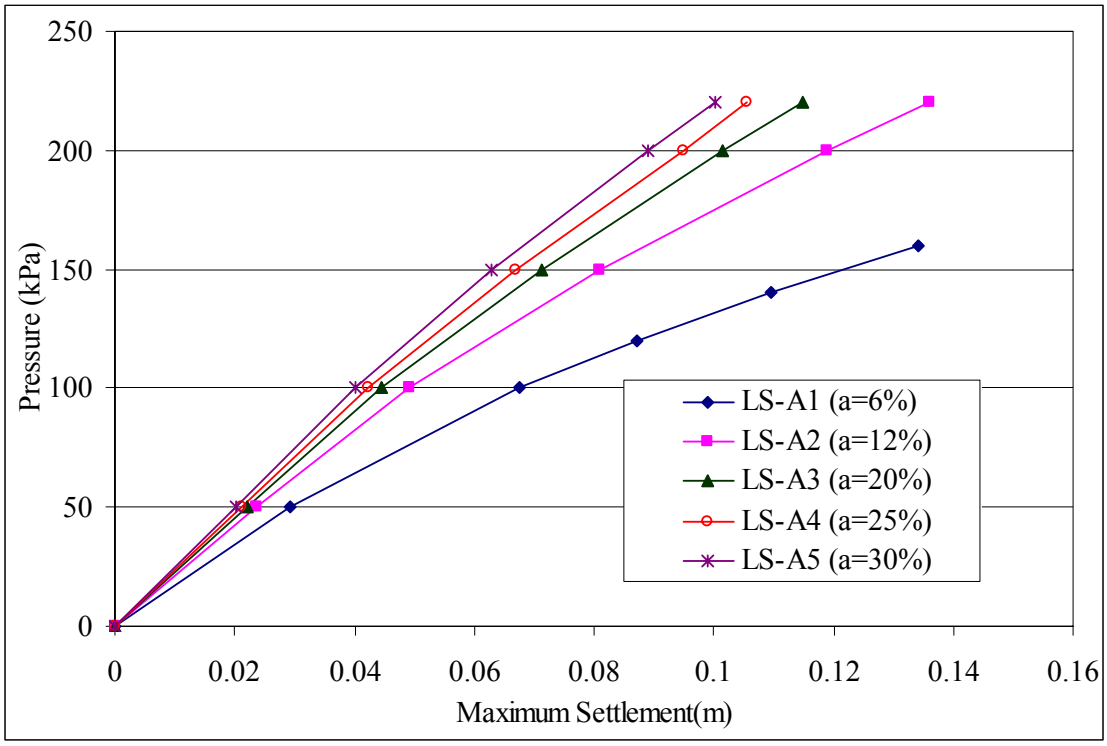

Figure 4.39 Development of maximum tank settlement with pressure from tank for model of test series 1 (loose sand bed layer).

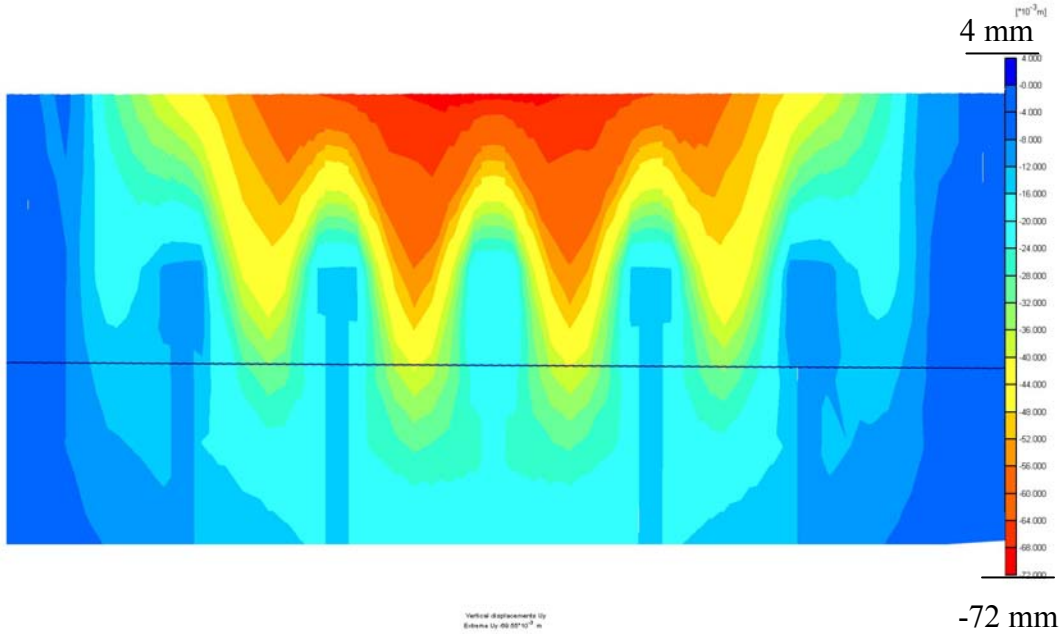

Figure 4.40 Vertical displacements at pressure of 180kPa (DS-A1) – cross section.

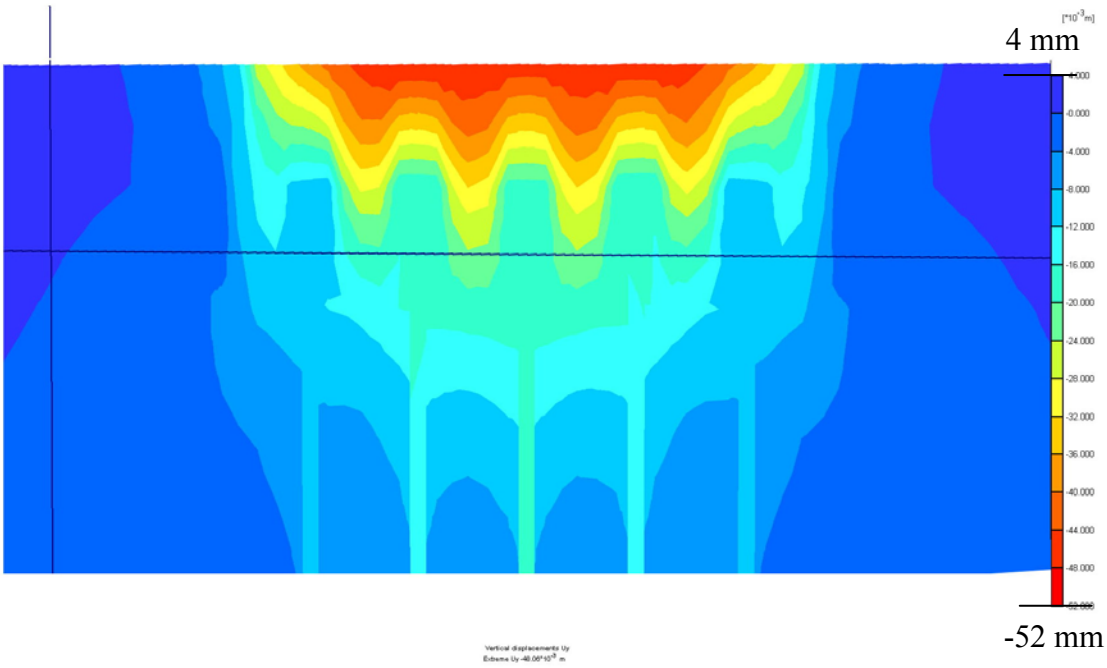

Figure 4.41 Vertical displacements at pressure of 220kPa (DS-A2) – cross section.

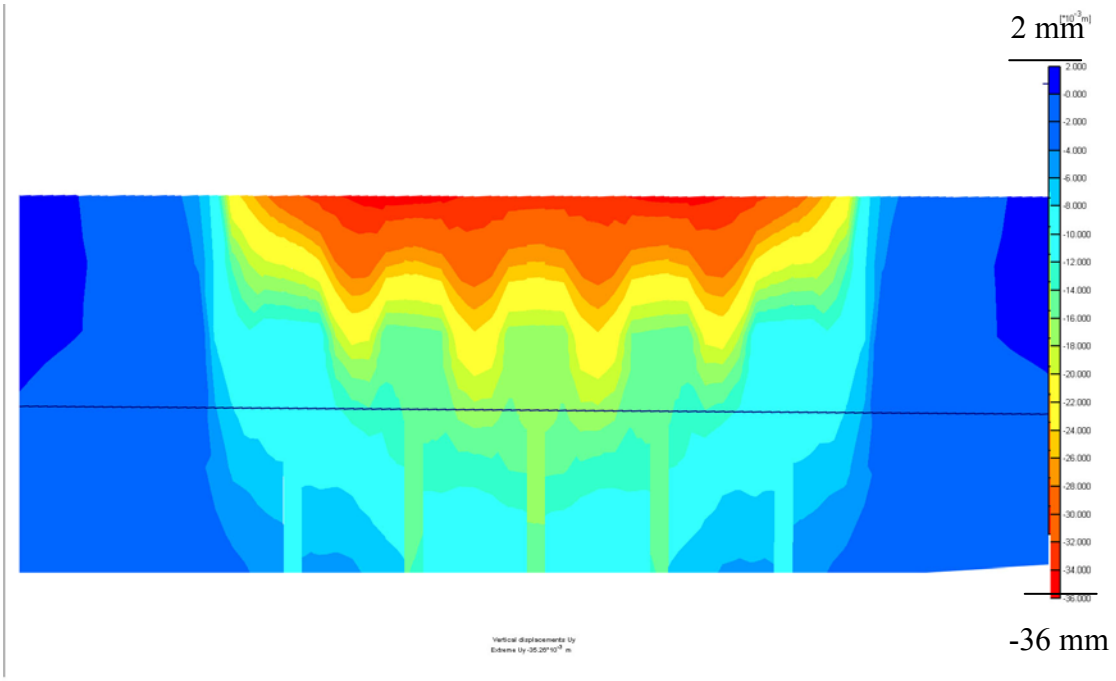

Figure 4.42 Vertical displacements at pressure of 220kPa (DS-A3) – cross section.

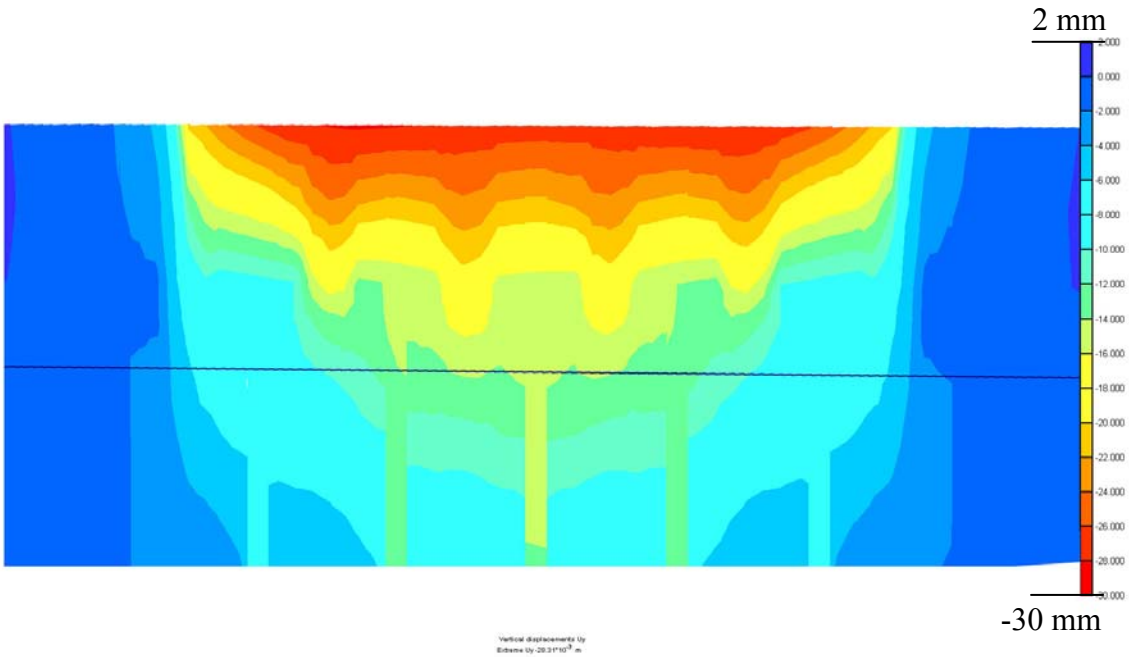

Figure 4.43 Vertical displacements at pressure of 220kPa (DS-A5) – cross section.

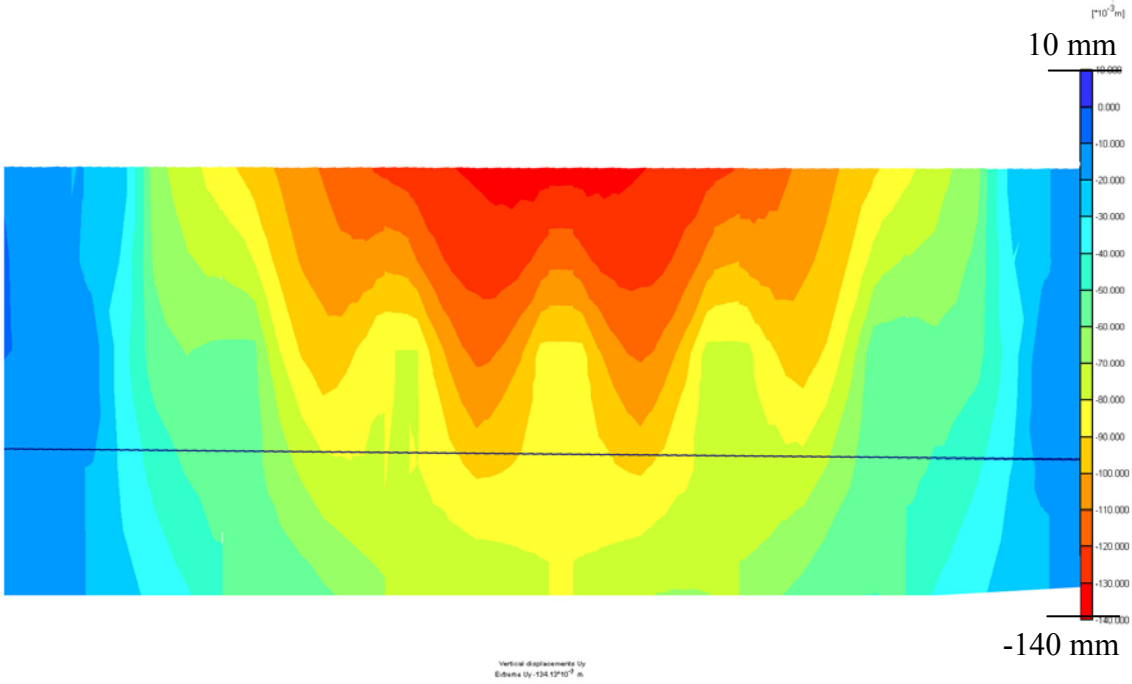

Figure 4.44 Vertical displacements at pressure of 160kPa (LS-A1) – cross section.

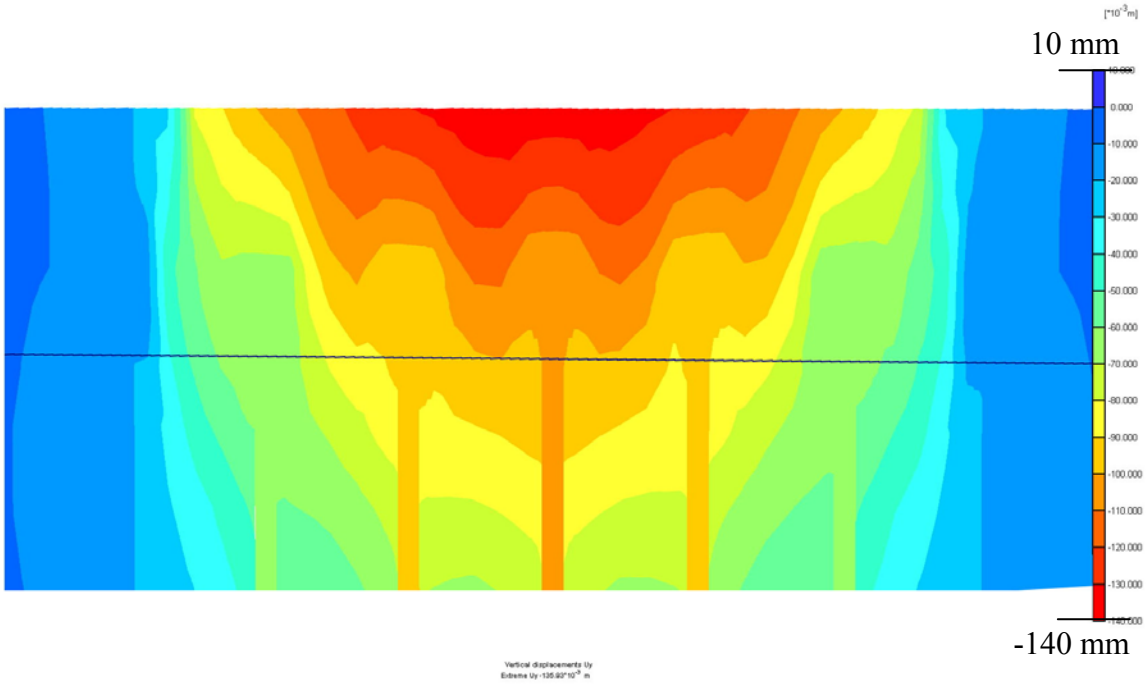

Figure 4.45 Vertical displacements at pressure of 220kPa (LS-A2) – cross section.

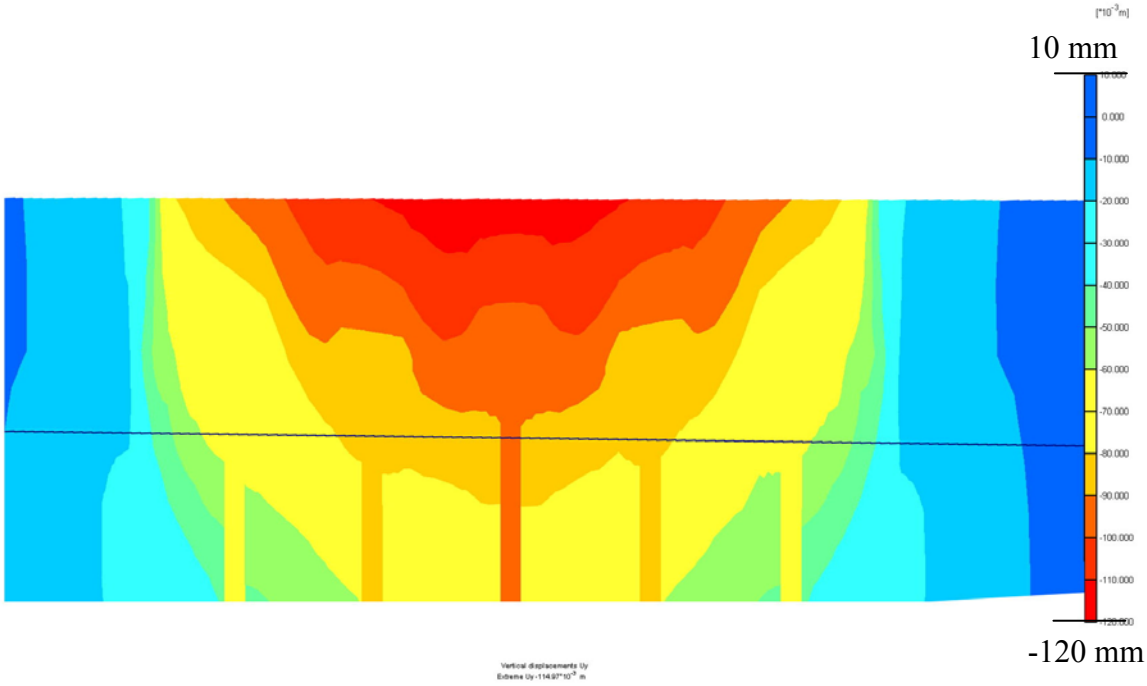

Figure 4.46 Vertical displacements at pressure of 220kPa (LS-A3) – cross section.

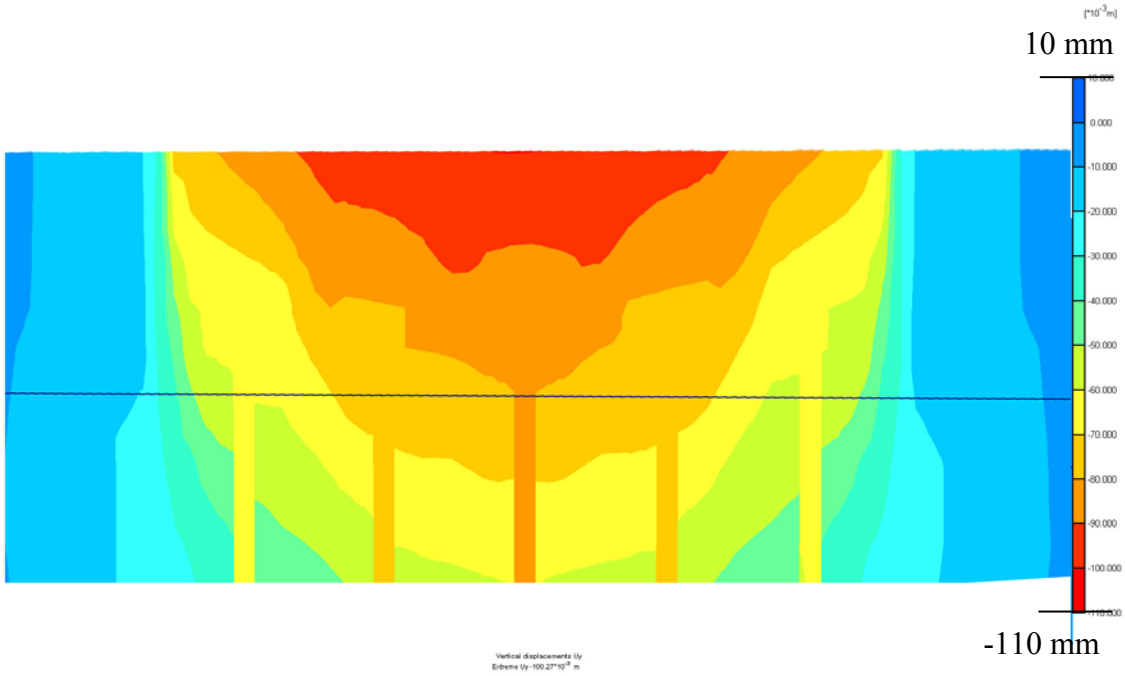

Figure 4.47 Vertical displacements at pressure of 220kPa (LS-A5) – cross section.

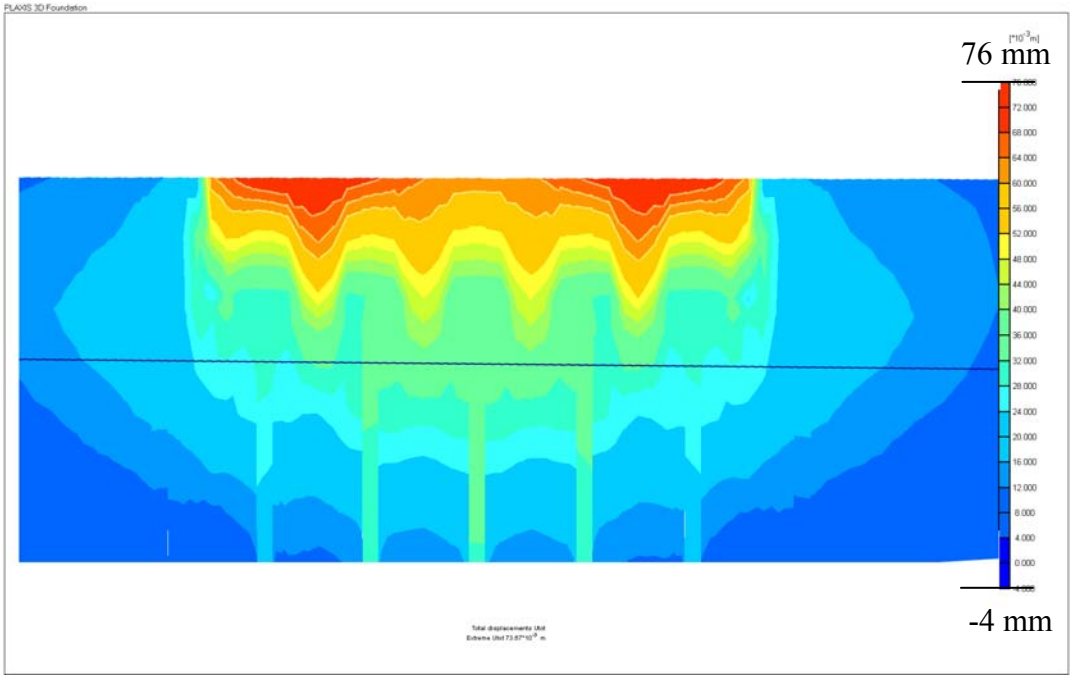

Figure 4.48 Total displacements at pressure of 400kPa (DS-A3) – cross section.

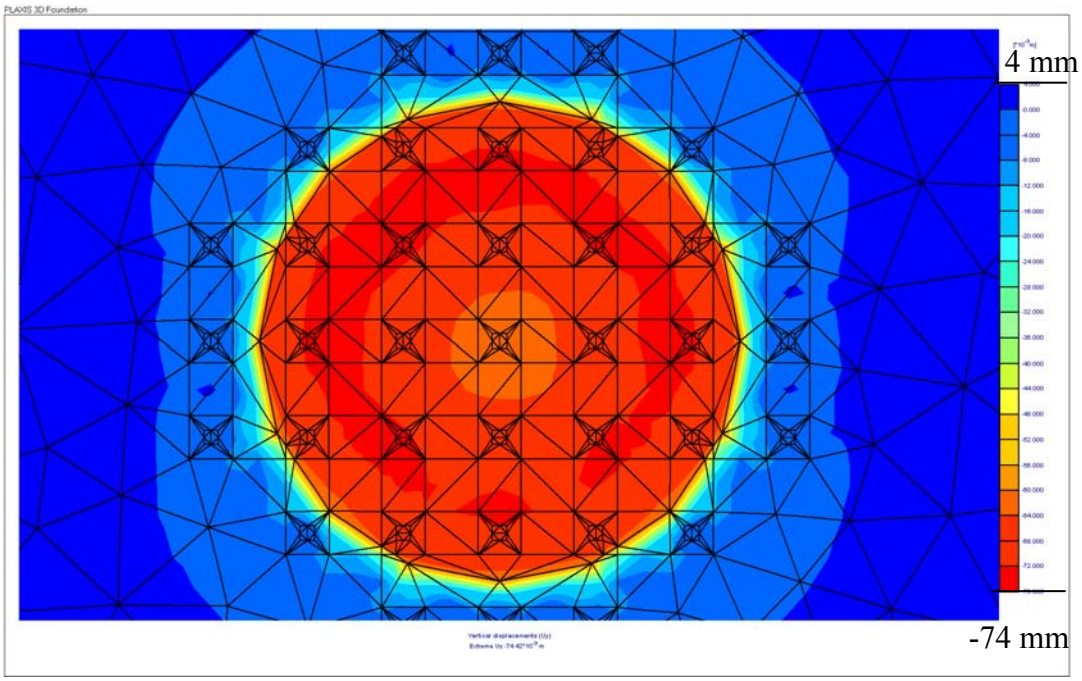

Figure 4.49 Vertical displacements at pressure of 400kPa (DS-A3) – plan view.

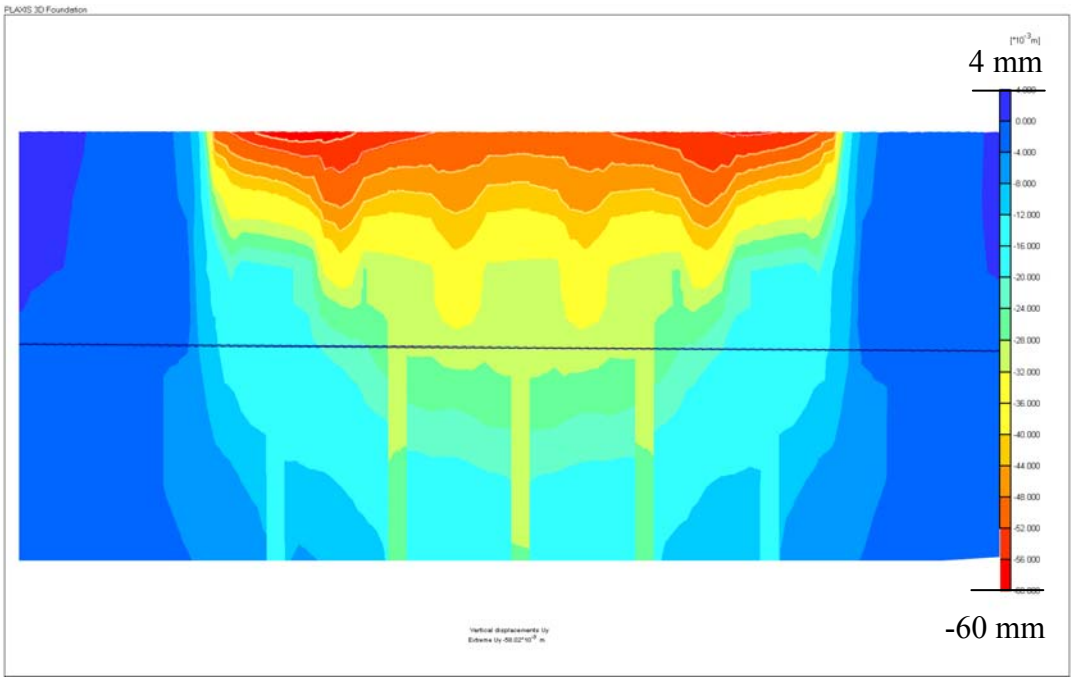

Figure 4.50 Vertical displacements at pressure of 400kPa (DS-A5) – cross section.

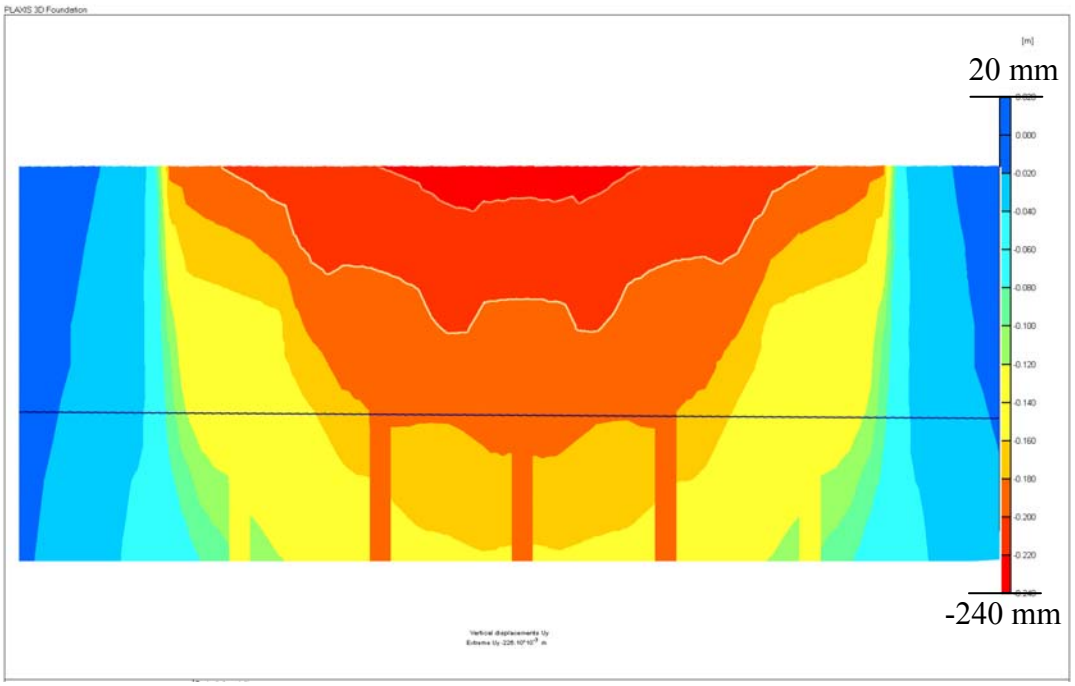

Figure 4.51 Vertical displacements at pressure of 400kPa (LS-A5) – cross section.

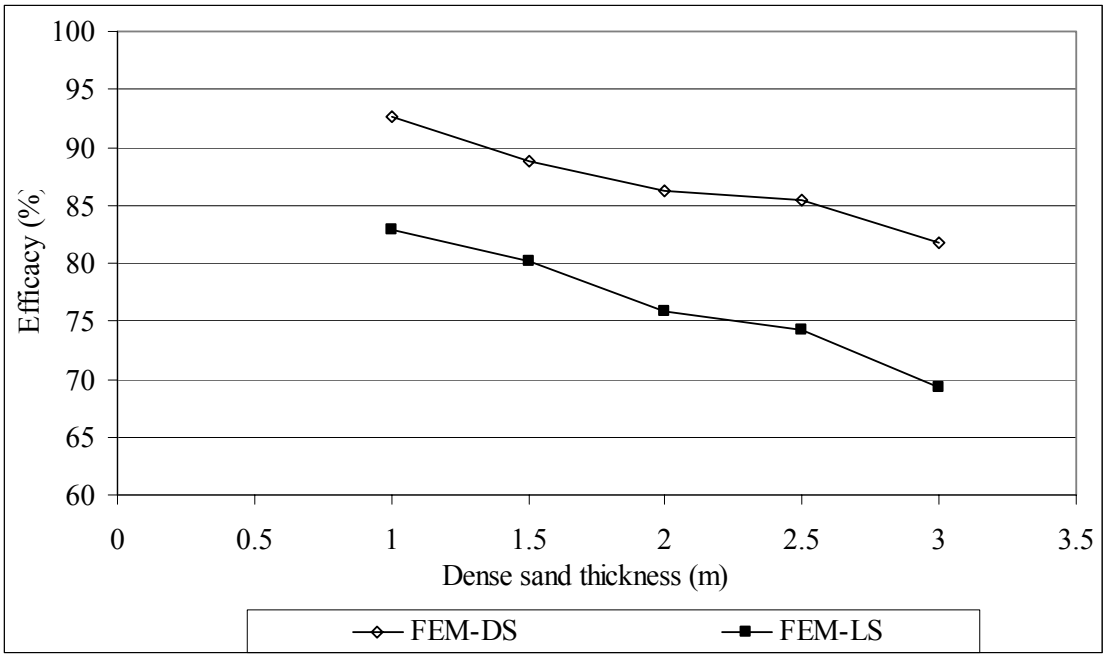

Figure 4.52 Development of efficacy with thickness of sand pad for model of test series 2.

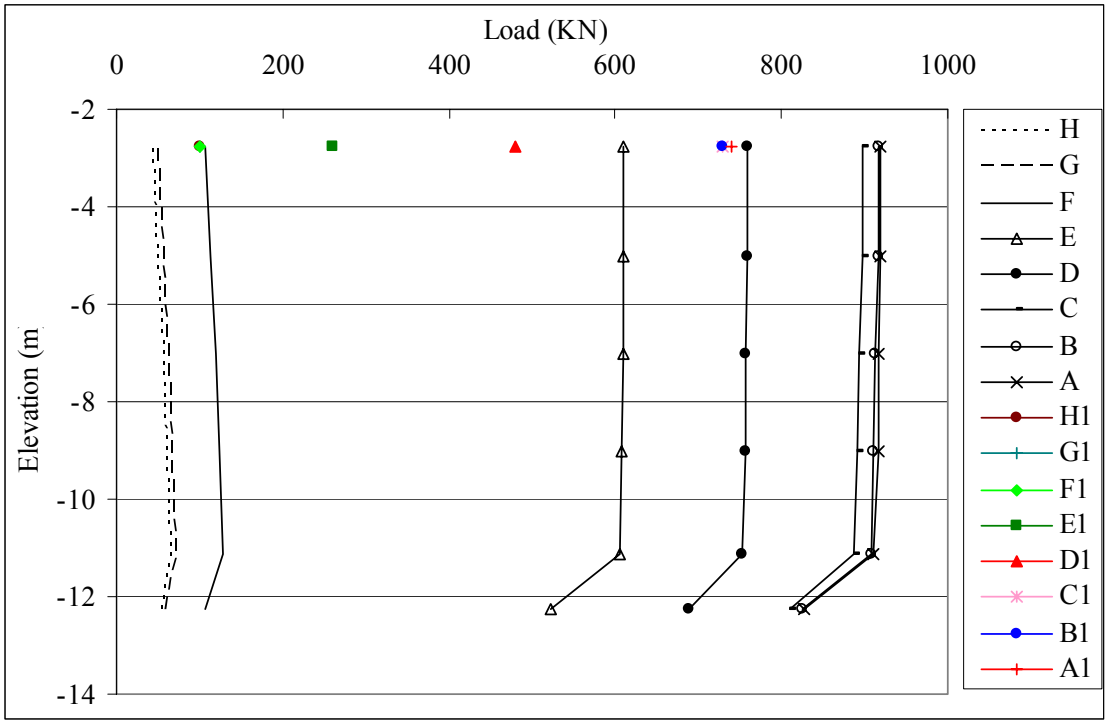

Figure 4.53 Load transfer curves in model of test DS-N1, 220kPa pressure. (Black lines present load transfer curve from FEM analysis; Color dots present load distribution from Centrifuge observation)

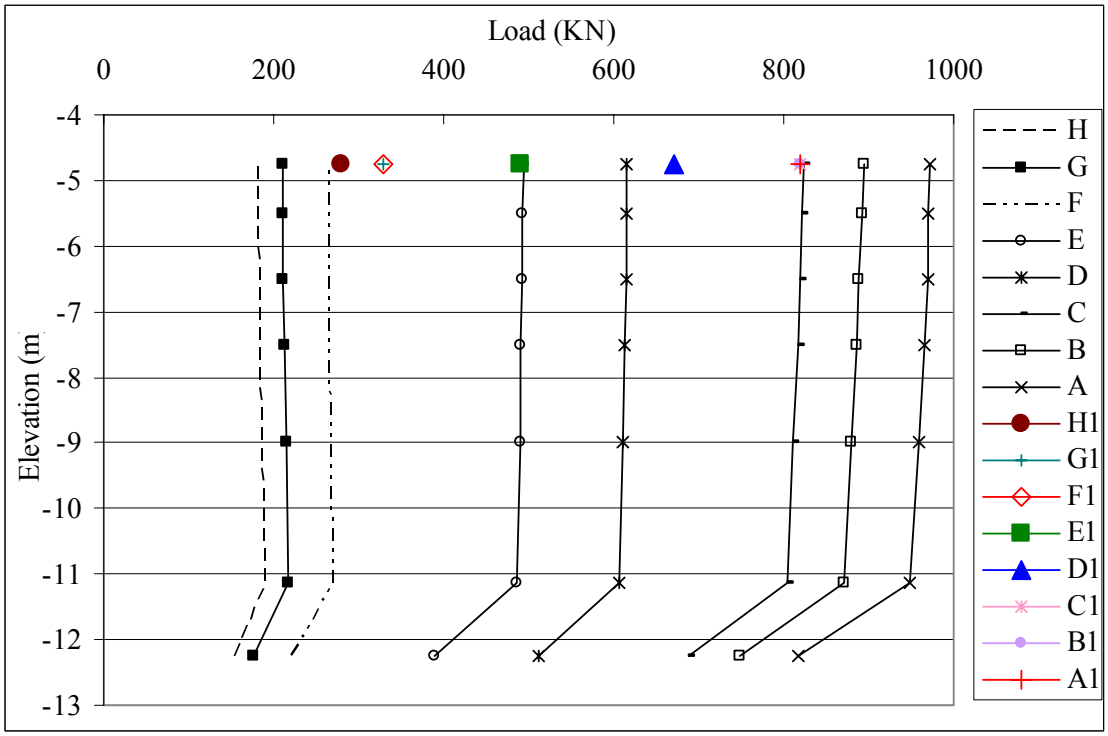

Figure 4.54 Load transfer curves in model of test DS-N4, 220kPa pressure. (Black lines present load transfer curve from FEM analysis; Color dots present load distribution from Centrifuge observation)

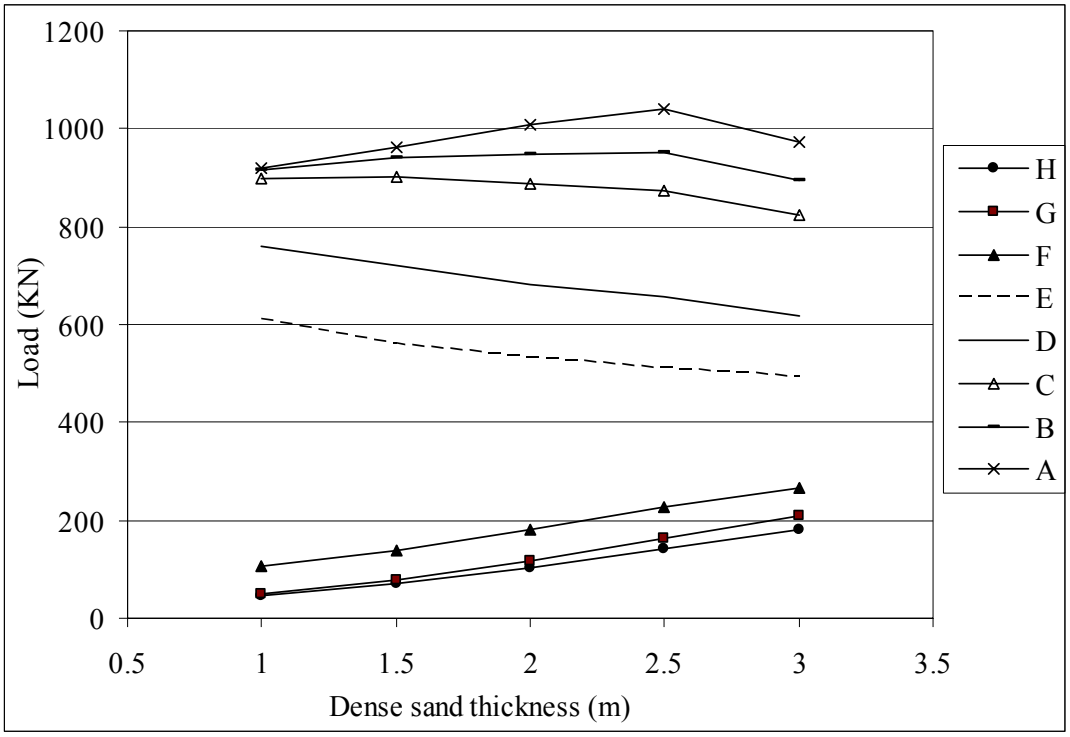

Figure 4.55 Comparision of load distribution among pile when overlying dense sand thickness increasing (dense sand bed layer) (Loads was taken at 1.75m below the pile cap).

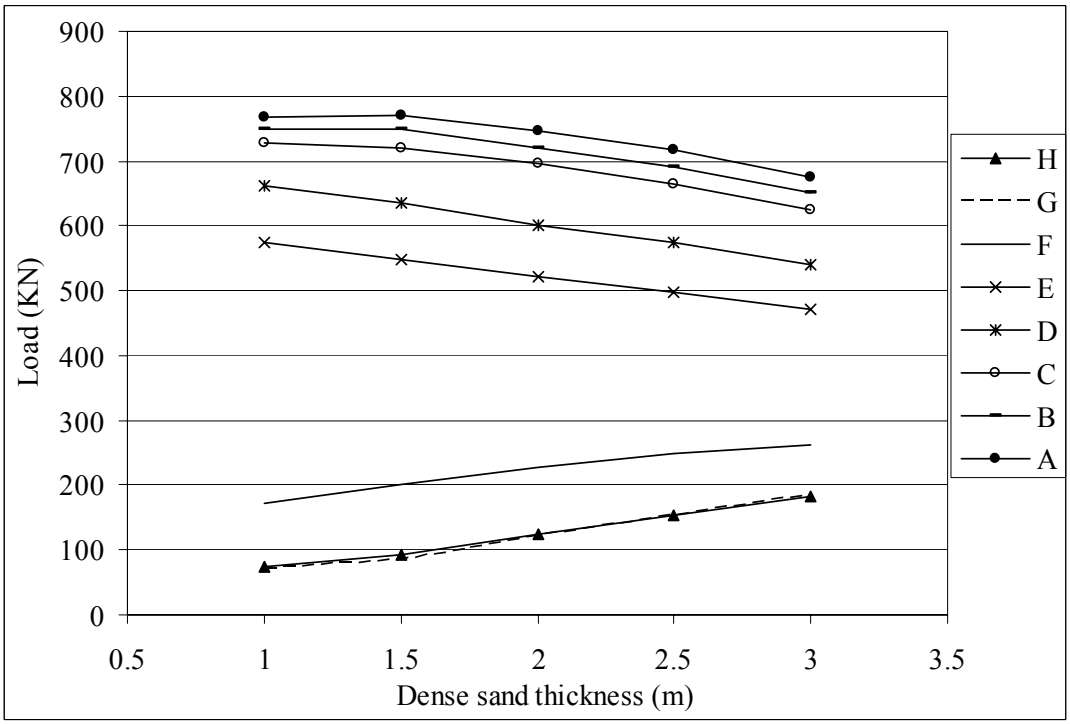

Figure 4.56 Comparision of load distribution among pile when overlying dense sand thickness increasing (loose sand bed layer) Loads was taken at 1.75m below the pile cap.

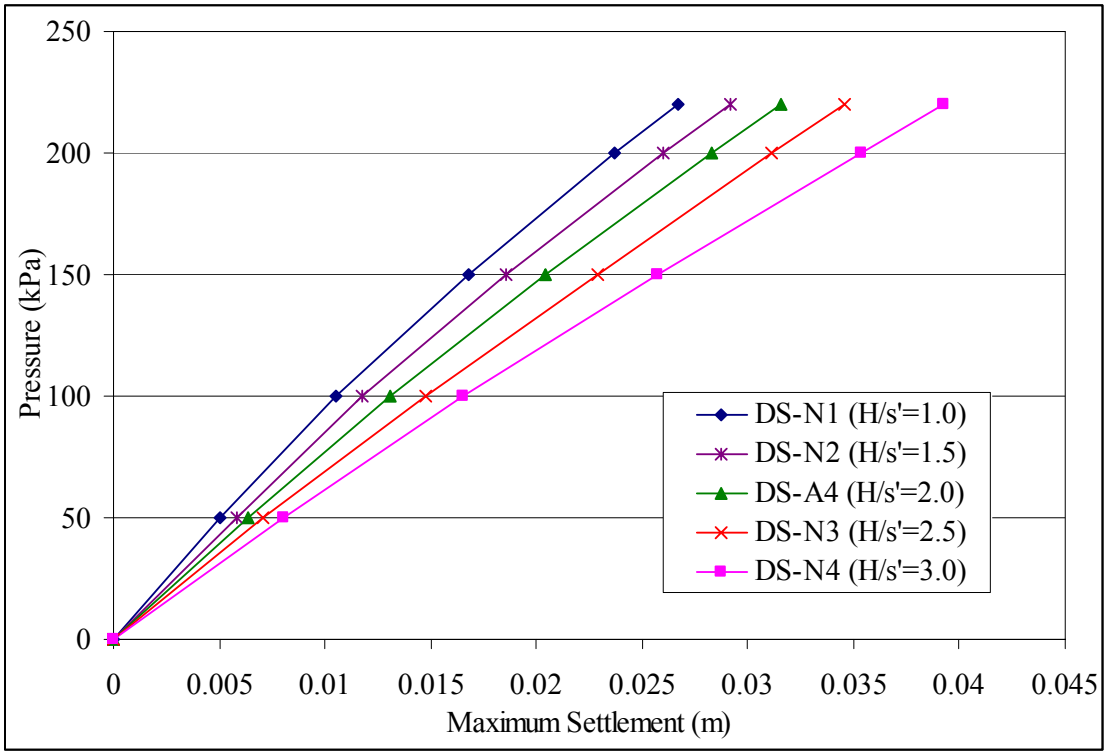

Figure 4.57 Development of maximum tank settlement with pressure from tank for model of test series 2 (dense sand bed layer).

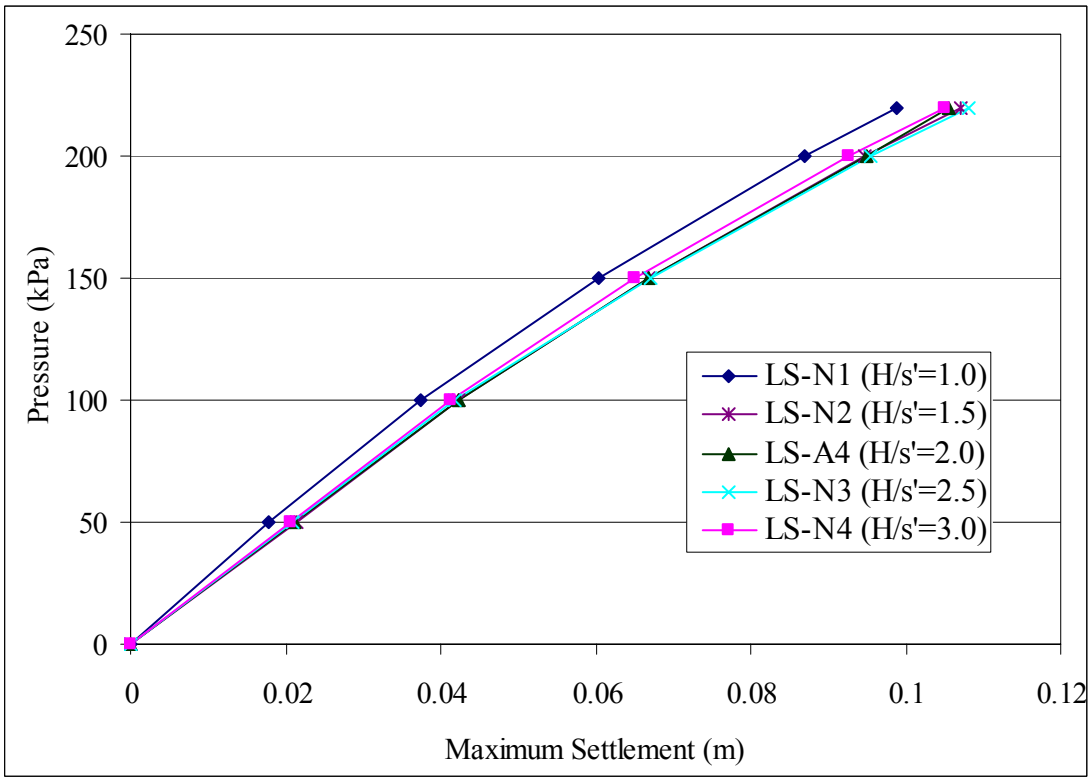

Figure 4.58 Development of maximum tank settlement with pressure from tank for model of test series 2 (loose sand bed layer).

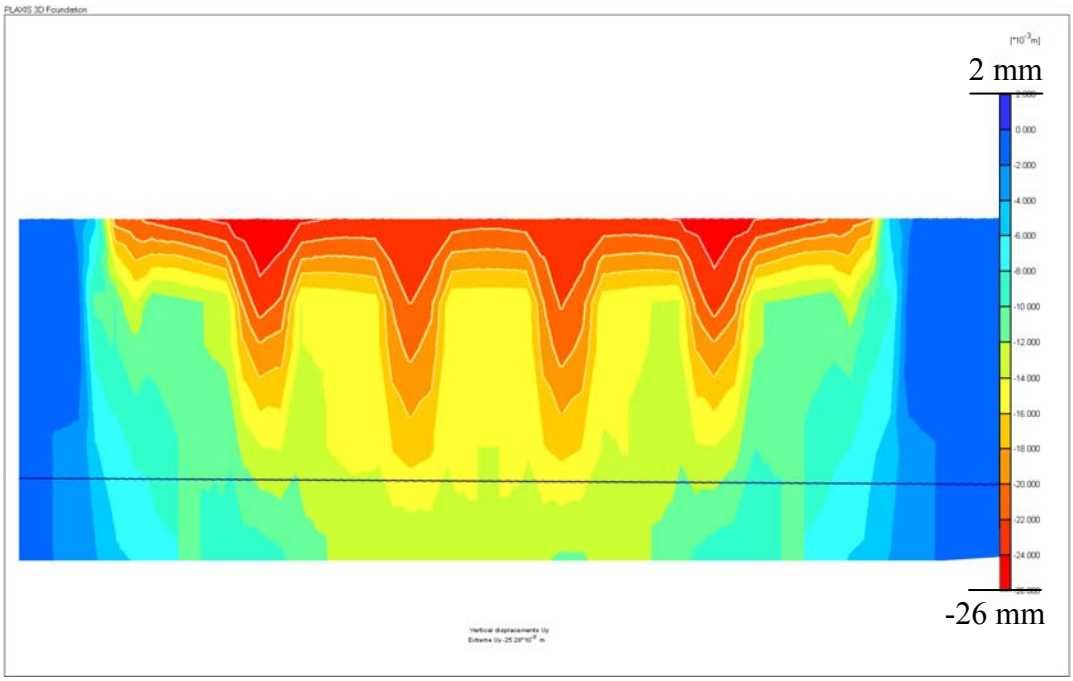

Figure 4.59 Vertical displacements at pressure of 220kPa (DS-N1) – cross section.

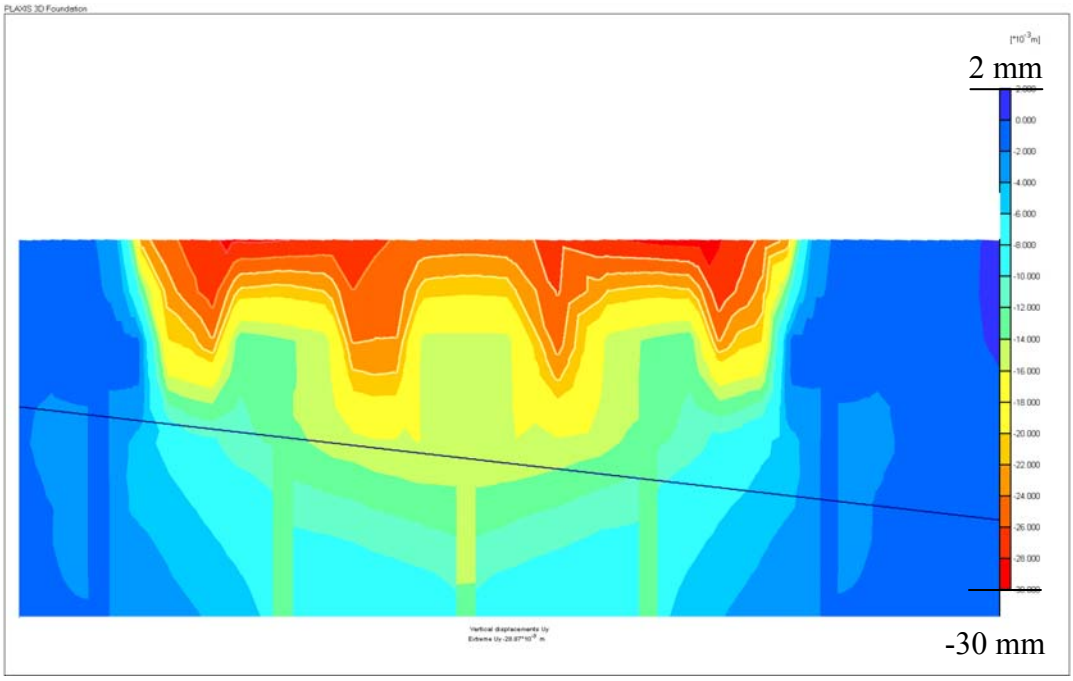

Figure 4.60 Vertical displacements at pressure of 220kPa (DS-N2) – cross section.

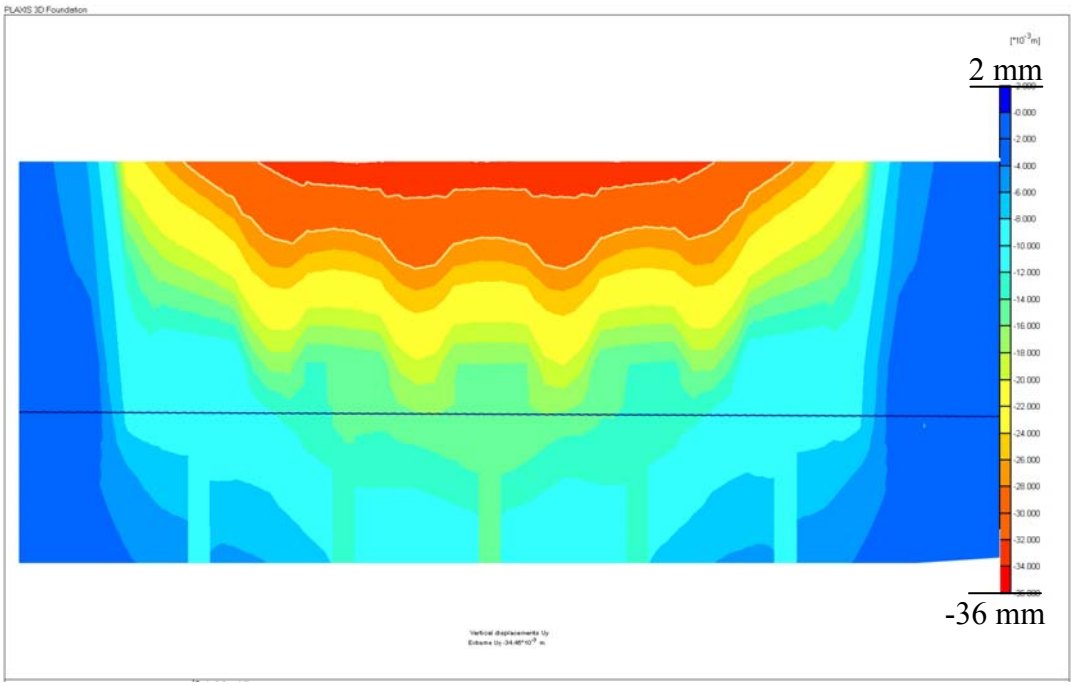

Figure 4.61 Vertical displacements at pressure of 220kPa (DS-N3) – cross section.

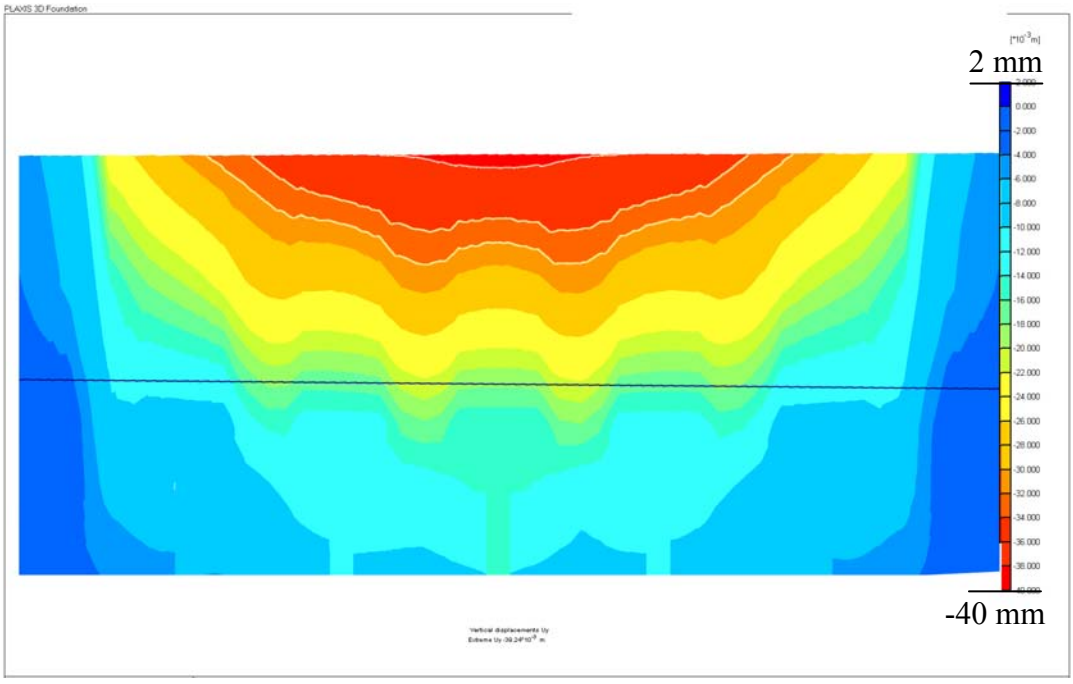

Figure 4.62 Vertical displacements at pressure of 220kPa (DS-N4) – cross section.

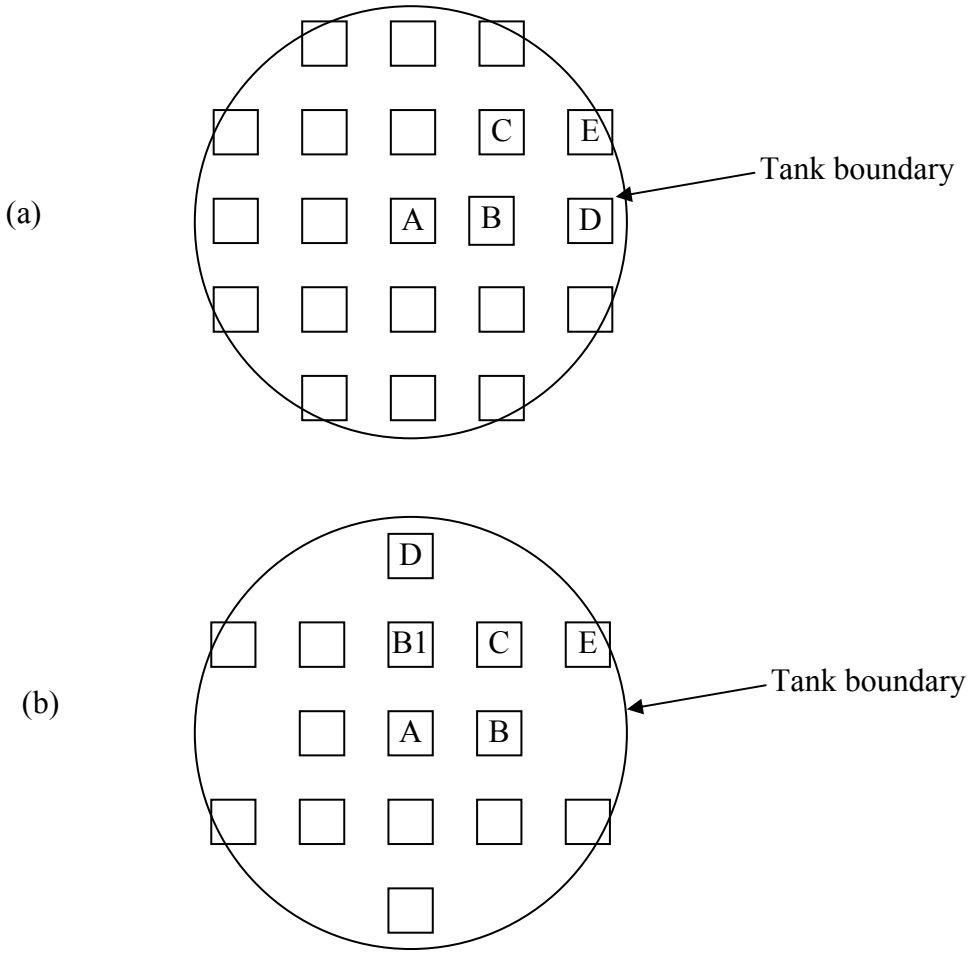

Figure 4.63 Configuration of pile plan layout (a) model test S2; (b) model test S3 (after S.C. Lee, 2004)

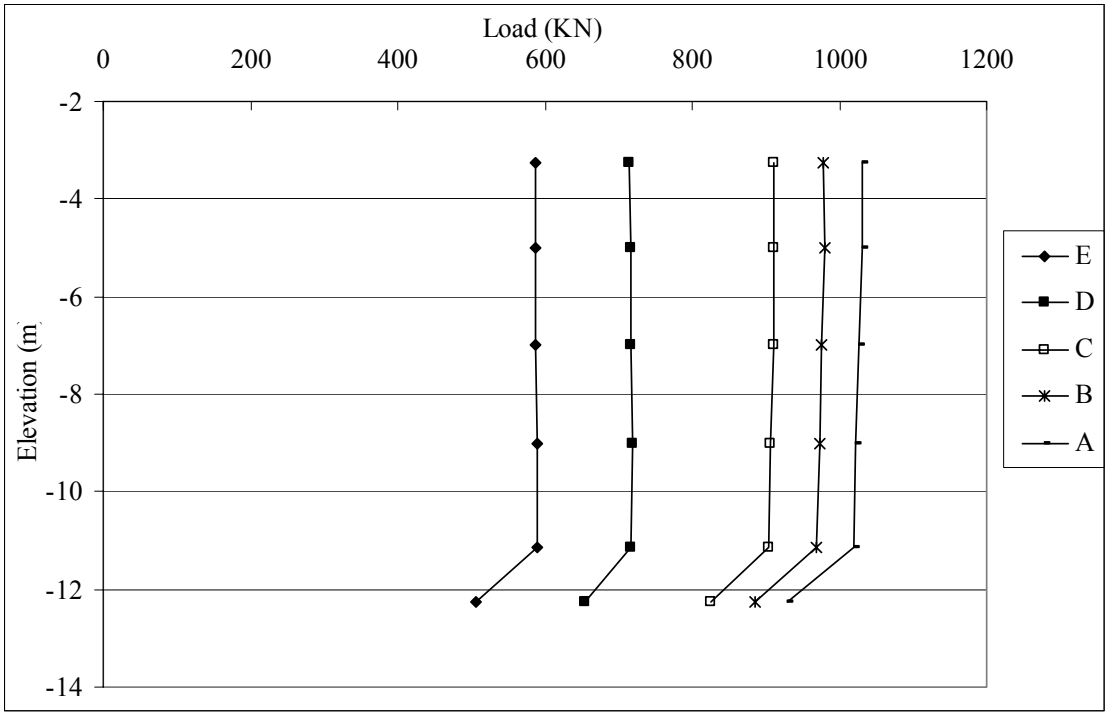

Figure 4.64 Load transfer curves in model of test DS-S2, 220kPa pressure.

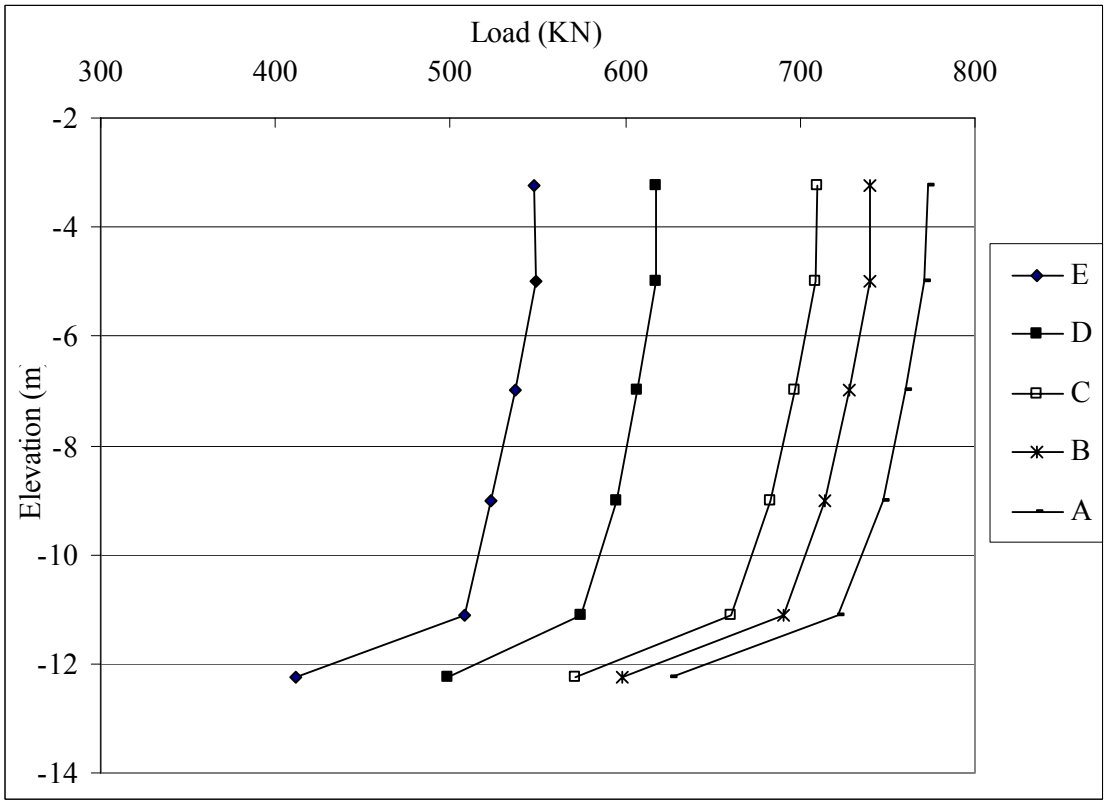

Figure 4.65 Load transfer curves in model of test LS-S2, 220kPa pressure.

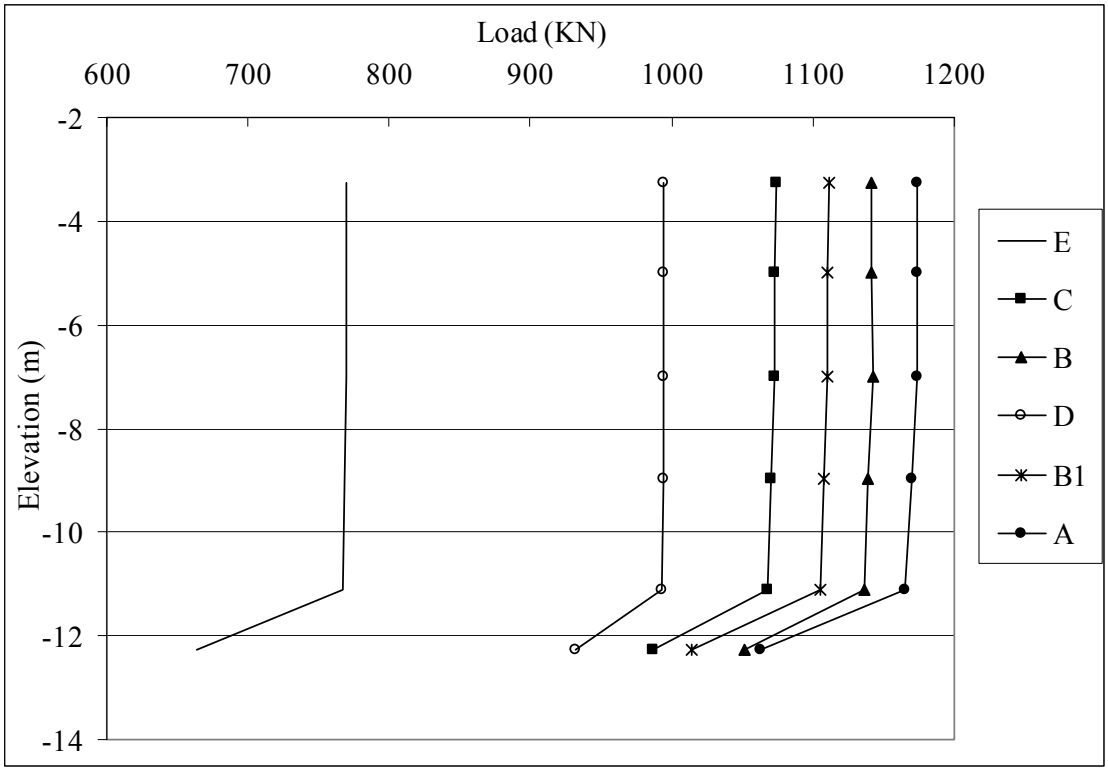

Figure 4.66 Load transfer curves in model of test DS-S3, 220kPa pressure.

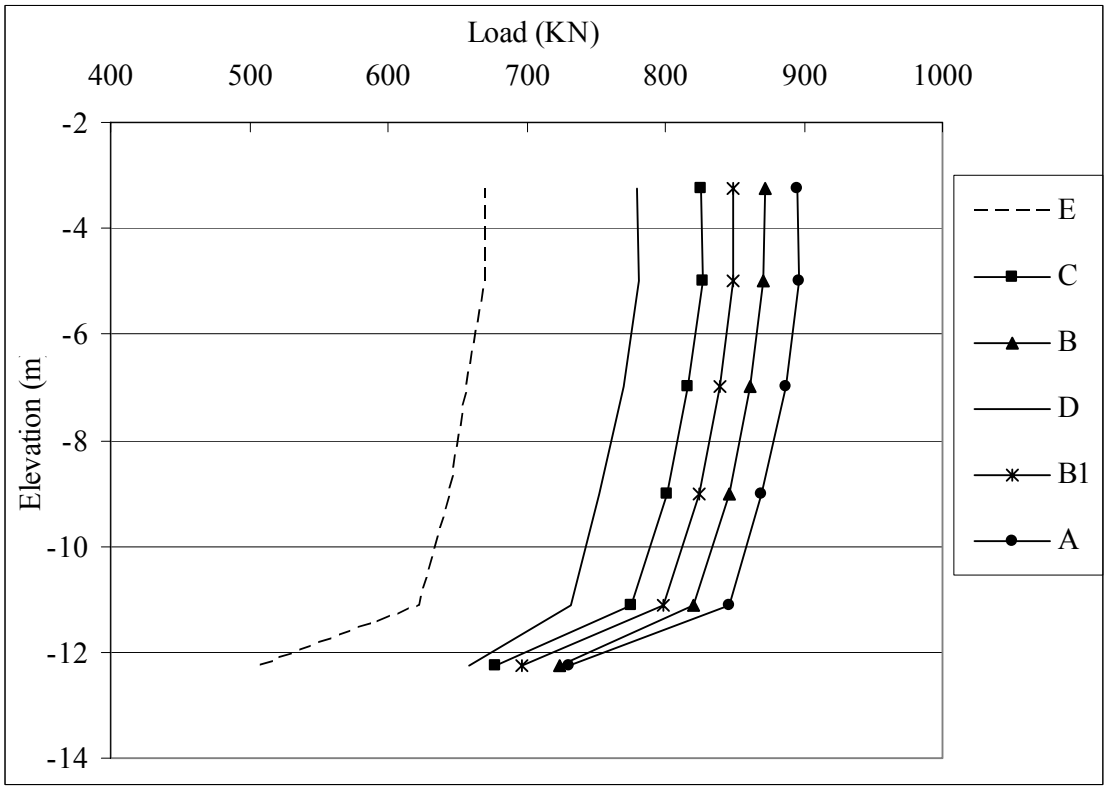

Figure 4.67 Load transfer curves in model of test LS-S3, 220kPa pressure.

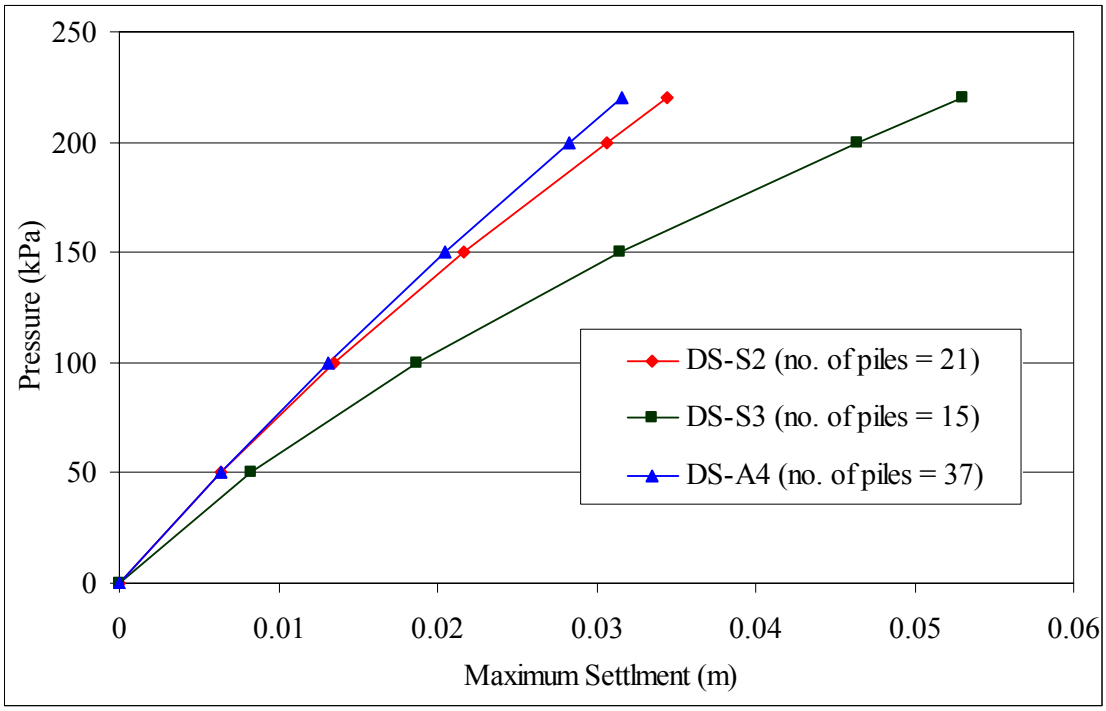

Figure 4.68 Development of maximum tank settlement with pressure from tank for model of test series 3 (dense sand bed layer).

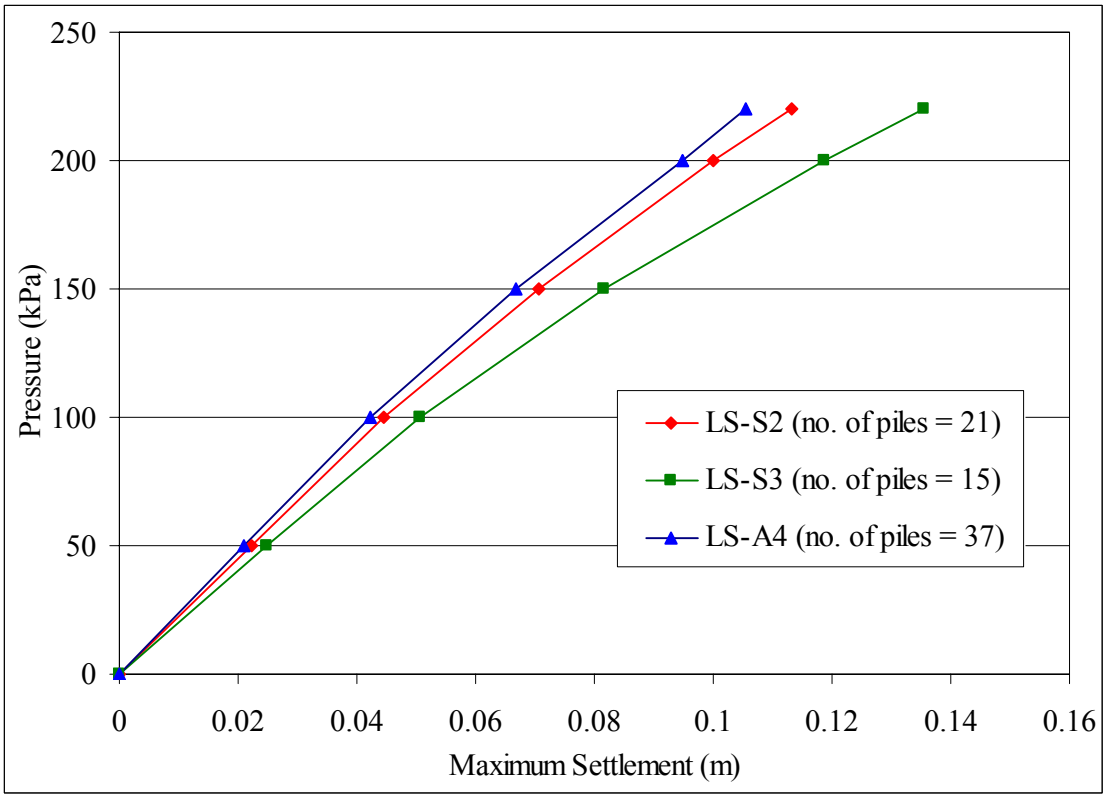

Figure 4.69 Development of maximum tank settlement with pressure from tank for model of test series 3 (loose sand bed layer).

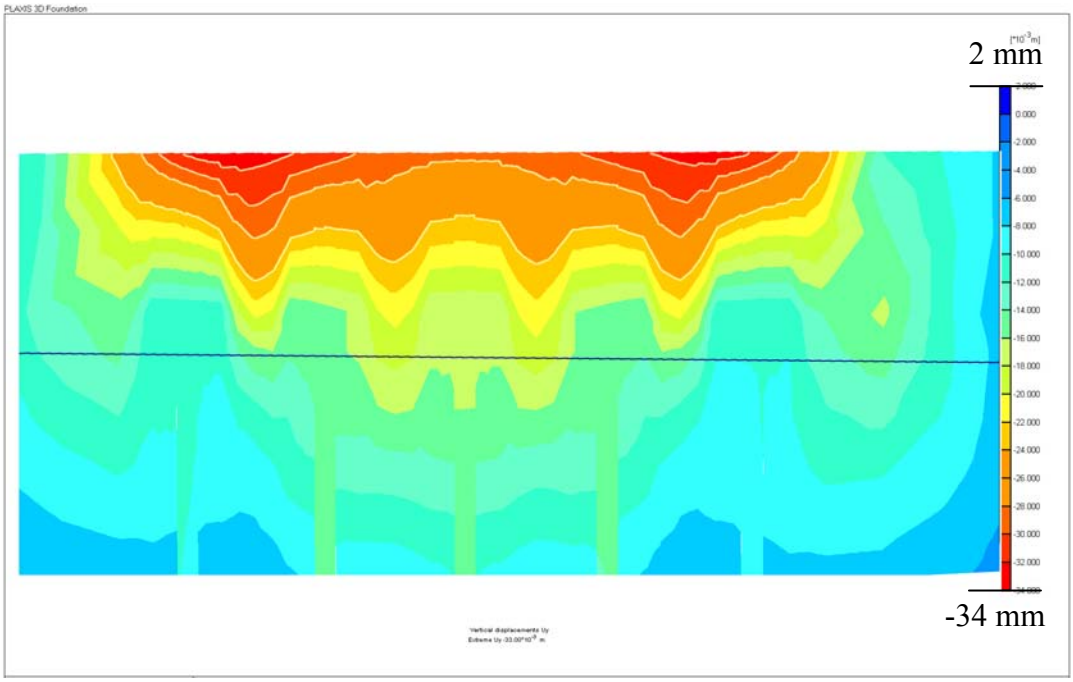

Figure 4.70 Vertical displacements at pressure of 220kPa (DS-S2) – cross section.

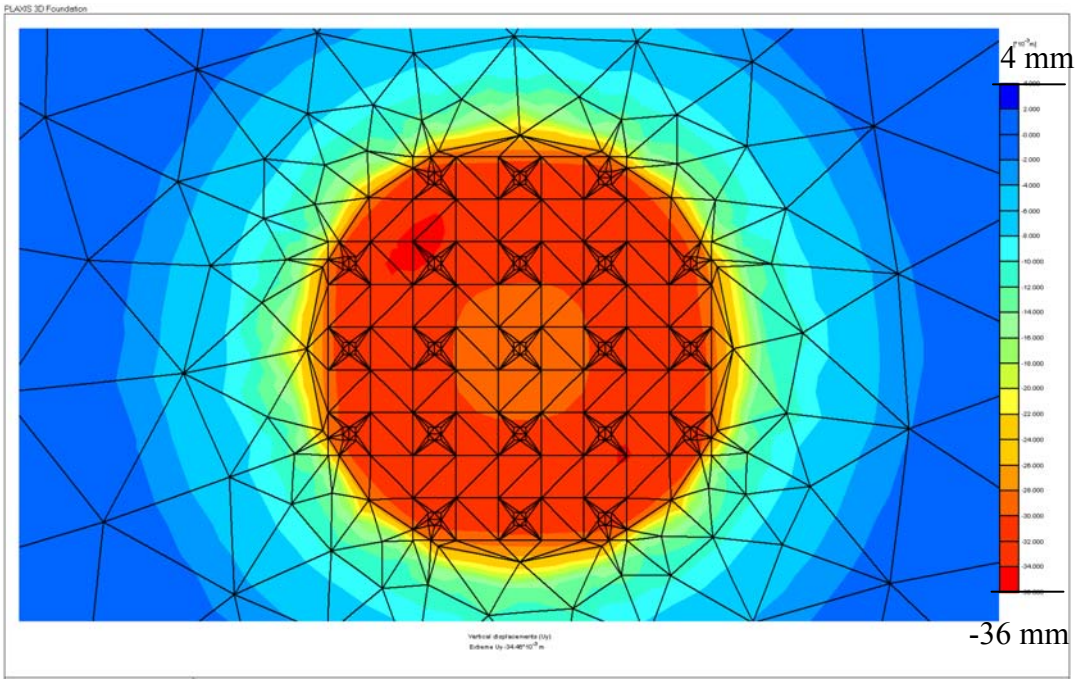

Figure 4.71 Vertical displacements at pressure of 220kPa (DS-S2) – plan view.

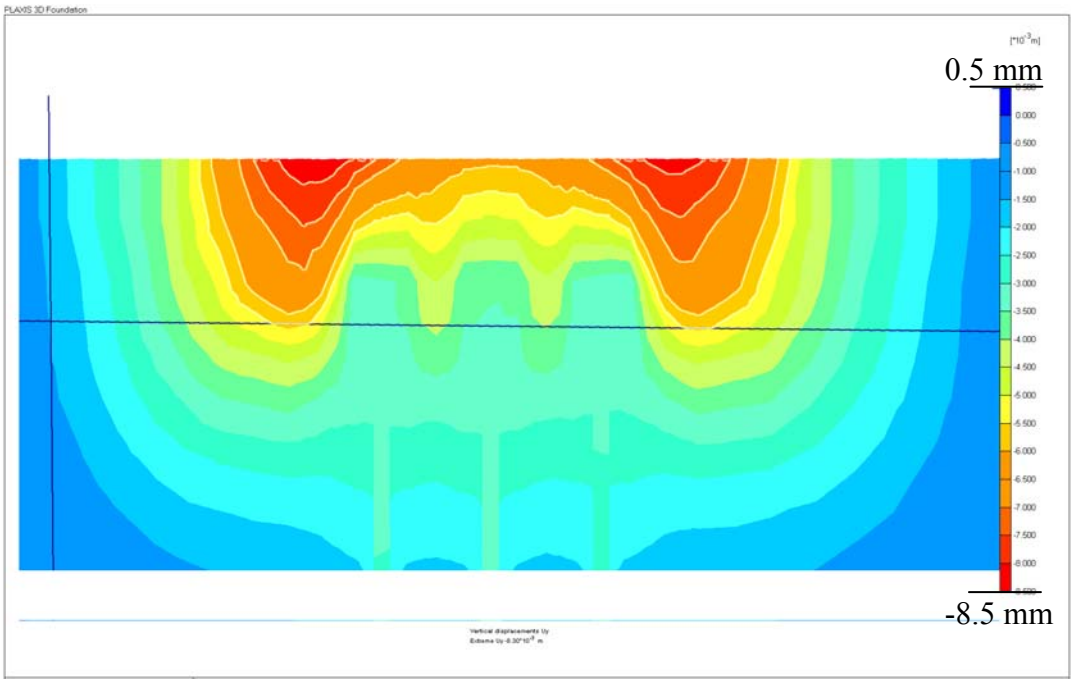

Figure 4.72 Vertical displacements at pressure of 50kPa (DS-S3) – cross section.

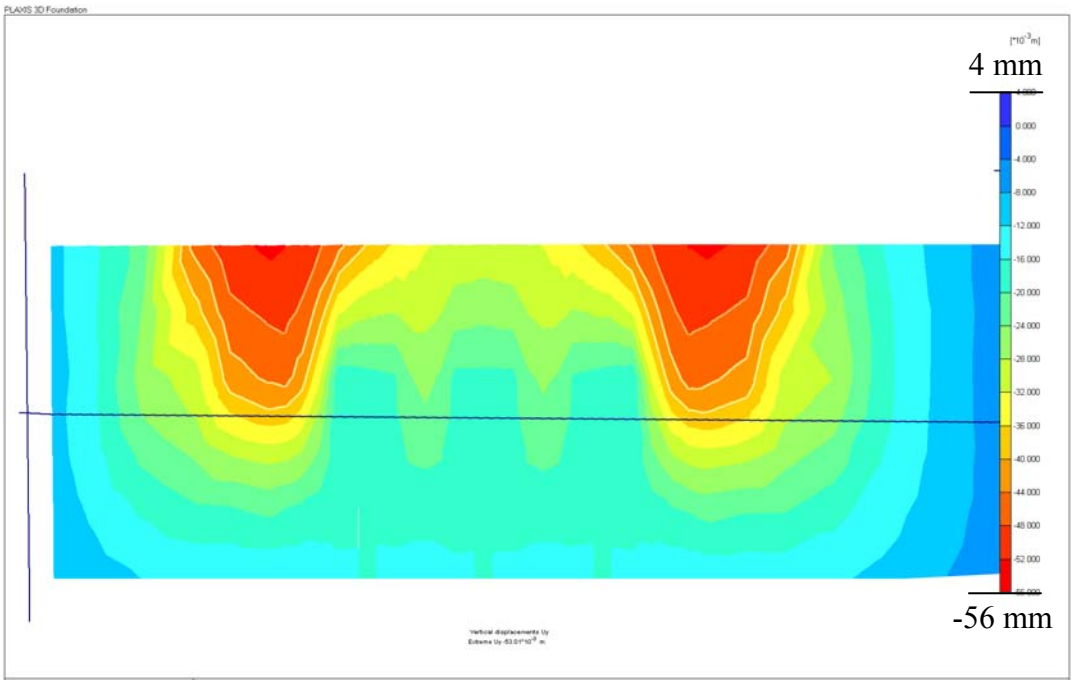

Figure 4.73 Vertical displacements at pressure of 220kPa (DS-S3) – cross section.

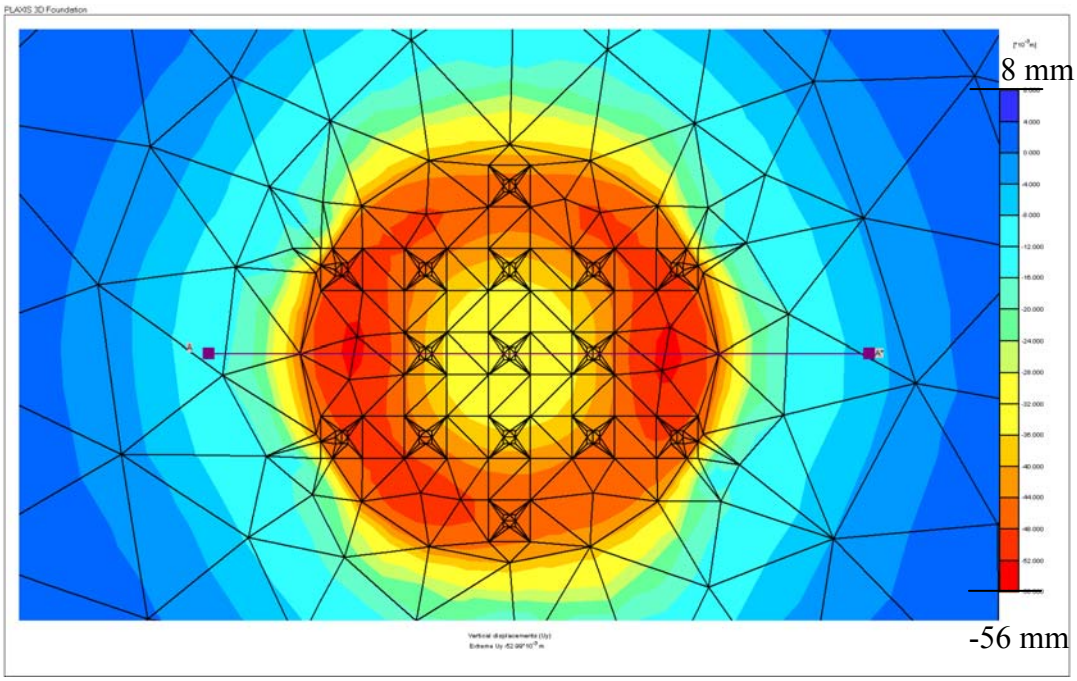

Figure 4.74 Vertical displacements at pressure of 220kPa (DS-S3) – plan view.

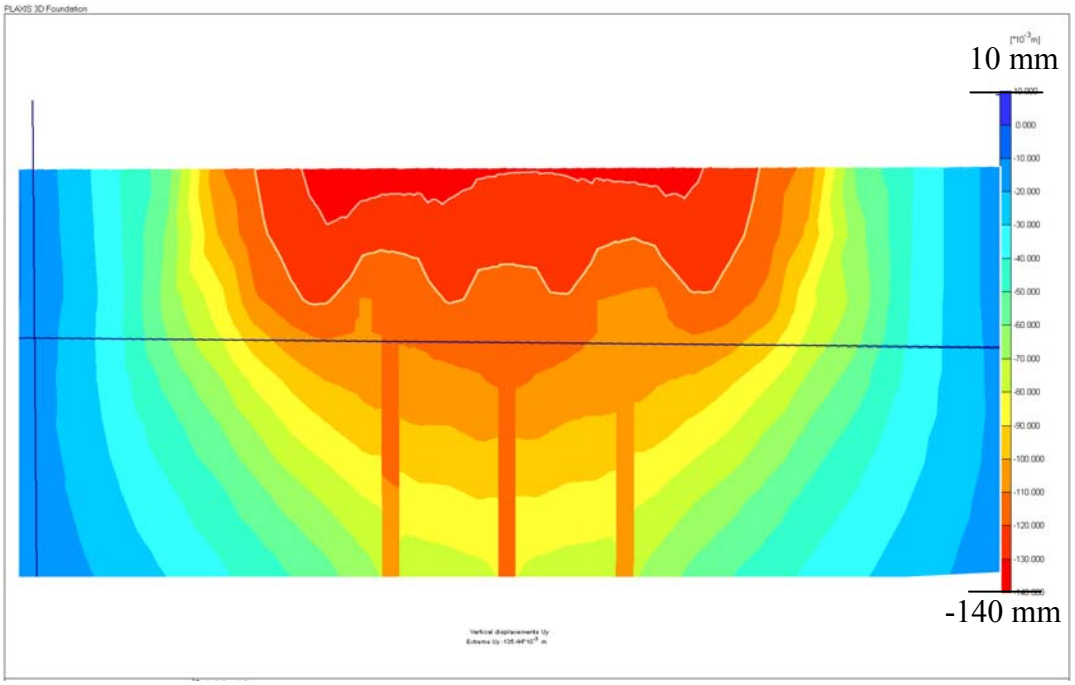

Figure 4.75 Vertical displacements at pressure of 220kPa (LS-S3) – cross section.

No.	Bed layer	Purpose	Test Number	Pile cap area ratio	Sand pad thickness	H/S'
1	Dense sand	Preliminary Test	DS-P1	No piles	2m	
2		Model series 1: Pile cap ratio	DS-A1	0.06	2m	1.33
3			DS-A2	0.12	2m	1.54
4			DS-A3	0.20	2m	1.82
5			DS-A4	0.25	2m	2.00
6			DS-A5	0.30	2m	2.22
7		Model series 2: Thickness of dense sand pad	DS-N1	0.25	1m	1.00
8			DS-N2	0.25	1.5m	1.50
9			DS-N3	0.25	2.5m	2.50
10			DS-N4	0.25	3m	3.00
11		Model series 3: Reduced number of piles	DS-S2	0.25	2m	2.00
12			DS-S3	0.25	2m	2.00
13	Loose sand	Model series 1: Pile cap ratio	LS-A1	0.06	2m	1.33
14			LS-A2	0.12	2m	1.54
15			LS-A3	0.20	2m	1.82
16			LS-A4	0.25	2m	2.00
17			LS-A5	0.30	2m	2.22
18		Model series 2: Thickness of dense sand	LS-N1	0.25	1m	1.00
19			LS-N2	0.25	1.5m	1.50
20			LS-N3	0.25	2.5m	2.50
21			LS-N4	0.25	3m	3.00
22		Model series 3: Reduced number of piles	LS-S2	0.25	2m	2.00
23			LS-S3	0.25	2m	2.00

Table 4.1 Summary of FEM model tests

Materials	Type	Young's Modulus E (MPa)	Poisson ratio ν	Frictional angle φ(deg)	drained shear strength c (kPa)	Unit weight γ (kN/m^3)
Sand pad	M-C	50	0.25	32	1	20
Soft soil	M-C	2+0.35z	0.35	22	0.1	16
Loose sand	M-C	13	0.30	31	1	20
Dense sand	M-C	200	0.25	35	25	20
Concrete	elastic	7.2E+04	0.2	-	-	24

Table 4.2 Soil properties

Name	Type	Young's Modulus E (MPa)	Poisson ratio ν	Unit weight γ (kN/m^3)	Poisson ratio ν	Size (m)	
						width	height
Pile	Elastic	7.2E+04	0.20	24	0.20	0.3	0.3
Plate	Elastic	7.2E-02	0.20	24	0.20	0.3	-
Floor	Elastic	2.1E+05	0.20	78.5	0.20	-	-

Table 4.3 Structural element properties.

Stage		P1	A1	A2	A3	A4	A5	N1	N2	N3	N4	S2	S3
Initial stage		√	√	√	√	√	√	√	√	√	√	√	√
Pile installation			√	√	√	√	√	√	√	√	√	√	√
Wall installation			√	√	√	√	√	√	√	√	√	√	√
Floor installation		√	√	√	√	√	√	√	√	√	√	√	√
Loading	20	√											
	40	√											
	50	□	√	√	√	√	√	√	√	√	√	√	√
	60	√											
	80	√											
	100	√	√	√	√	√	√	√	√	√	√	√	√
	110	√											
	120	√	√										
	140		√										
	150			√	√	√	√	√	√	√	√	√	√
	160		√										
	180		√										
	200			√	√	√	√	√	√	√	√	√	√
	220			√	√	√	√	√	√	√	√	√	√
	250			√	√	√	√	√	√	√	√	√	√
	300				√	√	√	√	√	√	√	√	√
	350				√	√	√	√	√	√	√	√	√
	400				√	√	√	√	√	√	√	√	√

Table 4.4 List of loading stages.

Time	Test model	H	G	F	E	D	C	B	B1	A	Total load on pile	Total load (45 degree)	Total load (90 degree)	Efficacy (45 degree)	Efficacy (90 degree)
	(kN)	(kN)	(kN)	(kN)	(kN)	(kN)	(kN)	(kN)	(kN)	(kN)	(kN)	(kN)	(%)	(%)	(kN)
After loading	A1	120	100	100	220	370	570	580		600	10200.00	19057.67	18429.35	54%	55%
	A2	140	140	140	320	485	710	710		720	13140.00	19057.67	18429.35	69%	71%
	A3	140	140	140	360	620	840	840		840	15160.00	19057.67	18429.35	80%	82%
	A4	180	150	140	400	660	870	870		890	16290.00	19057.67	18429.35	85%	88%
	A5	145	145	145	420	670	860	870		900	16180.00	19057.67	18429.35	85%	88%
	N1	100	100	100	260	480	730	730		740	12180.00		17011.71		72%
	N4	280	330	330	490	670	820	820		820	18860.00		19846.99		95%
	S2				430	640	890	890		890	14010.00		18429.35		76%
	S3				430	690	880	890	890	890	11070.00		18429.35		60%
One month after loading	A1	120	100	100	205	380	600	620		620	10420.00	19057.67	18429.35	55%	57%
	A2	135	130	130	280	520	780	790		800	13520.00	19057.67	18429.35	71%	73%
	A3	140	140	140	340	580	910	910		920	15480.00	19057.67	18429.35	81%	84%
	A4	160	140	140	360	620	950	950		965	16325.00	19057.67	18429.35	86%	89%
	A5	140	140	140	400	680	920	960		960	16640.00	19057.67	18429.35	87%	90%
	N1	100	100	100	280	490	770	770		770	12730.00		17011.71		75%
	N4	290	330	330	490	720	870	870		880	19600.00		19846.99		99%
	S2				410	640	960	960		960	14480.00		18429.35		79%
	S3				410	690	940	960	960	970	11590.00		18429.35		63%
Three months after loading	A1	120	100	100	195	360	630	630		640	10440.00	19057.67	18429.35	55%	57%
	A2	130	120	120	260	535	830	830		840	13700.00	19057.67	18429.35	72%	74%
	A3	140	140	140	300	550	940	940		950	15310.00	19057.67	18429.35	80%	83%
	A4	140	140	140	360	620	980	980		1000	16440.00	19057.67	18429.35	86%	89%
	A5	140	140	140	380	680	1000	1010		1010	17050.00	19057.67	18429.35	89%	93%
	N1	100	100	100	280	490	790	790		790	12910.00		17011.71		76%
	N4	295	320	320	480	720	880	880		900	19580.00		19846.99		99%
	S2				380	640	1000	1000		1000	14600.00		18429.35		79%
	S3				400	690	980	980	1010	1010	11890.00		18429.35		65%

Table 4.5 Axial load and efficacy from centrifuge models (After S.C. Lee, 2004).

Test model	H	G	F	E	D	C	B	B1	A	Total load on pile	Total load (45 degree)	Total load (90 degree)	Efficacy (45 degree)	Efficacy (90 degree)
	(kN)	(kN)	(kN)	(kN)	(kN)	(kN)	(kN)	(kN)	(kN)	(kN)	(kN)	(kN)	(%)	(%)
DS-A2	104.6	128.4	150.9	527.0	651.0	881.0	961.0		1027.0	17168.8	20667.4	20014.0	83%	86%
DS-A3	104.9	122.6	191.8	511.6	672.7	877.4	935.9		1023.3	17155.7	20667.4	20014.0	83%	86%
DS-A4	103.8	116.8	182.3	522.7	677.1	881.5	947.0		1014.5	17246.0	20667.4	20014.0	83%	86%
DS-A5	100.2	121.4	192.4	528.8	673.4	884.5	945.4		998.2	17297.9	20667.4	20014.0	84%	86%
DS-N1	70.3	78.3	138.3	560.1	719.6	900.3	940.8		963.7	17116.3		18474.4		93%
DS-N2	44.5	50.6	107.2	609.3	758.8	898.2	916.5		918.1	17073.5		19244.2		89%
DS-N3	141.2	161.9	227.5	512.8	657.7	873.9	950.8		1040.5	17760.2		20783.7		85%
DS-N4	182.2	209.8	266.0	494.7	616.1	823.7	893.6		973.0	17624.9		21553.5		82%
DS-S2				587.2	714.9	911.4	979.0		1030.9	16149.3		20014.0		81%
DS-S3				769.6	994.5	1073.6	1141.8	1111.0	1173.3	15040.7		20014.0		75%
LS-A2	110.8	112.7	156.0	530.4	601.2	719.6	757.8		790.3	15308.3	20667.4	20014.0	74%	76%
LS-A3	117.2	114.7	235.9	507.1	596.0	690.2	720.9		754.4	15178.8	20667.4	20014.0	73%	76%
LS-A4	118.1	113.1	220.8	516.7	598.0	691.1	714.0		737.6	15163.0	20667.4	20014.0	73%	76%
LS-A5	116.5	124.3	228.4	521.8	602.7	693.2	714.6		737.9	15297.4	20667.4	20014.0	74%	76%
LS-N1	83.3	74.5	190.8	549.0	636.8	721.8	748.6		770.5	15319.6		18474.4		83%
LS-N2	62.2	58.3	163.3	581.3	667.4	732.8	752.6		770.3	15415.5		19244.2		80%
LS-N3	151.7	151.6	248.1	504.9	584.1	674.8	703.2		729.0	15429.0		20783.7		74%
LS-N4	182.2	184.6	262.9	470.3	539.9	624.3	650.2		673.9	14941.7		21553.5		69%
LS-S2				548.2	618.0	709.5	740.3		773.5	13430.3		20014.0		67%
LS-S3				671.0	780.1	826.2	872.3	848.4	895.8	11886.3		20014.0		59%

Table 4.6 Axial load on different pile types and efficacy from FEM models.

CHAPTER 5

CONCLUSIONS AND RECOMENDATIONS

5.1 Conclusions

Three dimensional FEM study on pile foundation for oil tank on soft soil was carried out. The study investigates the efficacy of pile foundation system, the load sharing in the piles, the load transfer curves and soil arching for various pile cap area ratio, the thickness of the dense sand layer, the number of piles and the stiffness bedding layer in a typical oil tank foundation. The results are compared with the centrifuge model results. The following conclusions can be made on:

1. Efficacy:
    - The efficacy of the tank increases with the increase of tank pressure.
    - When the pile cap ratio increased from 12% to 30%, the efficacy does not change significantly because of the fully mobilized soil arching.
    - When the sand pad ratio is greater than 1, the efficacy seems to reduce as the sand pad ratio increases.
    - The efficacy decreases with decreasing of number of piles
    - The efficacy depends on the stiffness of bed layer.
2. Load distribution among the piles:
    - The load carried by the central piles is much higher as compared to corner piles and piles outside the tank.
    - When the load increases, the rate of load distribution to the center piles increases faster than the load transferred to the edge and outside piles.

- The greater the pile cap ratio, the better the load spread to the piles, it means that when the pile cap ratio increases, the load applied to the central piles reduces and the load applied to the corner piles and the outside piles increases.
- When the sand pad ratio increases, the axial force on outside piles increases and that of pile C, D, E decreases. But the axial force on pile type A and B in model of loose sand bed layer decreases with increasing overlying dense sand thickness layer while that of dense sand bed layer changes differently (it increases when the thickness sand pad increases from 1m to 2.5m and decreases when the overlying dense sand thickness layer increases to 3m).
- The axial force in edge piles increases faster than that of center piles with the decreasing number of piles but the change is small when the number of piles is reduced from 37 to 21. The difference is much larger when the number of pile is reduced from 21 to 15. This feature also is affected by the stiffness the bed layer, the stiffer the bed layer the larger the increase in axial load in the edge piles.

3. Settlement:
   - The maximum settlement and differential settlement of the tank decreases with increasing pile cap area ratio. The maximum tank settlement is reduced by half when the pile cap area ratio increases from 0.06 to 0.12.
   - The gradient of the load-settlement response of the tank decreases with increasing pile cap area ratios.
   - The models with dense sand bed layer reveal an increasing maximum and differential tank settlement when the thickness of dense sand layer increases whereas the results are similar for loose sand bed layer.
   - The maximum and differential tank settlement increase with decreasing number

of piles but the change is small when the number of pile reduces from 37 to 21 and much bigger when the number of pile reduces from 21 to 15.

4. Settlement profile shape:
    - The location of maximum settlement depends on the stiffness of bed layer. When bed layer is loose sand, maximum settlement occurs near to the center of oil tank for all loading levels. Whereas the location of maximum settlement in the model of dense sand bed layer occurs at about two third of the radius from the center of oil tank when the tank pressure is greater than 200kPa.
    - The location of maximum settlement depends on the magnitude of pressure applied. For the pile cap ratio less than 12%, maximum settlement occurs near to the center of oil tank for all loading levels. When the pile cap ratio is greater than 12%, the location of maximum settlement occurs about two third of the radius from the center of oil tank when the tank pressure is greater than 200kPa.
    - The location of maximum settlement depends on the sand pad thickness ratio. The larger the sand pad thickness ratio, the larger of tank pressure is needed to shift the location of maximum settlement out of center of the tank.
    - The shape of settlement dish depends on the arrangement of piles in group. When some piles in tank base area were omitted, the location of maximum settlement is shifted to the missing piles.
5. Arching: Arching seems fully mobilize with sand pad thickness ratio greater than 1.

5.2 Recommendations for Further Research

In the course of study, several areas have shown potential for improvement in further research. The following further studies are recommended:

1. As the performance of flexible oil tank foundation is largely a settlement control

problem, research on how settlement developed under various oil tank parameters is useful for the oil tank foundation designer.

2. Some parameters such as ratios between magnitude of loading and stiffness of oil underneath the oil tank, ratios between oil tank diameter and depth of the hard strata and inclined angle of bed strata should be further investigated. This can be effectively done with a reliable 3D FEM code that can correctly model the soil-structure interaction of the full scale oil tank foundation. The results of 3D FEM study should be compared with full scale field instrumented oil tanks.
3. As above study reveals pile group under the sand pad behaved like pile raft to some extent, the optimization of a pile raft system for oil tanks has potential for future research.

REFERENCES

Bell, R.A., and Iwakiri, J. (1980). Settlement comparion used in tank-failure study. Journal of the Geotechnical Engineering Division, ASCE, Vol. 106, No.2, 153-172.

British Standards BS8006: 1995 Code of practice for strengthened/Reinforced soils and other fills. Section 8.3.3 British Standard Institution.

Broms, B.B and Wong, I. H. (1985). Embankment piles. Third International Geotechnical Seminar, Soil Improvement Methods, Singaropre, 167-178.

Broms, J.F., and Paterson, W. G. (1964). Failure of an oil storage tank founded on a sensitive marine clay. Canadian Geotechnical Journal. Vol. 1, No. 4, 205-214.

Clarke, J. S. (1969). Survey of oil storage tank failures. Annales de l'institute Belge du Petrol, Belgium, No. 6, 15-24.

Duncan, J. M. and D'Orazio, T. B. (1984). Stability of oil storage tanks. Journal of Geotechnical Engineering, ASCE, Vol. 110, No. 9, 1219-1238.

D'Orazio, T. B. and Duncan, J. M. (1987). Deferential settlement in steel tank. Journal of Geotechnical Engineering, ASCE, Vol. 113, No. 9, 967-983.

Green, P. A. and Height, D. W. (1975). The failure of two oil storage tanks caused by differential settlement. Proceedings British Geotechnical Society Conference on Settlement of Structures, Pentech Press, London, England.

Hewlett, W. H. and Randolph, M. F. (1988). Analysis of piled embankments. Ground Engineering, London, England, 21(3), 12-18.

Biarez, J & Hicher, P.-Y. (1994). Elementary Mechanics of Soil Behavior.

Khoo, C. N. (2001). Design of Oil Tank Foundation, Bachelor of Civil Engineering (Civil) Thesis, Department of Civil Engineering, National University of Singapore.

Low, B. K., Tang, S. K. and Choa, V. (1994). Arching in piled embankments. Journal of Geotechnical Engineering ASCE, Vol. 120, No. 11, 1917-1938.

Marr, W. A., Ramos, J. A., and Lambe, T. W. (1982). Criterial for settlement of tanks. Journal of Geotechnical Engineering, ASCE, Vol. 108, No. 8, 1017-1039.

Lee, S. C. (2004).Centrifuge model study of pile foundation system for oil tank, M eng Thesis, Department of Civil Engineering, National University of Singapore.

Spangler, M. G. and Handy, R. L. (1982). Soil Engineering, 4th ed., Harper & Row, New York.

Thornburn, S., Laird, C. L. and Randolph, M. F. (1984). Storage tanks founded on soft soils reinforced with driven piles. Pilling and Ground Treatment, No. 9, 157-164.

Tung, Y. C. (1994). Load Transfer Mechanism of Embankment Piles, Bachelor of Civil Engineering (Civil) Thesis, Department of Civil Engineering, National University of Singapore.

Randolph, M. F. (1994). Design methods for pile groups and pile rafts. Proceeding 13th International Conference on Soil Mechanic and Foundation Engineering, New Delhi. Vol. 5. 61-82.

Horikoshi, K. & Randolph, M. F. (1998). A contribution to the optimum design of pile rafts, Geotechnique 48, No. 2, 301-317.

Schanz, T., Vermeer, P.A., (1998). Special issue on Pre-failure deformation behaviour of geomaterials, Geotechnique 48, pp. 383-387.

Knodner, R.L., (1963). A Hyperbolic Stress Strain Formulation for Sands. 2. Pan. Am. ICOSFE Brazil, Vol. 1, pp. 289-324.

Duncan, J.M., Chang, C.-Y., (1970). Nonlinear Analysis of Stress and Strain in Soil. ASCE J. of the Soil Mech. And Found. Div. Vol. 96, pp. 1629-1653.

Brinkgreve, R.B.J., (1994). Geomaterial Models and Numerical Analysis of Softening. Dissertation. Delft University of Technology.

PLAXIS 2002. “Plaxis Computer Program”, Version 8.2 manual

PLAXIS 2004. “Plaxis Computer Program”, Plaxis 3D Foundation manual